Justus-Liebig-University Giessen

Department of Geography

Climatology, Climate Dynamics and Climate Change

PhD dissertation

by

Zhang, Mingyue

“Regional Paleo Climate Simulation Over Eastern Mediterranean and the Nile River Basin with COSMO-CLM”

A dissertation submitted

for the degree of

Doctor rerum naturalium (Dr. rer. nat.)

by

Zhang, Mingyue

Examiner: Prof. Jürg Luterbacher

Co-Examiner: Prof. Andreas Dittmann

2023

Abstract

The complex interaction between climate variability, extreme events, and societal dynamics within the Eastern Mediterranean (EM) and Nile River (NR) basin (EMNR) has captivated scholarly attention for years. Despite the importance of climate's influence on societies, most of the research primarily relied on proxy records, with limited attention to the detailed/regional/local information provided by Regional Climate Model (RCM) simulations. The primary objective of this study is to increase the understanding of regional and local climatic patterns within the EM and NR basin over two millennia based on a regional climate model - COSMO-CLM. This study highlights the necessity of bridging the gap of the coarse GCM resolution by employing RCMs, focusing on the paleo climate simulation over EM and NR region with COSMO-CLM (COnsortium for Small-scale MOdelling in CLimate Mode) model.

More specifically, the first part of this thesis provides a sensitivity analysis of different land cover schemes in convective-permitting simulations within COSMO-CLM. Key among the external forcings is land use change, which significantly alters land surface properties affecting energy, water, and momentum exchanges between the land and atmosphere. By analyzing the simulated air temperature, the leaf area index and the plant coverage, this study underscored the need to carefully select appropriate Land Cover (LC) maps for regional climate modeling, as LC maps and fractions had substantial impacts on simulated air temperature, Leaf Area Index (LAI), and plant coverage. The study also indicated that analyzing the effects of heterogeneous land cover types on seasonal climate, as well as assessing the role of land cover in regional climate modeling, would be crucial for future research. Further investigations are also required to understand how regional climate responds to varying land cover distributions.

The second part involves developing a transient paleo climate simulation for the past 2000 years using the COSMO-CLM model with its enhanced horizontal resolution up to 50 x 50 km, which incorporates several external forcings (solar, orbital, volcanic, greenhouse gases and land use change) to make the paleo simulations more realistic and more independent. By implementing those

external forcings into COSMO-CLM, the study provides a dataset characterized by enhanced spatial (50 km) and temporal (monthly to hourly depending on the output variables) resolution. This approach can not only enable a comparative analysis between simulation outputs and proxy data but also foster the possibility of a comprehensive understanding of historical socio-climatic conditions.

The research further compares the mean climate condition of EMNR between the ERP (Early Rome Period: 400-362 BCE) and PI (Pre-Industrial: 1800 -1850 CE), further, offering insights into large-scale circulation processes and their impact on regional climate conditions between ERP and PI. The results show that the mean climate conditions of the two selected periods are similar in terms of annual cycle but with increased variability from ERP to PI. In addition, the relationship between large-scale circulation features to regional temperature/precipitation patterns reveals stable large-scale circulation influence during both ERP and PI periods.

Zusammenfassung

Die komplexe Wechselwirkung zwischen Klimaschwankungen, Extremereignissen und gesellschaftlicher Dynamik im östlichen Mittelmeerraum (EM) und im Einzugsgebiet des Nils (NR) zieht seit Jahren die Aufmerksamkeit der Wissenschaft auf sich. Trotz der Bedeutung des Einflusses des Klimas auf die Gesellschaft stützten sich die meisten Forschungsarbeiten in erster Linie auf Proxy-Datensätze und schenkten den detaillierten/regionalen/lokalen Informationen, die von regionalen Klimamodell-Simulationen (RCM) geliefert werden, nur wenig Aufmerksamkeit. Das Hauptziel dieser Studie ist es, das Verständnis der regionalen und lokalen Klimamuster im EM- und NR-Becken über zwei Jahrtausende auf der Grundlage eines regionalen Klimamodells - COSMO-CLM - zu verbessern. Diese Studie unterstreicht die Notwendigkeit, die Lücke der groben GCM-Auflösung durch den Einsatz von RCMs zu überbrücken, wobei der Schwerpunkt auf der Paläoklimasimulation über die EM- und NR-Region mit dem Modell COSMO-CLM (COnsortium for Small-scale MOdelling in CLimate Mode) liegt.

Genauer gesagt, bietet der erste Teil dieser Arbeit eine Sensitivitätsanalyse verschiedener Landbedeckungsschemata in konvektiven Simulationen innerhalb von COSMO-CLM. Zu den externen Einflüssen gehört vor allem die veränderte Landnutzung, die die Eigenschaften der Landoberfläche erheblich verändert und den Energie-, Wasser- und Impulsaustausch zwischen Land und Atmosphäre beeinflusst. Durch die Analyse der simulierten Lufttemperatur, des Blattflächenindexes und der Pflanzenbedeckung unterstrich diese Studie die Notwendigkeit, geeignete Landnutzungskarten für die regionale Klimamodellierung sorgfältig auszuwählen, da die Landnutzungskarten und -anteile erhebliche Auswirkungen auf die simulierte Lufttemperatur, den Blattflächenindex (LAI) und die Pflanzenbedeckung haben. Die Studie zeigte auch, dass die Analyse der Auswirkungen heterogener Landbedeckungsarten auf das saisonale Klima sowie die Bewertung der Rolle der Landbedeckung bei der regionalen Klimamodellierung für die künftige Forschung von entscheidender Bedeutung sind. Weitere Untersuchungen sind auch erforderlich, um zu verstehen, wie das regionale Klima auf unterschiedliche Landbedeckungen reagiert.

Der zweite Teil umfasst die Entwicklung einer instationären Paläo-Klimasimulation für die letzten 2000 Jahre unter Verwendung des COSMO-CLM-Modells mit seiner erhöhten horizontalen Auflösung von bis zu 50 x 50 km, das mehrere externe Einflüsse (Sonneneinstrahlung, Orbitalstrahlung, Vulkanismus, Treibhausgase und Landnutzungsänderungen) einbezieht, um die Paläo-Simulationen realistischer und unabhängiger zu machen. Durch die Implementierung dieser externen Einflüsse in COSMO-CLM liefert die Studie einen Datensatz, der sich durch eine verbesserte räumliche (50 km) und zeitliche (je nach Ausgangsvariablen monatlich bis stündlich) Auflösung auszeichnet. Dieser Ansatz kann nicht nur eine vergleichende Analyse zwischen Simulationsergebnissen und Proxydaten ermöglichen, sondern auch die Möglichkeit eines umfassenden Verständnisses historischer sozioklimatischer Bedingungen fördern.

Die Forschung vergleicht außerdem die mittleren Klimabedingungen des EMNR zwischen der ERP (Early Rome Period: 400-362 v. Chr.) und der PI (Pre-Industrial: 1800-1850 n. Chr.) und bietet Einblicke in großräumige Zirkulationsprozesse und ihre Auswirkungen auf die regionalen Klimabedingungen zwischen ERP und PI. Die Ergebnisse zeigen, dass die mittleren Klimabedingungen der beiden ausgewählten Zeiträume in Bezug auf den Jahreszyklus ähnlich sind, jedoch mit einer erhöhten Variabilität von ERP zu PI. Darüber hinaus zeigt die Beziehung zwischen großräumigen Zirkulationsmerkmalen und regionalen Temperatur-/Niederschlagsmustern einen stabilen Einfluss der großräumigen Zirkulation sowohl während der ERP- als auch der PI-Perioden.

Contents

List of Figures

List of Tables

1. Introduction

1.1 Motivation

Over the past two millennia, the interaction between climate variability, climate extreme events, and societies within the EMNR has gained significant attention. This timeframe has experienced significant moments including the ascendancy of notable civilizations like the Romans, and Byzantium, and the expansion of Islamic societies, all of which have collectively contributed to a rich and intricate historical narrative across the region. This poses a chance of an interdisciplinary study over the region in investigating the impacts of climate and climate change on societies changes.

However, the influence of climate on societies is examined only from the proxy records perspective (García-Herrera et al., 2007), without the detail of the processes that are offered by RCM simulations. While the proxy data are highly restricted to their geographical location and currently there is only coarse resolution Global Climate Modelling (GCM)/ Earth System Modelling (ESM) data exists in this region. Therefore, by only comparing the proxy data to the GCM/ESM data will be lacking of regional processes and inaccurate (Giorgi and Lionello, 2008). Other than this, on longer time scales covering the last two millennia, the climate system changes with several major external forcings. These include orbital variations, solar activity fluctuations, and volcanic activity, in conjunction with changes in GHG and land use (Gomez-Navarro et al., 2012). While the RCM used in this study COSMO-CLM, currently is designed for simulations from 1850 CE, and has not yet been modified for the paleo climate application, especially, those external forcings haven't been implemented into the COSMO-CLM transiently. To study the past climate and its variability at the regional scale, regional climate models (RCM) are therefore needed which should allow a considerably increased horizontal resolution and implementation of important external forcings.

Between those external forcings, the land use over the last two millennia of the study region has experienced changes that cannot be neglected. Land use can have a significant impact on regional and local climate through changes in surface properties and conditions. There are many surface properties that can be affected by land use, such as surface albedo, surface roughness (surface

texture), and the amount of vegetation cover. These attributes, when influenced by land use change, in turn will affect the exchange of energy, water and momentum between the surface and the atmosphere, which further affects regional climate (Hong et al., 2022). For example, deforestation (the conversion of forested areas to agricultural land) can increase the albedo of the land surface, which results in more sunlight being reflected back into the atmosphere. Therefore there is not enough energy to heat up the land surface, and in consequence, lowers the surface temperature and further affects the patterns of atmospheric circulation. Similarly, removal of vegetation will correspondingly reduce evapotranspiration (the combined process of evaporation and transpiration) from the surface, leading to a decrease in humidity and rainfall in the area (Sieber et al., 2022). Land use changes can also have indirect effects on regional climate by altering the emissions of greenhouse gases and aerosols from the land surface. For example, deforestation can increase the amount of carbon dioxide in the atmosphere, which can contribute to global warming and climate change (Jones et al., 2013). It is important to understand the impact of land use on regional climate because it can have significant implications for human societies and ecosystems. Changes in regional climate can affect agriculture, water resources, and human health, and can also lead to changes in biodiversity and ecosystem services. Therefore, it is essential to account for land use in regional climate models in order to make accurate predictions of future climate change and to inform land use policy decisions that aim to mitigate its impact.

Other than this, volcanic eruptions have a short-term but strong impact on climate, especially the volcanic eruptions near the equator. Explosive volcanic eruptions exert the strongest short-term influence on the climate. Strong tropical eruptions release large amounts of sulfate aerosols into the stratosphere causing lower tropospheric temperatures on a global scale (Robock, 2000). Over the past 2000 years, volcanic eruptions have played a role in shaping the global climate, especially in affecting the predominantly agricultural societies. Large tropical volcanic eruptions have the capacity to influence the global climate over the subsequent 3-5 years, indicating significant spatial variability. An illustrative instance is the occurrence of the cold spell during the newly identified Late Antique Little Ice Age (LALIA), which has been observed across extensive regions in Eurasia (Luterbacher et al., 2016). This cooling period in the LALIA era is believed to have been triggered by a series of potent tropical volcanic eruptions towards the late 530s and early 540s (Toohey and Sigl, 2017).

In addition to volcanic eruptions, solar radiation is as well a critical factor in shaping Earth's climate (Lean and Rind, 1998). Solar radiation is the major source of Earth energy, its variations in solar activity are induced by dynamic processes within the Sun (Cubasch et al., 2006). This solar radiation drives various processes that influence the Earth's temperature, weather patterns, and overall climate (Budyko, 1969; Cubasch et al., 2006). Solar radiation is a fundamental driver of Earth's climate. Its variations and interactions with the atmosphere, oceans, and land play a vital role in shaping weather patterns, temperature distribution, and long-term climate trends.

Furthermore, the changes in the orbital parameters of the Earth related to its eccentricity, obliquity and precession play a significant role in influencing the latitudinal and seasonal distribution of the solar forcing on different timescales (Cubasch et al., 2006). Likewise, land use and land cover change can also affect climate by directly altering the surface solar and longwave radiation and indirectly changing atmospheric turbulence (Pielke Sr et al., 2011). Hence, the respective changes in external forcings such as solar, orbital, volcanic, GHG and land use change must be implemented in COSMO-CLM to make the RCM more realistic and consistent with its driving GCM.

Because of the significant interest of the climate impacts on historical civilizations and the limitations of using proxy records, we strengthen the need for regional climate models (RCMs) with external forcings such as land use, volcanic eruptions, and solar radiation. The aim of this study is to enhance our understanding of the influence of land use on regional climate. Additionally, the study aims at developing a transient paleoclimate simulation covering the past 2000 years. Especially, to prepare the regional climate model COSMO-CLM in the paleo application with fully forced external forcings, such as solar, orbital, volcanic, greenhouse gas and land use changes. Furthermore, to gain insights into historical climatic conditions within the Eastern Mediterranean (EM) and Nile River (NR) basin at a regional level.

Within the scope of the study, also as the first part of the whole research, a sensitivity study of COSMO-CLM to different land cover schemes in convective permitting simulations over a large part of Europe will be conducted. Continually, by developing the fully forced paleo climate simulation with COSMO-CLM over 500 BCE to 1850 CE, we aspire to investigate in detail the changes in mean climate of 2500 years ago compared to the Pre-Industrial time, together with a

comprehensive analysis of the large-scale circulation processes and their impact on the regional climate in EM and the Nile basin.

In the sensitivity study of investigating the impact of various land cover (LC) maps and fractions on climate using the COSMO-CLM model, simulations are performed over a large part of Europe at a 3 km horizontal resolution with three different LC maps (GlobCover 2009, GLC2000, and ESACCI-LC) as lower boundary input data. With the analysis focused on air temperature, leaf area index (LAI), and plant coverage. The results highlighted the sensitivity of COSMO-CLM to different LC maps and fractions. The simulated air temperature closely matched observational data for all three LC maps over most of the research area, but discrepancies were observed in the Alpine region. The study demonstrated that temperature sensitivity to LC fractions was higher in summer than in winter. Different LC maps also affected LAI and plant coverage, with heterogeneous forested areas showing significant sensitivities to variations in land cover. Moreover, the study pointed out that the COSMO-CLM output did not always mirror differences in LC fractions, indicating the importance of considering both LC fraction and distribution discrepancies.

As the second and third parts of this thesis, a fully forced CCLM (COSMO-CLM) was introduced for paleo region climate simulation application, including the implementation of the external forcings such as volcanic, solar, land-use, greenhouse gas, and orbital. Simulations are performed using this model over a region encompassing the Eastern Mediterranean and the Nile River Basin at a spatial resolution of 0.44 degrees. The model's performance was evaluated for the present time (1980-2018) and compared with observational (GPCC) and reanalysis (ERA-Interim) data. The study demonstrated that the fully forced CCLM can adequately represent the climate across the selected domain. The model showed better accuracy in simulating seasonal air temperatures compared to seasonal precipitation. However, limitations were observed, such as the erroneous representation of precipitation over the Nile River domain due to challenges in capturing convective processes linked to the ITCZ. Notably, temperature patterns exhibited both underestimations and overestimations across different latitudinal bands.

Further, in this study, the simulated climates for the Early Roman Period (ERP, 400-362 BCE) and the Pre-Industrial period (PI, 1800-1850 CE) over the study region are compared. Despite similar mean climate conditions between the ERP and PI periods, different variations were noted across

the study area. The ERP appeared to be generally wetter than the PI in both summers and winters in the EM region, with increased variability in summers. ERP summers were discovered to be wetter and more variable than the compared PI era, but ERP winters over the Nile River (NR) area did not show any noticeable wetter or drier conditions compared to PI winters. There were not many statistically significant different variations in summer and winter precipitation between PI and ERP. Temperature-wise, the ERP exhibited a colder winter by around 0.5 °C compared to the PI period within the EMNR (Eastern Mediterranean and Nile River) region from 10 to 25 degrees north, while differences of summer temperature between the two periods were relatively minor. Variability in ERP temperature was found to be lower in winter but higher in summer compared to PI. The study employed regression analysis of sea level pressure to principal components to attribute large-scale features to regional patterns, revealing stable large-scale circulation influence during both ERP and PI periods.

Finally, this research aims to provide valuable insights for future investigations into climate change and foster interdisciplinary explorations of the intricate relationship between climate and society. Another advantage of studying this region in the past two millennia on a regional scale is that we can link the already existing proxy data with our simulation results.

1.2 Climate over EM/NR

Various patterns of atmospheric circulation impact the Eastern Mediterranean and the Nile River Basin (Zittis et al., 2022). Mid-latitude, subtropical, and tropical weather systems have an impact on EM (Alpert et al., 2005). These weather systems can cause a variety of extremes, such as windstorms, hydrological extremes, and temperature extremes (Hochman et al., 2022). Located at an atmospheric crossroad and in a transitional zone between subtropical and mid-latitude climates, the region is directly impacted by a range of atmospheric circulation patterns and meteorological processes on several continents (Hochman et al., 2022). For instance, the Eastern Mediterranean is greatly influenced by the South Asian Monsoon in the summer, but the region may also be impacted by the variability of continental circulation anomalies associated with the Siberian High-Pressure System in the winter (Cramer et al., 2018; Paz et al., 2003). Large-scale atmospheric circulation and its interactions with regional synoptic systems—such as Cyprus Lows, Red Sea Troughs, Persian Troughs, and "Sharav" Lows—as well as high-pressure systems mostly control the extreme

weather across EM. Extreme weather is also largely influenced by complex orographic features (Hochman et al., 2022).

Multiple atmospheric circulation patterns affect the NR region and the water availability of the huge drainage basin that crosses different hydroclimatic zones. The West African monsoon, which is influenced by the dynamics of the Indian monsoon, is the primary cause of the precipitation regime along the Nile basin (Ménot et al., 2020). 70% of the yearly precipitation in the Blue Nile's source region, the central Ethiopian Highlands, occurs during the summer months of June through September, when the region is impacted by tropical convection clusters over continental areas and the Intertropical Convergence Zone's (ITCZ) rain belt (Conway, 2000). Monsoonal systems that prevail near Lake Victoria and in parts of the Ethiopian highlands also have an impact on the region's climate (Camberlin, 2009). The moisture sources that actually affect the NR Basin originate from the Gulf of Guinea, the Indian Ocean and the flow from the north through the Mediterranean Sea and the Red Sea (Viste and Sorteberg, 2013). According to Veste and Sorteberg (2013), the majority of Ethiopia's rainy seasons coincide with increased moisture inflow from the northern branches. The variability of rainfall in Eastern Africa including the source region of the Nile River basin: Lake Victoria, is also shaped by a range of climatic phenomena, which encompass the Indian Ocean Dipole (IOD), El Niño–Southern Oscillation (ENSO), the Madden–Julian Oscillation (MJO), and the Quasi-Biennial Oscillation (QBO). Although those climatic phenomena are not discussed in this research, it is necessary to be aware the complexity of the climate over the NR region. The IOD, characterized by disparities in sea surface temperatures between the western and eastern Indian Ocean, has a direct impact on the short rains in Eastern Africa. A positive IOD phase brings with it heavier precipitation, while a negative phase brings with it less short rains. Furthermore, ENSO conditions are crucial in determining the short rains; El Niño is generally linked to higher short rain amounts, while La Niña is typically associated with drier conditions.

Just as it has in the past, the Nile River continues to serve as the primary source of agricultural and economic sustenance for multiple African nations today. Among these nations, Egypt has historically been profoundly reliant on the flow of the Nile River, as it represents one of the ancient world's "hydraulic civilizations" (Singh et al., 2023). Egypt offers a unique case study for examining how societies respond to climatic fluctuations and their vulnerabilities (Manning et al.,

2017). To illustrate, the Nile floods have exerted significant impacts on the Egyptian population, prompting the development of various strategies to mitigate the consequences of flooding. These strategies encompass advancements in water-lifting technology and innovations in agricultural practices, underscoring the critical importance of effectively managing the variability of the Nile's flow (Manning et al., 2017).

1.3 Atmospheric regional climate model COSMO-CLM (CCLM)

The COSMO-CLM (COnsortium for Small-scale MOdelling in CLimate Mode - CCLM), as introduced by Rockel et al., (2008), stands as a widely recognized Regional Climate Model (RCM) extensively employed for examining climate change under various influences. Specifically, the atmospheric model CCLM operates as a non-hydrostatic RCM.

Its original design enables simulations starting from the year 1850 CE onwards (from the model source code, but modifications have been made in this study to perform simulations over the past 2000 years). And the performance of the CCLM is notably influenced by the driving Global Climate Model (GCM), which typically exhibits a coarser spatial resolution, as indicated by Armstrong et al., (2019). Notably, recent studies within the framework of the CORDEX (Coordinated Regional Climate Downscaling EXperiment) initiative have performed multiple CCLM simulations at diverse resolutions, from 50 km up to very high convection-permitting resolutions, reaching approximately 2.2 kilometers (Raffa et al., 2023).

1.4 External forcings in COSMO-CLM

External forcing refers to the factors that can influence the Earth's climate from outside of the Earth system itself. These factors include orbital variations, solar radiation, volcanic activity, greenhouse gases and land use changes. Earth system models (ESMs) use these external forcing factors to simulate and predict the Earth's climate under different scenarios (Jungclaus et al., 2017). Mathematical equations are used in ESM to link the interactions between these external forcing factors and the Earth's climate system itself. By changing the values of these external forcing parameters in the models, one can simulate different scenarios (for example, different CO2

concentrations, different periods of the past or in the future)and further learn from the paleoclimate and make predictions about the future climate of the Earth (Jungclaus et al., 2017).

1.4.1 Solar

Solar forcing in COSMO-CLM, is to change the solar radiation according to the sun's activity in order to have a more realistic set-up for the climate model. The solar forcing in this study is implemented as the total solar irradiance according to the MPI-ESM-P "Mythos" simulation (Jungclaus et al., 2017). Total solar irradiance is read in by COSMO-CLM in the source code on a monthly basis.

Solar radiation, which comes from the Sun, is the primary source of energy that drives the Earth's climate and is also a critical factor in shaping Earth's climate (Petersen et al., 2010b). Changes in solar radiation, such as variations in the Sun's brightness or in the amount of income radiation that reaches the Earth's surface, can affect the Earth's climate (Petersen et al., 2010d). These variations can occur over short time periods, such as solar flares or sunspot cycles (11-year solar cycle), or over longer time periods, such as changes in the Sun's output over millions of years (Gray et al., 2010).

The very basic principle followed by some climate models (Energy Balance Model) is to balance the incoming solar radiation and outgoing infrared radiation from Earth. Many factors affect the amount of solar radiation, which is received by the earth's surface (Lean and Rind, 1998). For example, the tilt of the Earth's axis causes the amount of solar radiation received at different latitudes to vary throughout the year and this is responsible for the changing of seasons. Solar radiation differentially heats Earth's surface, creating temperature gradients. These temperature differences drive atmospheric circulation patterns, such as the formation of high and low-pressure systems and the development of trade winds and jet streams (Gray et al., 2010). In summary, solar radiation is a fundamental driver of Earth's climate. Its variations and interactions with the atmosphere, oceans, and land play a vital role in shaping weather patterns, temperature distribution, and long-term climate trends (Budyko, 1969; Gray et al., 2010; Lean and Rind, 1998).

1.4.2 Orbital

Orbital forcing refers to the variations in Earth's orbit around the Sun that can influence climate over long timescales. These orbital changes are collectively known as Milankovitch cycles (Spiegel et al., 2010), named after the Serbian scientist Milutin Milankovitch who extensively studied them. The three main components of orbital forcing are eccentricity, axial tilt (obliquity), and axial precession (Jungclaus et al., 2017; Petersen et al., 2010c). The orbital forcing in this study is represented by the eccentricity, the obliquity and the longitude of perihelion (Berger, 1978; Schmidt et al., 2014). Those parameters related to the orbital changes in the earth's system is implemented into the COSMO-CLM in the source code on a yearly basis, with reference to the previous work from Ludwig et al., (2016, 2017) for the LGM (Last glacial maximum) simulation.

Earth's orbit refers to the not perfect circle but slightly elliptical in which the Earth is moving around the Sun. Eccentricity refers to the changing shape of this elliptical orbit over thousands of years. The elliptical level of this orbit can influence the amount of solar radiation received and contribute to climate change. Earth's axis is tilted relative to its orbital plane, causing the change in seasons. Obliquity refers to the angle of this tilt, which varies between about 22.1 and 24.5 degrees over a cycle of around 41,000 years An increased axial tilt can result in more pronounced seasonal fluctuations, impacting temperature variations and the extent of snow and ice coverage. The precession, which refers to Earth's rotational axis experiences a wobbling motion similar to that of a spinning top, primarily due to gravitational interactions with the Moon and the Sun, following a cycle lasting approximately 26,000 years. Precession has the ability to influence the timing of seasons and alter the orientation of Earth's axial tilt (Milankovitch (Orbital) Cycles and Their Role in Earth's Climate, 2023).

The effects of these orbital variations on climate are complex and can manifest in various ways. Changes in eccentricity, obliquity, and precession influence the distribution and amount of solar radiation Earth receives. It's important to note that while orbital forcing sets the stage for long-term climate changes (Cubasch et al., 2006).

1.4.3 Volcanic

Volcanic forcing plays a significant role in shaping Earth's climate by temporarily cooling the planet due to the release of aerosols and gases during eruptions (Robock, 2000). Understanding the interactions between volcanic activity and climate helps scientists better model and predict the behaviors of the Earth's climate system (Petersen et al., 2010e). The volcanic forcing in this simulation is based on the stratospheric aerosol optical depth (AOD) at 550 nm wavelength by Toohey and Sigl, (2017). It is read in by the source code of COSMO-CLM on a monthly basis as well.

Volcanic forcing in the climate modelling world often refers to the impact of volcanic eruptions on the Earth's climate. After major volcanic eruptions, large amounts of sulfur dioxide and other particles can be injected into the atmosphere, which can reflect and absorb incoming solar radiation (Robock, 2000). This can lead to short-term cooling of the Earth's climate. Some of the most well-known examples of volcanic forcing include the eruption of Mount Pinatubo in 1991, which caused a temporary cooling of global temperatures (Volcano Watch — The Pinatubo Effect: Can geoengineering mimic volcanic processes? | U.S. Geological Survey, 2023).

Volcanic eruptions emit large amounts of sulfur dioxide (SO2) and other gases into the atmosphere. In the stratosphere, sulfur dioxide can react with water vapor to form sulfate aerosols (Robock, 2000). These aerosols are tiny particles that reflect sunlight back into space, leading to a temporary cooling effect on the planet's surface. The sulfate aerosols produced by volcanic eruptions can remain in the stratosphere for months to years, depending on the size of the eruption. Especially, the eruptions occurring in the tropics can have a more pronounced global impact as the aerosols can be dispersed by the Brewer-Dobson circulation to high latitudes in both hemispheres (Pauling et al., 2023). Thus, volcanic eruptions contribute to short-term climate variability, affecting weather patterns, precipitation, and temperature.

1.4.4 Greenhouse gases

According to Ramanathan and Feng (2009), greenhouse gases, such as carbon dioxide and methane, prevent the long wave radiation from going out from the Earth's atmosphere and, in consequence, lead to the warming of the Earth's climate (Ramanathan and Feng, 2009). Numerous

studies have demonstrated that since the Industrial Revolution, human activities like the burning of fossil fuels and deforestation have significantly increased the concentrations of greenhouse gases in the atmosphere (Meinshausen et al., 2017). This increase in greenhouse gas concentrations is one of the primary drivers of current climate change (Causes of climate change, 2023). Greenhouse gas is the major driver of climate change, which in turn leads to global warming, shifts in weather patterns, sea level rise, and numerous ecological and societal impacts (Hennessy et al., 2022). The changes in GHG concentrations in this study consist of CO2, CH4 and N2O (Meinshausen et al., 2017) and it is implemented as CO2 ebullient in the COSMO-CLM on a monthly basis, see Eq. (1):

$$CO_2 + 25 * CH_4 + 298 * N_2O \quad (1)$$

As the global warming happens, it will trigger various feedback mechanisms that will further affect the climate of the Earth. For example, warming can lead to ice and snow melting, and consequently, reducing the Earth's albedo, which might cause further warming. Increased temperatures can disrupt traditional weather patterns, leading to changes in precipitation, droughts, heatwaves, and more intense and frequent extreme weather events (Hennessy et al., 2022; Chapter 11: Weather and Climate Extreme Events in a Changing Climate, 2023, p.11).

1.4.5 Land use changes and land use

Land use information is an important input parameter in regional climate models COSMO-CLM, as it can significantly influence surface energy and water balance, and hence the regional climate (Zhang et al., 2021; Wouters et al., 2017). COSMO-CLM incorporates land use information through the use of land surface parameters, such as albedo, roughness, soil properties, and vegetation cover, which are derived from land use datasets (Schättler and Blahak, 2017). In this study, we derived the necessary parameters (maximum and minimum Leaf Area Index: LAI; plant coverage: PLANT; fraction of deciduous forest: FOR_D; fraction of everlasting forest: FOR_E) which can indicate the land use change from the MPI-ESM-P “Mythos” simulation output (LAI and PLCOV) and implemented into COSMO-CLM for the transient simulation from 500 BCE to 1850 CE. COSMO-CLM read in the land use change information from an external file in the interpolation step with INT2LM.

In more recent years, much effort has been made to incorporate dynamic land use change into COSMO-CLM. This has involved the integration of the use of high-resolution land cover datasets that allow for a more detailed representation of land surface properties, such as vegetation cover, albedo, and roughness, which can significantly affect the surface energy balance and regional climate, furthermore, helps the model better capture the spatial heterogeneity of land surface properties (Zhang et al., 2021).

1.5 Simulations

The COSMO model version 5.0 with CLM version 15 (COSMO-CLM v5.0-clm15) was used for the following simulations (see, Table 1). The interpolation was carried out with INT2LM in version 2.05 with CLM version 1 (INT2LM-v2.05 clm1). The time integration is the two time-level Runge–Kutta scheme, the difference in the model time step is shown in Table 1.

Table 1.1. List of simulations performed with COSMO-CLM in this study.

Study	Simulation Name	Resolution	Domain	Time step
Sensitivity Simulation with Different Land Use Input	Land Use Sensitivity – GlobCover2009	0.0275	EURO-CORDEX (see Figure 1a)	25s
	Land Use Sensitivity – GLC2000	0.0275	EURO-CORDEX (see Figure 1a)	25s
	Land Use Sensitivity – ESACCI-LC	0.0275	EURO-CORDEX (see Figure 1a)	25s
Paleo Transient Simulation	Transient 500 BCE – 1850 CE	0.44	MENA (see Figure 1b)	300s

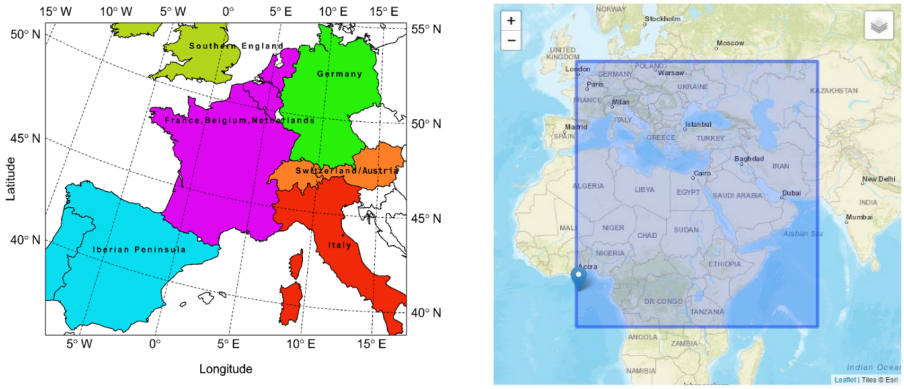

Figure 1.1. The simulation domains, a: sensitivity Simulation with Different Land Use Input, b: Paleo Transient Simulation.

1.6 Large-scale circulation

Large-scale circulation, often referred to as atmospheric or oceanic circulation, is a fundamental and major system governing the motion of air and water on a global scale. This motion plays an important role in shaping the Earth's climate, influencing weather patterns, and the distribution of heat and energy across our Earth's surface, as well as our study region EM and NR. Here we will introduce the major circulations that are affecting our study area, such as the North Atlantic Oscillation (NAO), the South Asia Monsoon affecting the EM and the West Africa Monsoon (WAM), the Sahara Heat Low (SHL), the India Monsoon, the ITCZ affecting the NR region. For better organizing this part, the NAO will be discussed in section “1.6.1” and all these different monsoon systems including the SHL will be discussed under subsection “1.6.2”, and in the end the ITCZ in section “1.6.3”.

1.6.1 North Atlantic Oscillation

According to Quante et al. (2016) and Hurrell (2003) in “An Overview of the North Atlantic Oscillation - Geophysical Monograph Series - Wiley Online Library, 2023”, the NAO is the dominant pattern of near-surface pressure fluctuations over the North Atlantic Ocean and Europe. It influences a large part of the Northern Hemisphere.

During the positive phase of NAO, a stronger than usual westerly airflow results from the enhancement of the pressure difference between the two main centers—the Subtropical High and the Subpolar Low— is enhanced compared to the average condition (Hurrell, 1995). Consequently, the storm track extends northeastward, resulting in an increased frequency of storms over the North Sea and northern Europe. As a result, these regions receive more and milder precipitation than normal, especially in the winter. On the other hand, during this phase, the Mediterranean region typically experiences colder and drier weather.

On the other hand, the pressure differential between the Subtropical High and Subpolar Low reduces during the NAO's negative phase. This alteration causes the storm track to adopt a more east-west orientation, shifting southward and extending into the western Mediterranean. Consequently, the resultant airflow is weaker than usual, as observed in studies by Xoplaki et al.,

(2004). In the case of significantly negative NAO indices, there is a potential for the atmospheric flow to reverse, characterized by higher pressure prevailing over Iceland compared to the Azores. This atmospheric pattern can lead to severe winters affecting extensive regions of Europe including the EM, as was the case in the record-breaking cold winter of 2009/2010 (Wang et al., 2010).

1.6.2 Monsoon system

The global wind system reflects latitudinal imbalances in temperature. On a regional and local scale, wind develops in response to different temperature conditions. Winds are an example that develops in response to variations in temperature and pressure. Many regions experience differences in wind directions and conditions over the seasons, this is often called Monsoon. (Petersen et al., 2010c). The term monsoon originates from the Arabic word “mausim”, meaning season. The Arabic sailors have used this word to describe seasonal changes in wind direction across the Arabian Sea between Arabia and India for many centuries. In meteorological terminology, a monsoon denotes the shift of wind direction between seasons. Typically, a monsoon manifests when moist winds from the ocean blow towards the land during the summer but then transition to dry, cooler winds blowing seaward off the land during the winter. A characteristic of a monsoon is the complete 180° reversal in wind direction between seasons (Petersen et al., 2010c).

The most well-known monsoon system is of southern Asia, which is normally referred to as South Asia Monsoon (SAM). In the winter, Asia's enormous landmass creates a large high-pressure cell from which there is a substantial air outflow because it gets considerably colder than the nearby waters. From the Asia continent, these chilly, dry winds travel southward toward the tropical low that is positioned over the warmer waters. Due to the air's origin in a dry continental region, the winter monsoon is a dry season. The Asian continent is quite warm in the summer and forms a sizable low-pressure system, which attracts warm, humid air from the oceans. This hot, humid air rises and cools due to convective uplift or landform barriers, bringing heavy precipitation. The summer monsoon may bring with it extremely severe rains and flooding in the foothills of the Himalayas, in other regions of India, and in portions of Southeast Asia. The Mediterranean climate is exposed to and affected by South Asian Monsoon (SAM) and the SAM is largely responsible for the summertime descent and dryness over the Mediterranean (Cherchi et al., 2014). The precipitation over the Mediterranean is a result of the interaction between westward propagating

Rossby waves, which are generated by the diabatic heating associated with the summer monsoon rainfall in South Asia, and the mean westerly flow north of the region (Rodwell and Hoskins, 2001).

The West African Monsoon (WAM), another monsoon system that is connected to our research region, is a significant wind system that mostly affects West African countries but also has an influence on the EM and NR regions (Gaetani et al., 2011). WAM is a pronounced seasonal wind shift that is produced by thermodynamic contrasts between the land Sahara and the equatorial Atlantic Ocean (Nicholson, 2018). It is characterized by winds that blow southwesterly in the warmer months and northeasterly in the winter. The shallow, humid layer of surface air that makes up the southwest winter monsoon replaces the major northeast trade wind, which originates from the Sahara (Sahara Heat Low - SHL) as a deep stream of dry, dusty air. The rainfall over the NR region is largely affected by WAM in combination with SAM.

1.6.3 Intertropical Convergence Zone (ITCZ)

The Intertropical Convergence Zone (ITCZ) is a fixed low-pressure area which located along the equatorial trough, where surface trade winds carrying heat and moisture converge, leading to enhanced convection, cloud formation, and increased precipitation (Adam et al., 2016). The study area NR is located on the ITCZ and its climate is also influenced by the ITCZ. It also shows that in our study, the precipitation of NR is moving northward together with ITCZ north–south displacement "follows" the sun from winter to summer. Nevertheless, there has been many discussions regarding the conception of ITCZ, especially regarding the equatorial Africa area, where there are two rainy seasons (during the boreal spring and summer) (Nicholson, 2018). The ITCZ, which accounts for 32 per cent of global precipitation, influences the climate and society in the tropics. Climate change will have an impact on the ITCZ and the tropical regions affected by the ITCZ. Further, due to its impact on the global radiation budget, the ITCZ is likely to influence global temperature and precipitation and their response to climate change (Byrne et al., 2018).

In this study, when comparing the mean climate of the 2000 years apart, we found that the not only the precipitation but also the temperature variability over the NR region is closely related to the ITCZ. Nevertheless, currently, many studies focus on the rainfall over the equatorial region, and very limited research addresses the characteristics of temperature and its association with ITCZ.

Since this, we have tried to use a regression study between the large-scale circulation presented by Sea Level Pressure (SLP) and temperature principal component to give insight into the temperature behavior over the studied region.

1.7 Reference

Adam, O., Schneider, T., Brient, F., and Bischoff, T.: Relation of the double-ITCZ bias to the atmospheric energy budget in climate models, Geophysical Research Letters, 43, 7670–7677, https://doi.org/10.1002/2016GL069465, 2016.

Alpert, P., Price, C., Krichak, S. O., Ziv, B., Saaroni, H., Osetinsky, I., Barkan, J., and Kishcha, P.: Tropical tele-connections to the Mediterranean climate and weather, Advances in Geosciences, 2, 157–160, https://doi.org/10.5194/adgeo-2-157-2005, 2005.

A Central European precipitation climatology – Part I: Gene...: Ingenta Connect: https://www.ingentaconnect.com/content/schweiz/mz/2013/00000022/00000003/art00001, last access: 25 May 2020.

An Overview of the North Atlantic Oscillation - Hurrell - 2003 - Geophysical Monograph Series - Wiley Online Library: https://agupubs.onlinelibrary.wiley.com/doi/10.1029/134GM01, last access: 20 September 2023.

Causes of climate change: https://climate.ec.europa.eu/climate-change/causes-climate-change_en, last access: 20 September 2023.

Chapter 11: Weather and Climate Extreme Events in a Changing Climate: https://www.ipcc.ch/report/ar6/wg1/chapter/chapter-11/, last access: 20 September 2023.

The ERA-Interim reanalysis: configuration and performance of the data assimilation system - Dee - 2011 - Quarterly Journal of the Royal Meteorological Society - Wiley Online Library: https://rmets.onlinelibrary.wiley.com/doi/full/10.1002/qj.828, last access: 25 May 2020.

Volcano Watch — The Pinatubo Effect: Can geoengineering mimic volcanic processes? | U.S. Geological Survey: https://www.usgs.gov/observatories/hvo/news/volcano-watch-pinatubo-effect-can-geoengineering-mimic-volcanic-processes, last access: 20 September 2023.

Armstrong, E., Hopcroft, P. O., and Valdes, P. J.: Reassessing the Value of Regional Climate Modeling Using Paleoclimate Simulations, Geophysical Research Letters, 46, 12464–12475, https://doi.org/10.1029/2019GL085127, 2019.

Asensio, H. and Messmer, M.: External Parameters for Numerical Weather Prediction and Climate Application EXTPAR v5 0 User and Implementation Guide, 45, n.d.

Berger, A.: Long-Term Variations of Daily Insolation and Quaternary Climatic Changes, American Meteorological Society, 1978.

Bernabé, S. and Plaza, A.: A new system to perform unsupervised and supervised classification of satellite images from Google Maps, in: Satellite Data Compression, Communications, and Processing VI, Satellite Data Compression, Communications, and Processing VI, 261–270, https://doi.org/10.1117/12.863243, 2010.

Bounoua, L., DeFries, R., Collatz, G. J., Sellers, P., and Khan, H.: Effects of land cover conversion on surface climate, Climatic Change, 52, 29–64, 2002.

Budyko, M. I.: The effect of solar radiation variations on the climate of the Earth, Tellus, 21, 611–619, https://doi.org/10.3402/tellusa.v21i5.10109, 1969.

Byrne, M. P., Pendergrass, A. G., Rapp, A. D., and Wodzicki, K. R.: Response of the Intertropical Convergence Zone to Climate Change: Location, Width, and Strength, Curr Clim Change Rep, 4, 355–370, https://doi.org/10.1007/s40641-018-0110-5, 2018.

Camberlin, P.: Nile basin climates, in: The Nile, Springer, 307–333, 2009.

Cherchi, A., Annamalai, H., Masina, S., and Navarra, A.: South Asian Summer Monsoon and the Eastern Mediterranean Climate: The Monsoon–Desert Mechanism in CMIP5 Simulations, Journal of Climate, 27, 6877–6903, https://doi.org/10.1175/JCLI-D-13-00530.1, 2014.

Conway, D.: The climate and hydrology of the Upper Blue Nile River, Geographical Journal, 166, 49–62, 2000.

Cramer, W., Guiot, J., Fader, M., Garrabou, J., Gattuso, J.-P., Iglesias, A., Lange, M. A., Lionello, P., Llasat, M. C., Paz, S., Peñuelas, J., Snoussi, M., Toreti, A., Tsimplis, M. N., and Xoplaki, E.: Climate change and interconnected risks to sustainable development in the Mediterranean, Nature Clim Change, 8, 972–980, https://doi.org/10.1038/s41558-018-0299-2, 2018.

Crowley, T., GA, Z., Vinther, B., Udisti, R., Kreutzs, K., Cole-Dai, J., and Castellano, E.: Volcanism and the Little Ice Age, PAGES Newslett., 16, 22–23, https://doi.org/10.1029/2002GL0166335, 2008.

Cubasch, U., Zorita, E., Kaspar, F., Gonzalez-Rouco, J. F., Storch, H. von, and Prömmel, K.: Simulation of the role of solar and orbital forcing on climate, Advances in Space Research, 37, 1629–1634, https://doi.org/10.1016/j.asr.2005.04.076, 2006.

Davin, E. L., Stöckli, R., Jaeger, E. B., Levis, S., and Seneviratne, S. I.: COSMO-CLM2: a new version of the COSMO-CLM model coupled to the Community Land Model, Clim Dyn, 37, 1889–1907, https://doi.org/10.1007/s00382-011-1019-z, 2011.

Gaetani, M., Pohl, B., Douville, H., and Fontaine, B.: West African Monsoon influence on the summer Euro-Atlantic circulation, Geophysical Research Letters, 38, https://doi.org/10.1029/2011GL047150, 2011.

García-Herrera, R., Luterbacher, J., Lionello, P., González-Rouco, F., Ribera, P., Rodó, X., Kull, C., and Zerefos, C.: Reconstruction of past Mediterranean climate, Eos, Transactions American Geophysical Union, 88, 111–111, https://doi.org/10.1029/2007EO090010, 2007.

Giorgi, F. and Lionello, P.: Climate change projections for the Mediterranean region, Global and Planetary Change, 63, 90–104, https://doi.org/10.1016/j.gloplacha.2007.09.005, 2008.

Gómez-Navarro, J. J. and Zorita, E.: Atmospheric annular modes in simulations over the past millennium: No long-term response to external forcing, Geophysical Research Letters, 40, 3232–3236, https://doi.org/10.1002/grl.50628, 2013.

Gomez-Navarro, J. J., Wagner, S., Zorita, E., and Montavez, J. P.: Changes in distribution of daily temperature and precipitation between the Late Maunder Minimum and the 2nd half of the 20th century: A regional model study, 2012, PP21B-1990, 2012.

Gray, L. J., Beer, J., Geller, M., Haigh, J. D., Lockwood, M., Matthes, K., Cubasch, U., Fleitmann, D., Harrison, G., Hood, L., Luterbacher, J., Meehl, G. A., Shindell, D., van Geel, B., and White, W.: Solar Influences on Climate, Reviews of Geophysics, 48, https://doi.org/10.1029/2009RG000282, 2010.

Hennessy, K., Lawrence, J., and Mackey, B.: IPCC Sixth Assessment Report (AR6): Climate Change 2022 - Impacts, Adaptation and Vulnerability: Regional Factsheet Australasia, 2022.

Hochman, A., Marra, F., Messori, G., Pinto, J. G., Raveh-Rubin, S., Yosef, Y., and Zittis, G.: Extreme weather and societal impacts in the eastern Mediterranean, Earth System Dynamics, 13, 749–777, https://doi.org/10.5194/esd-13-749-2022, 2022.

Hong, T., Wu, J., Kang, X., Yuan, M., and Duan, L.: Impacts of Different Land Use Scenarios on Future Global and Regional Climate Extremes, Atmosphere, 13, 995, https://doi.org/10.3390/atmos13060995, 2022.

Hurrell, J. W.: Decadal Trends in the North Atlantic Oscillation, Science (New York, N.Y.), 269, 676–9, https://doi.org/10.1126/science.269.5224.676, 1995.

Jog, S. and Dixit, M.: Supervised classification of satellite images, in: 2016 Conference on Advances in Signal Processing (CASP), 2016 Conference on Advances in Signal Processing (CASP), 93–98, https://doi.org/10.1109/CASP.2016.7746144, 2016.

Jones, A. D., Collins, W. D., Edmonds, J., Torn, M. S., Janetos, A., Calvin, K. V., Thomson, A., Chini, L. P., Mao, J., Shi, X., Thornton, P., Hurtt, G. C., and Wise, M.: Greenhouse Gas Policy Influences Climate via Direct Effects of Land-Use Change, Journal of Climate, 26, 3657–3670, https://doi.org/10.1175/JCLI-D-12-00377.1, 2013.

Jungclaus, J. H., Bard, E., Baroni, M., Braconnot, P., Cao, J., Chini, L. P., Egorova, T., Evans, M., González-Rouco, J. F., Goosse, H., Hurtt, G. C., Joos, F., Kaplan, J. O., Khodri, M., Klein

Goldewijk, K., Krivova, N., LeGrande, A. N., Lorenz, S. J., Luterbacher, J., Man, W., Maycock, A. C., Meinshausen, M., Moberg, A., Muscheler, R., Nehrbass-Ahles, C., Otto-Bliesner, B. I., Phipps, S. J., Pongratz, J., Rozanov, E., Schmidt, G. A., Schmidt, H., Schmutz, W., Schurer, A., Shapiro, A. I., Sigl, M., Smerdon, J. E., Solanki, S. K., Timmreck, C., Toohey, M., Usoskin, I. G., Wagner, S., Wu, C.-J., Yeo, K. L., Zanchettin, D., Zhang, Q., and Zorita, E.: The PMIP4 contribution to CMIP6 – Part 3: The last millennium, scientific objective, and experimental design for the PMIP4 *past1000* simulations, Geoscientific Model Development, 10, 4005–4033, https://doi.org/10.5194/gmd-10-4005-2017, 2017.

Kelley, C. P., Mohtadi, S., Cane, M. A., Seager, R., and Kushnir, Y.: Climate change in the Fertile Crescent and implications of the recent Syrian drought, Proceedings of the National Academy of Sciences, 112, 3241–3246, https://doi.org/10.1073/pnas.1421533112, 2015.

Milankovitch (Orbital) Cycles and Their Role in Earth's Climate: https://climate.nasa.gov/news/2948/milankovitch-orbital-cycles-and-their-role-in-earths-climate, last access: 20 September 2023.

Lamarche, C., Santoro, M., Bontemps, S., D'Andrimont, R., Radoux, J., Giustarini, L., Brockmann, C., Wevers, J., Defourny, P., and Arino, O.: Compilation and Validation of SAR and Optical Data Products for a Complete and Global Map of Inland/Ocean Water Tailored to the Climate Modeling Community, Remote Sensing, 9, 36, https://doi.org/10.3390/rs9010036, 2017.

Lean, J. and Rind, D.: Climate Forcing by Changing Solar Radiation, Journal of Climate, 11, 3069–3094, 1998.

Ludwig, P., Schaffernicht, E., Shao, Y., and Pinto, J.: Regional atmospheric circulation over Europe during the Last Glacial Maximum and its links to precipitation, Journal of Geophysical Research Atmospheres, 121, 2130–2145, https://doi.org/10.1002/2015JD024444, 2016.

Ludwig, P., Pinto, J. G., Raible, C. C., and Shao, Y.: Impacts of surface boundary conditions on regional climate model simulations of European climate during the Last Glacial Maximum, Geophysical Research Letters, 44, 5086–5095, https://doi.org/10.1002/2017GL073622, 2017a.

Ludwig, P., Pinto, J., Raible, C., and Shao, Y.: Impacts of Surface Boundary Conditions on Regional Climate Model Simulations of European Climate during the Last Glacial Maximum, Geophysical Research Letters, 44, 5086–5095, https://doi.org/10.1002/2017GL073622, 2017b.

Luterbacher, J., Werner, J. P., Smerdon, J. E., Fernández-Donado, L., González-Rouco, F. J., Barriopedro, D., Ljungqvist, F. C., Büntgen, U., Zorita, E., Wagner, S., Esper, J., McCarroll, D., Toreti, A., Frank, D., Jungclaus, J. H., Barriendos, M., Bertolin, C., Bothe, O., Brázdil, R., Camuffo, D., Dobrovolný, P., Gagen, M., García-Bustamante, E., Ge, Q., Gómez-Navarro, J. J., Guiot, J., Hao, Z., Hegerl, G. C., Holmgren, K., Klimenko, V. V., Martín-Chivelet, J., Pfister, C., Roberts, N., Schindler, A., Schurer, A., Solomina, O., Gunten, L. von, Wahl, E., Wanner, H., Wetter, O., Xoplaki, E., Yuan, N., Zanchettin, D., Zhang, H., and Zerefos, C.: European summer temperatures since Roman times, Environ. Res. Lett., 11, 024001, https://doi.org/10.1088/1748-9326/11/2/024001, 2016.

Manning, J. G., Ludlow, F., Stine, A. R., Boos, W. R., Sigl, M., and Marlon, J. R.: Volcanic suppression of Nile summer flooding triggers revolt and constrains interstate conflict in ancient Egypt, Nat Commun, 8, 900, https://doi.org/10.1038/s41467-017-00957-y, 2017.

Meinshausen, M., Vogel, E., Nauels, A., Lorbacher, K., Meinshausen, N., Etheridge, D. M., Fraser, P. J., Montzka, S. A., Rayner, P. J., Trudinger, C. M., Krummel, P. B., Beyerle, U., Canadell, J. G., Daniel, J. S., Enting, I. G., Law, R. M., Lunder, C. R., O'Doherty, S., Prinn, R. G., Reimann, S., Rubino, M., Velders, G. J. M., Vollmer, M. K., Wang, R. H. J., and Weiss, R.: Historical greenhouse gas concentrations for climate modelling (CMIP6), Geoscientific Model Development, 10, 2057–2116, https://doi.org/10.5194/gmd-10-2057-2017, 2017.

Ménot, G., Pivot, S., Bouloubassi, I., Davtian, N., Hennekam, R., Bosch, D., Ducassou, E., Bard, E., Migeon, S., and Revel, M.: Timing and stepwise transitions of the African Humid Period from geochemical proxies in the Nile deep-sea fan sediments, Quaternary Science Reviews, 228, 106071, https://doi.org/10.1016/j.quascirev.2019.106071, 2020.

Nicholson, S. E.: Climate of the Sahel and West Africa, in: Oxford Research Encyclopedia of Climate Science, https://doi.org/10.1093/acrefore/9780190228620.013.510, 2018.

Pauling, A. G., Bitz, C. M., and Armour, K. C.: The Climate Response to the Mt. Pinatubo Eruption Does Not Constrain Climate Sensitivity, Geophysical Research Letters, 50, e2023GL102946, https://doi.org/10.1029/2023GL102946, 2023.

Paz, S., Tourre, Y. M., and Planton, S.: North Africa-West Asia (NAWA) sea-level pressure patterns and their linkages with the Eastern Mediterranean (EM) climate, Geophysical Research Letters, 30, https://doi.org/10.1029/2003GL017862, 2003.

Petersen, J., Sack, D., and Gabler, R. E.: Atmospheric Pressure, Winds, and Circulation, in: Fundamentals of Physical Geography, Cengage Learning, 2010a.

Petersen, J., Sack, D., and Gabler, R. E.: Fundamentals of Physical Geography, Cengage Learning, 499 pp., 2010b.

Petersen, J., Sack, D., and Gabler, R. E.: Physical Geography: Earth Environments and Systems, in: Fundamentals of Physical Geography, Cengage Learning, 2010c.

Petersen, J., Sack, D., and Gabler, R. E.: Solar Energy and Atmospheric Heating, in: Fundamentals of Physical Geography, Cengage Learning, 2010d.

Petersen, J., Sack, D., and Gabler, R. E.: Volcanic and Tectonic Processes and Landforms, in: Fundamentals of Physical Geography, Cengage Learning, 2010e.

Pielke Sr, R., Pitman, A., Niyogi, D., Mahmood, R., Mcalpine, C., Hossain, F., Klein Goldewijk, K., Nair, U., Betts, R., Fall, S., Reichstein, M., Kabat, P., and de NOBLET, N.: Land Use/Land Cover Changes and Climate: Modeling Analysis and Observational Evidence, Wiley Interdisciplinary Reviews: Climate Change, 2, 828–850, https://doi.org/10.1002/wcc.144, 2011.

Planton, S., Lionello, P., Artale, V., Aznar, R., Carrillo, A., Colin, J., Congedi, L., Dubois, C., Elizalde, A., Gualdi, S., Hertig, E., Jacobeit, J., Jordà, G., Li, L., Mariotti, A., Piani, C., Ruti, P., Sánchez Gómez, E., Sannino, G., and Tsimplis, M.: The Climate of the Mediterranean Region in Future Climate Projections, in: The Climate of the Mediterranean Region, 449–502, https://doi.org/10.1016/B978-0-12-416042-2.00008-2, 2012.

Quante, M., Colijn, F., Bakker, J. P., Härdtle, W., Heinrich, H., Lefebvre, C., Nöhren, I., Olesen, J. E., Pohlmann, T., Sterr, H., Sündermann, J., and Tölle, M. H.: Introduction to the Assessment—Characteristics of the Region, in: North Sea Region Climate Change Assessment, edited by: Quante, M. and Colijn, F., Springer International Publishing, Cham, 1–52, https://doi.org/10.1007/978-3-319-39745-0_1, 2016.

Raffa, M., Adinolfi, M., Reder, A., Marras, G. F., Mancini, M., Scipione, G., Santini, M., and Mercogliano, P.: Very High Resolution Projections over Italy under different CMIP5 IPCC scenarios, Sci Data, 10, 238, https://doi.org/10.1038/s41597-023-02144-9, 2023.

Ramanathan, V. and Feng, Y.: Air pollution, greenhouse gases and climate change: Global and regional perspectives, Atmospheric Environment, 43, 37–50, https://doi.org/10.1016/j.atmosenv.2008.09.063, 2009.

Ritter, B. and Geleyn, J.-F.: A Comprehensive Radiation Scheme for Numerical Weather Prediction Models with Potential Applications in Climate Simulations, Monthly Weather Review, 120, 303–325, https://doi.org/10.1175/1520-0493(1992)120<0303:ACRSFN>2.0.CO;2, 1992.

Robock, A.: Volcanic eruptions and climate, Reviews of Geophysics, 38, 191–219, https://doi.org/10.1029/1998RG000054, 2000.

Rockel, B., Will, A., and Hense, A.: Regional climate modelling with COSMO-CLM (CCLM), Meteorol. Z. (Stuttg.), 17, 2008.

Rodwell, M. J. and Hoskins, B. J.: Subtropical Anticyclones and Summer Monsoons, Journal of Climate, 14, 3192–3211, https://doi.org/10.1175/1520-0442(2001)014<3192:SAASM>2.0.CO;2, 2001.

Schättler, U. and Blahak, U.: in: A Description of the Nonhydrostatic Regional COSMO-Model, 2017.

Schmidt, G. A., Annan, J. D., Bartlein, P. J., Cook, B. I., Guilyardi, E., Hargreaves, J. C., Harrison, S. P., Kageyama, M., LeGrande, A. N., Konecky, B., Lovejoy, S., Mann, M. E., Masson-Delmotte, V., Risi, C., Thompson, D., Timmermann, A., Tremblay, L.-B., and Yiou, P.: Using palaeo-climate

comparisons to constrain future projections in CMIP5, Climate of the Past, 10, 221–250, https://doi.org/10.5194/cp-10-221-2014, 2014.

Schulz, J.-P., Vogel, G., Becker, C., Kothe, S., Rummel, U., and Ahrens, B.: Evaluation of the ground heat flux simulated by a multi-layer land surface scheme using high-quality observations at grass land and bare soil, Meteorologische Zeitschrift, 25, 607–620, https://doi.org/10.1127/metz/2016/0537, 2016.

Sieber, P., Ericsson, N., Hammar, T., and Hansson, P.-A.: Albedo impacts of current agricultural land use: Crop-specific albedo from MODIS data and inclusion in LCA of crop production, Science of The Total Environment, 835, 155455, https://doi.org/10.1016/j.scitotenv.2022.155455, 2022.

Singh, R., Tsigaridis, K., LeGrande, A. N., Ludlow, F., and Manning, J. G.: Investigating hydroclimatic impacts of the 168–158 BCE volcanic quartet and their relevance to the Nile River basin and Egyptian history, Climate of the Past, 19, 249–275, https://doi.org/10.5194/cp-19-249-2023, 2023.

Smiatek, G., Rockel, B., and Schättler, U.: Time invariant data preprocessor for the climate version of the COSMO model (COSMO-CLM), Meteorologische Zeitschrift, 17, 395–405, https://doi.org/10.1127/0941-2948/2008/0302, 2008.

Smiatek, G., Helmert, J., and Gerstner, E.-M.: Impact of land use and soil data specifications on COSMO-CLM simulations in the CORDEX-MED area, metz, 25, 215–230, https://doi.org/10.1127/metz/2015/0594, 2016.

Spiegel, D. S., Raymond, S. N., Dressing, C. D., Scharf, C. A., and Mitchell, J. L.: Generalized Milankovitch cycles and long-term climatic habitability, ApJ, 721, 1308, https://doi.org/10.1088/0004-637X/721/2/1308, 2010.

Tiedtke, M.: Parameterization of Cumulus Convection in Large-Scale Models, in: Physically-Based Modelling and Simulation of Climate and Climatic Change: Part 1, edited by: Schlesinger, M. E., Springer Netherlands, Dordrecht, 375–431, https://doi.org/10.1007/978-94-009-3041-4_9, 1988.

Toohey, M. and Sigl, M.: Volcanic stratospheric sulfur injections and aerosol optical depth from 500 BCE to 1900 CE, Earth System Science Data, 9, 809–831, https://doi.org/10.5194/essd-9-809-2017, 2017.

Viste, E. and Sorteberg, A.: Moisture transport into the Ethiopian highlands, International Journal of Climatology, 333, 249–263, https://doi.org/10.1002/joc.3409, 2013.

Wang, C., Liu, H., and Lee, S.-K.: The record-breaking cold temperatures during the winter of 2009/2010 in the Northern Hemisphere, Atmospheric Science Letters, 11, 161–168, https://doi.org/10.1002/asl.278, 2010.

Welch, B. L.: The Generalization of `Student's' Problem when Several Different Population Variances are Involved, Biometrika, 34, 28–35, https://doi.org/10.2307/2332510, 1947.

Wouters, H., Varentsov, M., Blahak, U., Schulz, J.-P., Schattler, U., Bucchignani, E., and Demuzere, M.: User guide for TERRA URB v2.2: The urban-canopy land-surface scheme of the COSMO model, 12, 2017.

Xoplaki, E., González-Rouco, J. F., Luterbacher, J., and Wanner, H.: Wet season Mediterranean precipitation variability: influence of large-scale dynamics and trends, Climate Dynamics, 23, 63–78, https://doi.org/10.1007/s00382-004-0422-0, 2004.

Young, K. C.: A Numerical Simulation of Wintertime, Orographic Precipitation: Part I. Description of Model Microphysics and Numerical Techniques, Journal of the Atmospheric Sciences, 31, 1735–1748, https://doi.org/10.1175/1520-0469(1974)031<1735:ANSOWO>2.0.CO;2, 1974.

Zhang, M., Tölle, M. H., Hartmann, E., Xoplaki, E., and Luterbacher, J.: A Sensitivity Assessment of COSMO-CLM to Different Land Cover Schemes in Convection-Permitting Climate Simulations over Europe, Atmosphere, 12, 1595, https://doi.org/10.3390/atmos12121595, 2021.

Zittis, G., Hadjinicolaou, P., Almazroui, M., Bucchignani, E., Driouech, F., El Rhaz, K., Kurnaz, L., Nikulin, G., Ntoumos, A., Ozturk, T., Proestos, Y., Stenchikov, G., Zaaboul, R., and Lelieveld, J.: Business-as-usual will lead to super and ultra-extreme heatwaves in the Middle East and North Africa, npj Clim Atmos Sci, 4, 1–9, https://doi.org/10.1038/s41612-021-00178-7, 2021.

Zittis, G., Almazroui, M., Alpert, P., Ciais, P., Cramer, W., Dahdal, Y., Fnais, M., Francis, D., Hadjinicolaou, P., Howari, F., Jrrar, A., Kaskaoutis, D. G., Kulmala, M., Lazoglou, G., Mihalopoulos, N., Lin, X., Rudich, Y., Sciare, J., Stenchikov, G., Xoplaki, E., and Lelieveld, J.: Climate Change and Weather Extremes in the Eastern Mediterranean and Middle East, Reviews of Geophysics, 60, e2021RG000762, https://doi.org/10.1029/2021RG000762, 2022.

2. A Sensitivity Assessment of COSMO-CLM to Different land Cover Schemes in Convection-Permitting Climate Simulations over Europe

Published on: Atmosphere, 12, 1595, https://doi.org/10.3390/atmos12121595, 2021

Mingyue Zhang [1],*, Merja H. Tölle [2], Eva Hartmann [1], Elena Xoplaki [1,3] and Jürg Luterbacher [1,3,4]

[1] Department of Geography, Climatology, Climate Dynamics and Climate Change, Justus-Liebig University of Giessen, 35390 Giessen, Germany; Eva.Hartmann@geogr.uni-giessen.de (E.H.); elena.xoplaki@geogr.uni-giessen.de (E.X.); jluterbacher@wmo.int (J.L.)

[2] Center for Environmental Systems Research (CESR), University of Kassel, Wilhelmshöher Allee 47, 34117 Kassel, Germany; merja.toelle@uni-kassel.de

[3] Centre of International Development and Environmental Research, Justus Liebig University of Giessen, 35390 Giessen, Germany

[4] Science and Innovation Department, World Meteorological Organization (WMO), CH-1211 Geneva 2, Switzerland

Correspondence: Mingyue.zhang@geogr.uni-giessen.de; Tel.: +49 6419936215

Abstract

The question of how sensitive the regional and local climates are to different land cover maps and fractions is important, as land cover affects the atmospheric circulation via its in-fluence on heat, moisture, and momentum transfer, as well as the chemical composition of the atmosphere. In this study, we used three independent land cover data sets, GlobCover 2009, GLC2000 and ESACCI-LC, as the lower boundary of the regional climate model COSMO-CLM (Consortium for Small Scale Modeling in Climate Mode, v5.0-clm15) to perform convection-permitting regional climate simulations over the large part of Europe covering the years 1999 and 2000 at a 0.0275° horizontal resolution. We studied how the sensitivity of the impacts on regional and local climates is represented by different land cover maps and fractions, especially between warm (summer) and cold (winter) seasons. We show that the simulated regional climate is sensitive to different land cover maps and fractions. The simulated temperature and observational data are generally in good agreement, though with differences between the seasons. In comparison to winter, the summer simulations are more heterogeneous across the study region. The largest deviation is found for the alpine area (−3 to +3 °C), which might be among different reasons due to different classification systems in land cover maps and orographical aspects in the COSMO-CLM model. The leaf area index and plant cover also showed different responses based on various land cover types, especially over the area with high vegetation coverage. While relating the differences of land cover fractions and the COSMO-CLM simulation results (the leaf area index, and plant coverage) respectively, the differences in land cover fractions did not necessarily lead to corresponding bias in the simulation results. We finally provide a comparative analysis of how sensitive the simulation outputs (temperature, leaf area index, plant cover) are related to different land cover maps and fractions. The different regional representations of COSMO-CLM indicate that the soil moisture, atmospheric circulation, evaporative demand, elevation, and snow cover schemes need to be considered in the regional climate simulation with a high horizontal resolution.

Keywords: land cover map; land cover fraction; sensitivity; EXTPAR; COSMO-CLM

2.1. Introduction

Land cover (LC, see Appendix A) plays an important role in regional climate via influencing the heat, moisture, momentum transfer, and chemical composition of the atmosphere. Currently, land cover data in regional climate modeling are static in time and provide different details depending on the land cover data. Land cover changes are among the main human-induced activities that significantly contribute to climate change (Wang et al., 2008; Betts et al., 2007). Long-term studies of the land surface in regional climate simulation show that land cover affects the atmospheric circulation (Betts et al., 2007; Wramneby et al., 2010; Arora and Montenegro, 2011). Many studies have revealed that land cover representation plays a substantial role in climate simulations (Davin et al., 2020). Modifications of land surface schemes in climate models result in differences in the modeled climate (Steiner et al., 2009; Lu et al., 2001; Davin et al., 2011). The effects of land cover on climate vary across different spatial resolutions (Pielke et al., 1998; Betts, 2007). Earlier studies by Avissar and Pielke (Pielke et al., 1998) showed that the representation of stomatal conductance affects the mesoscale atmospheric circulation, while the representation of stomatal conductance is highly dependent on the vegetation coverage of land (Avissar and Pielke, 1991). Therefore, land cover change is an important factor influencing regional and local climates (Bonan et al., 2002; Feddema et al., 2005). By transforming agricultural land into the forest for bioenergy production (Luca et al., 2016), convection-permitting climate model simulations have revealed lower summer temperatures in the order of 1–2 °C over the afforested areas. Thus, changes in local conditions with the underlying surface have the strongest impact on temperature due to the interplay between surface albedo and soil moisture changes and evapotranspiration efficiencies. This indicates that changes in temperature response are to be expected locally, underlying the im-portance of the convection-permitting scale when considering land cover changes. In addition, scientific evidence shows that land cover influences the Earth's water and energy cycles through heat, moisture, and momentum transfer as well as chemical composition (Pitman, 2003; Bonan et al., 2002; Brovkin et al., 2004). Especially in regions with strong land–atmosphere interactions, the differences in land cover types significantly affect weather and climate through atmospheric circulation. Therefore, a convection-permitting simulation with a higher horizontal resolution on a regional scale is needed, which al-lows us to investigate how sensitive the land–atmosphere interaction is with different land cover types (Stéfanon et al., 2014).

Regional climate models (RCMs) have been developed to overcome the coarse spatial resolution of global climate models (GCMs) and provide more detailed information on the regional and local aspects of climate (Giorgi and Mearns, 1991). RCMs allow for studying detailed land cover type effects on climate, which cannot be studied with coarse global climate models (Tölle et al., 2014; Luca et al., 2016; Added value of regional climate modeling over areas characterized by complex terrain—Precipitation over the Alps - Torma - 2015 - Journal of Geophysical Research: Atmospheres - Wiley Online Library, 2020). RCMs can realistically represent the climate in bio-geophysical, bio-geochemical, and bio-geographical aspects, and at the same time, with a high horizontal resolution (Alesta-lo, 1981). RCMs provide regional climate change projections and can be used to evaluate regional climate model performance through a set of experiments aiming at producing regional climate projections (cordex.org) (Jacob et al., 2014; Kotlarski et al., 2014). The challenge on how to represent the fraction of land surface in the regional climate modeling procedure is in the frame of the international initiative. The land surface scheme plays an important role in parameterizing the physical processes on the Earth's surface (Bonan et al., 2002). The land cover has a significant impact on the atmosphere's lower boundary via both bio-geochemical and bio-geophysical processes. It can influence the heat, moisture, momentum transfer as well as the chemical composition of the atmosphere as well as climate. Therefore, most research papers have focused on vegetation and land surface modeling by introducing the scheme into climate models (Diffenbaugh, 2005). Equilibrium vegetation models (EVMs) allow plants to "move" through the model grid cells ac-cording to the simulated climate change (Foley et al., 1998). New dynamic global vegetation models (DGVMs) have been developed to make use of the interactive plant biogeography from EVMs and the simplified plant succession and biogeochemistry (Diffenbaugh, 2005). In current regional climate simulations, the land cover stays static through the whole simulation period, which results in uncertainty in the model output (Yokohata et al., 2019). Consequently, it is necessary to perform research on a regional scale at a higher spatial resolution with different land cover data.

The role of past and future land cover changes (LUCs) forcing the occurrence of extremes on land, is still poorly studied, especially at regional and local scales. This is be-cause of the inadequately quantified effects of different land cover maps and fractions in regional climate models. Furthermore, the current GCMs and RCMs have a rather coarse horizontal resolution, which cannot

provide detailed and accurate information at smaller scales. Although the land cover has a detectable role in changes in temperature and precipitation extremes (Tölle et al., 2016; Wilhelm et al., 2015), convection-permitting modeling can improve the representation of the regional climate by better resolving the regional forcing and processes (Fosser et al., 2015). Topography and land cover are two of the rea-sons to increase the uncertainty in RCM simulations arising from the parameterization of sub-grid scale convection (Pal et al., 2019). Meanwhile, few studies have addressed the impacts of different land cover maps and fractions in climate modeling with a higher horizontal resolution than 5 km on a regional scale. For example, some of the research within EURO-CORDEX (Coordinated Downscaling Experiment - European Domain) has focused on either the precipitation variability or temperature representation in the COS-MO-CLM model (Meredith et al., 2021; Breil et al., 2020). Over Central Europe, the vegetation is highly diverse, containing many different land cover types such as cropland, forest, and pasture. By performing seasonal simulations with RCMs, sensitivity studies have explored the impact of land cover change, seasonal vegetation and soil scheme on the cli-mate (Heck et al., 2001). It is known that the vegetation cover in forest areas and seasonal crops play a major role in modifying the climate (Garnaud et al., 2015). Nevertheless, cur-rent research does not provide more insights on how the local and regional climates in Europe react to different land cover maps and fractions.

Therefore, a sensitivity study on the relationship between different land cover maps, land fractions, and regional climate at a high horizontal resolution scale is needed. The main objective of this study was to investigate the effects of different land cover maps on the regional climate with convection-permitting modeling. In this contribution, we anticipated answering the following questions:

- Do the three land cover maps in regional climate simulations reliably compare to observational data?
- Do regional and seasonal temperatures change according to the different land cover maps and fractions? If yes, why, where and in which season?
- How do the leaf area index (LAI) and plant coverage react or change according to the different land cover data sets?

- How do the different land cover fractions affect the temperature, LAI and plant coverage in COSMO-CLM regional climate simulation?

To address these questions, we performed convection-permitting simulations with the regional climate model COSMO-CLM (Wouters et al., n.d.) using three different land cover data sets. The simulation with the land cover data GlobCover 2009 was the reference simulation to which the simulations with the land cover data GLC2000 and ESACCI-LC were compared. All the LC maps were unified into the same LC types with respect to GLC2000 (see Appendix C) so that the differences in the results can be attributed to different land cover fractions. The simulation period covers two years, 1999 and 2000.

The remainder of this paper is as follows: Section 2 introduces the three different land cover sets and the data for evaluation. Then, the climate model setup, as well as the analysis methods, are explained in Section 3. Section 4 presents the results and discussion, followed by a conclusion and a short outlook for further research in Section 5.

2.2. Data

2.2.1. Input Land Cover Data Sets

The GlobCover 2009 (global land cover product of 2009) at 300 m spatial resolution (GLOBCOVER-products-description-and-validation-report.pdf, 2020), which is produced from the automated classification of satellite MERIS (MEdium Resolution Imaging Spectrometer) time series. The GlobCover 2009 classification consists of 23 different land cover types (Arino_et_al_GlobCover2009-a.pdf, 2020) (see Appendix C). It is a high horizontal resolution land surface product and has been used to compare the effects of different land cover types in atmospheric circulation (Yin et al., 2020; Zhong et al., 2019).

The GLC2000 (Global Land Cover map for the year 2000) has a spatial resolution of 1 × 1 km for its land cover data set and is compiled by the Joint Research Centre of the European Commission (JRC; Table 1). It is produced through the Global Land Cover 2000 Project (GLC2000), which aims to provide information to the International Conventions on Climate Change. Daily SPOT4 vegetation sensor data are the basic input data of this land cover product (GLC2000: a new

approach to global land cover mapping from Earth observation data: International Journal of Remote Sensing: Vol 26, No 9, 2020). GLC2000 is the former standard input land cover data in CCLM and it contains 23 LC types.

ESACCI-LC (European Space Agency Climate Change Initiative Land Cover) global land cover maps are available at the 300 m spatial resolution on an annual basis from 1992 to 2017 (Lamarche et al., 2017) (Table 1). It is produced by the European Space Agency (ESA) Climate Change Initiative (CCI) project. The Coordinate Reference System used for the global land cover database is a geographic coordinate system (GCS) based on the World Geodetic System 84 (WGS84) reference ellipsoid. It contains 37 land cover types on a regional scale.

The three land cover products are different in terms of source data, classification system, spatial resolution, and land cover types, as presented in Table 1. Different classification systems result in differences related to land cover fractions and distribution, even with the same source data. The impacts of different classification systems are addressed in the discussion of Section 4 below.

Table 2.1. Characteristics of the three different land cover data sets used in this study: GlobCover 2009 (Lamarche et al., 2017), GLC2000 (Bounoua et al., 2002), and ESACCI-LC (Wouters et al., 2017), created by author.

Characteristics/Data set	ESACCI-LC	GLC2000	GlobCover2009
Data Source	**Satellite, observation**	**SPOT4**	**MERIS**
Time Span	**1992–2015**	**2000**	**2009**
Temporal Resolution	**Yearly**	**--**	**--**
Land Use/Cover Types	**37**	**23**	**23**
Spatial Resolution	**300 m**	**1 km**	**300 m**
Classification System	**Unsupervised**	**Unsupervised**	**Unsupervised and supervised**
Data Format	**Tiff/netCDF**	**ESRI/Binary**	**Tiff**

ESACCI-LC maps also offer a global scale legend, which contains 23 classes. They are produced based on the view of as much compatibility as possible with GLC2000 and GlobCover 2009. With

these two legends offered by ESACCI-LC maps, according to the regional and global LC information offered by ESACCI-LC, and compared to the GlobCover 2009 LC class, we unified the ESACCI-LC class as GlobCover 2009. For example, in the 37 LC legends, LC type 61 (tree cover, broadleaved, deciduous, closed (>40%)) and 62 (tree cover, broadleaved, deciduous, open (15–40%)) is unified as 60 (tree cover, broadleaved, deciduous, closed to open (>15%)) in the 23 LC types. Based on this, the ESACCI-LC types were unified into 23, the same as GlobCover 2009. Although, after unifying the ESACCI-LC types, three LC maps have the same number of LC types. However, the LC types differ in names. Therefore, we transferred the GlobCover2009 and ESACCI-LC legends into GLC2000 (see details in Appendix C). However, there are some land cover types in GLC2000 that do not exist in GlobCover 2009, for example, class number 10: burned tree cover. While this land cover type shares a very low fraction in GLC2000, so in our research, we did not consider it as a factor affecting the COSMO-CLM results.

The fraction of the land cover is shown in Figure 1 (over the whole research domain) and Figure 2 (over the six different sub-domains) after unifying these three maps into the same land cover types. ESACCI-LC and GLC2000 share a similar fraction of land cover types for the whole of the domain, which is different to GlobCover2009. We studied the links between the different land cover factions and simulated output by comparing the differences in temperature, LAI, and plant coverage.

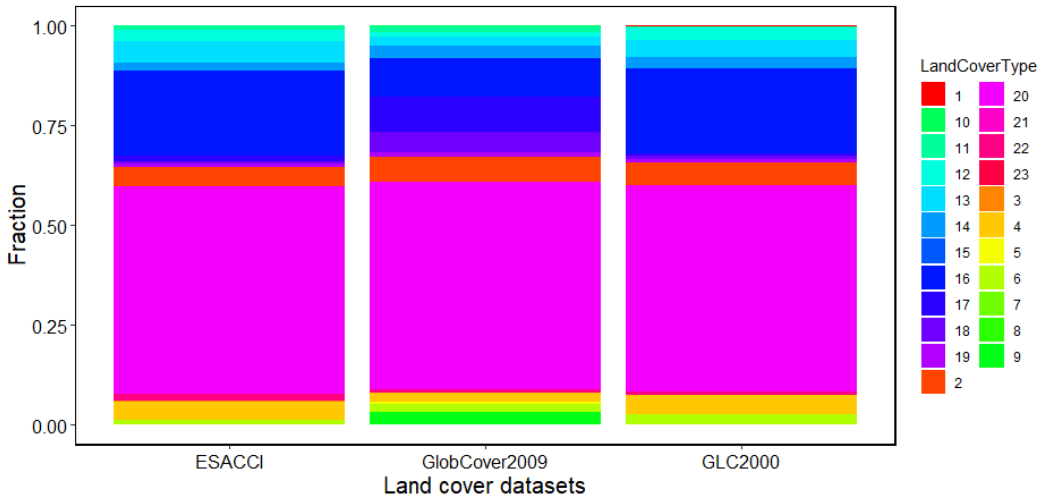

Figure 2.1. Land cover data sets of the fraction of three land cover maps over the whole study area based on unified land cover types (see Appendix C).

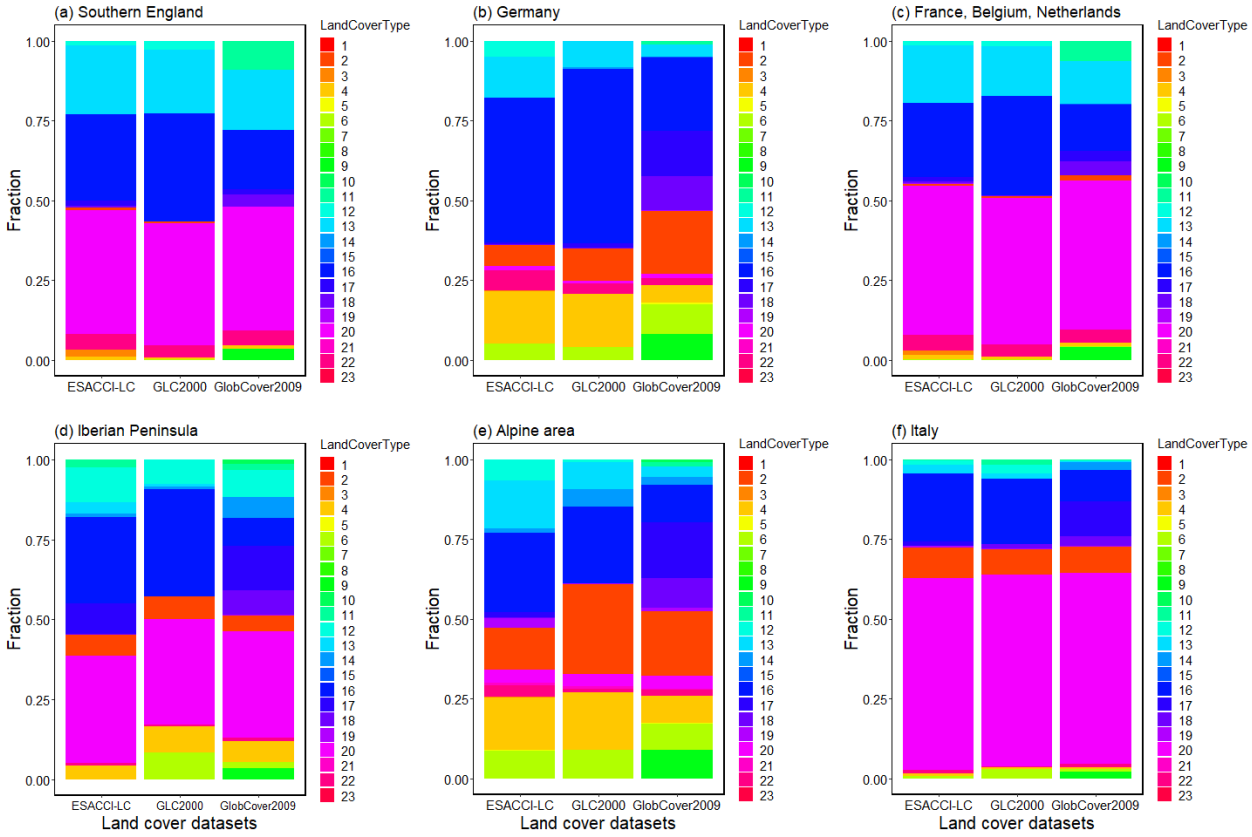

Figure 2.2. Land cover data sets of the fraction of three land cover maps over six different study areas based on unified land cover types (see Appendix C); (a) Southern England; (b) Germany; (c) France, Belgium, and Netherlands; (d) Iberian Peninsula; (e) Switzerland/Austria (the Alpine area); and (f) Italy.

2.2.2. HYRAS Data Sets

HYRAS (HYdrological RASter data sets) is a daily gridded data set based on observations from 1951 to 2015 with a resolution of 5 × 5 km for temperature. The HYRAS data set is used for bias correction of regionalized climate projection data and as input data for hydrological modeling. The data set is often used for various applications in climate modeling and impact research (A Central European precipitation climatology – Part I). Herein, we used this data set to evaluate our simulation results. We compared the mean temperature COSMO-CLM output with HYRAS data over Germany and the Alpine area to evaluate our simulation results for both summer and winter (described in Section 4.1).

2.2.3. ERA-Interim Data Sets

ERA-Interim is a global atmospheric reanalysis data set that contains re-analyzed and homogenized observation data by the computerized weather data from the European Centre for Medium-Range Weather Forecasts (ECMWF) (Tiedtke, 1988), at a maximum 0.125° horizontal resolution. It is continuously updated in real time, from 1979, and includes several surface parameters that describe weather, ocean-wave and land surface conditions. It is commonly used as driving data in COSMO-CLM, as well as in our simulation.

2.2.4. Model Description

COSMO-CLM (COnsortium for Small-scale MOdeling-CLimate Model) is a limited area model and the climate version of the COSMO model (Davin et al., 2011; Rockel et al., 2008). The COSMO model was introduced in 1998 and the model equations were formulated in rotated geographical coordinates and a generalized terrain-following height coordinate. Since 2005, COSMO-CLM has been the community model of the German regional climate research community jointly further developed by CLM-Community. It has been used in many simulations at different time scales and spatial resolutions from 1 to 50 km.

The COSMO model version 5.0 with CLM version 15 (COSMO-CLM v5.0-clm15) was used for the following simulations. The interpolation was carried out with INT2LM in version 2.05 with CLM version 1 (INT2LM-v2.05 clm1). The time integration is the two time-level Runge–Kutta scheme (Bounoua et al., 2002) and the model time step was 25 s. Following convection-permitting simulations, only shallow convection parameterization based on the Tiedtke scheme (Tiedtke, 1988) was used. COSMO-CLM includes a variety of physical processes, and the energy and water balance are simulated at the land surface and the ground, providing the surface temperature and humidity as the lower boundary conditions (Wouters et al., 2017; Schulz et al., 2016). The radiation scheme of COSMO-CLM is based on the solution of the δ two-stream version of the radiative transfer equation, allowing for a very flexible treatment of clouds by hiring partial cloud cover and relating the cloud optical properties to the cloud liquid water content (Ritter and Geleyn, 1992). Furthermore, the cloud microphysical processes were considered by developing different basic

microphysical processes, such as the nucleation of particles, particle growth by diffusion, and growth by interparticle collection (Young, 1974).

The investigated modeling domain was chosen according to the setup of the WCRP Coordinated Regional Downscaling Experiment (CORDEX) in its European realization (EURO-CORDEX), excluding northern Africa, Scandinavia, eastern European countries, and Northern England. The size of the computational domain was 760 × 600 grid cells at a horizontal resolution of 0.0275° (approximately 3 km) in a rotated grid; the left bottom point geographical coordinates are 7.6050973 degrees east longitude and 34.4874324 degrees north latitude.

2.3. Methods

2.3.1. External Data Acquiring

Regional climate models require geographically localized data sets including the topographic height of the Earth's surface, the plant cover, the distribution of land and sea, and a variety of other external parameters. These parameters are constant in COSMO-CLM. EXTPAR (Smiatek et al., 2008, 2016) (External Parameter for Numerical Weather Prediction and Climate Application) is used for generating appropriate external parameters such as plant coverage, LAI, and land fraction. EXTPAR can adapt all external data into the experimentally required horizontal resolution (Smiatek et al., 2008, 2016; Asensio and Messmer, n.d.). It contains three basic steps:

- Specify the target spatial resolution (rotated or non-rotated): In our simulations, the target grids were rotated.
- Aggregate the different raw data sets into the target horizontal resolution.
- Check the consistency of the different external parameter sets to make sure that the generated external data are consistent. This procedure includes a grid cell check, which ensures that all of the external parameters are of the same grid scale, either rotated or non-rotated. This step also checks the availability of the necessary variables for the simulation.

According to our needs, we used the following parameters as the input of EXTPAR (see Table 2.2). We acquired three different sets of external data with the GlobCover 2009, GLC2000, and

ESACCI-LC maps separately. These three external data sets were the input data for the three simulations.

Table 2.2. Input parameters for start EXTPAR software.

Parameters	Input Data
Topography data	GLOBE
Soil map	FAO digital soil map of the world
NDVI (normalized differential vegetation index)	NDVI Climatology from NASA
Lake fraction	Global lake database (DWD, RSHU, MétéoFrance)
Albedo	MODIS albedo (NASA)

2.3.2. Regional Climate Simulation

In Section 3.1, we described how to generate external parameters with the EXTPAR software based on the three LC maps. With the three generated external parameters, three simulations were conducted. Each simulation covered the period January of 1999 to March 2000, including the first three months of 1999 as spin-up. We chose this period because it is the initial year of our following study in the project, as the project aimed to investigate the regional climate behavior in the 21st century. All the simulations mentioned in this paper were driven by ERA-Interim reanalysis data (The ERA-Interim reanalysis: configuration and performance of the data assimilation system - Dee - 2011 - Quarterly Journal of the Royal Meteorological Society - Wiley Online Library, 2020). In this paper, we performed all of the simulations based on COSMO-CLM-v5.0-clm15, with the following initial and boundary data (Table 3).

Table 2.3. COSMO-CLM simulation set up.

Parameters	Input Setting
Interpolation	INT2LM-v2.05 clm15
Forcing	ERA-Interim
External data	GlobCover2009, GLC2000, ESACCI-LC

Domain	Middle Europe, approximately 3 km (0.0275°), 740 × 600 grid points
Time integration	Two time-level Runge–Kutta schemes
Model time step	25 s
Convection	Shallow convection based on Tiedtke scheme
Simulation period	1999.01.01 to 2000.03.31

2.3.3. Sensitivity Study

The simulated temperature was compared with the observational data from HYRAS. Furthermore, the COSMO-CLM outputs (plant coverage and LAI) were compared separately in six different sub-regions. The different LC fractions of these six regions are shown in Figure 2.2. To investigate how the different land cover maps and land cover fractions affect the COSMO-CLM output, the correlation between the temperature and the COSMO-CLM output (LAI and plant coverage) is shown by scatter plots (Figures A2.1 and A2.2). The sensitivity study included the following three parts:

- The temperature output from COSMO-CLM based on the three LC maps GlobCover 2009, GLC2000, and ESACCI-LC was compared with the observational data—HYRAS. We evaluated the COSMO-CLM results by comparing the mean temperature with the HYRAS observational data over Germany and the adjacent area: the Alpine area.
- Comparison of the COSMO-CLM results between three land cover sets: In this part, we focused on the differences between the output plant coverage and LAI by setting GlobCover 2009 as the reference simulation. The research domain was divided into six sub-domains, and the LC fraction of each domain is shown in Figure 2.1.
- The relation between the difference in the three LC data sets (LAI and plant coverage) and the simulated temperature are shown by scatter plots (Figures A2.1 and A2.2).

We concentrated on summer (June, July, and August) 1999 and winter (December, January, and February) 1999/2000, investigating the impacts of different land cover maps and fractions on

temperature, LAI, and plant cover. Furthermore, we also addressed the performance of COSMO-CLM in the two seasons.

2.3.4. Statistically Study

The performance of the three different land cover data sets was evaluated by the statistical significance *t*-test (Welch, 1947) and bias (calculated through mean bias error).

- The differences of the three land cover data sets with respect to the reference simulation (HYRAS or GlobCover 2009) were statistically assessed with a one side t-test under the following null hypothesis: the target simulation is not different compared to the reference. The degrees of freedom for the t-test was calculated as n−2, where n is the grid number for each group.
- For the evaluation of the simulated temperature, bias (see Equation (2.1)) was calculated through the sub-domain to see the average bias towards the observational data in the simulations. Where n indicates the total grid number, i indicates the specific grid box, and x presents the value of every grid box.

$$Bias = \frac{1}{n}\sum_{i=1}^{n}(x_i - \underline{x}) \tag{2.1}$$

2.4. Results and Discussion

2.4.1. Evaluation of Simulated Temperature Based on the Three LC Maps

There were two main questions we sought to answer. Is the simulated temperature based on three different land cover maps reasonably simulated compared to the observational data? How does the temperature react to different land cover maps and fractions in the summer and winter seasons? To evaluate the simulations and study the temperature response to different LC maps and fractions, we first calculated the mean seasonal temperature difference between the three COSMO-CLM outputs and the observational data HYRAS for each grid point over the summer (JJA) in 1999 and winter (DJF) in 1999/2000 (Figures 2.3 and 2.4).

In summer, the simulated mean temperature over southern Germany is overestimated by approximately 2 °C but underestimated in parts of the Alpine region (Figure 2.3). There are

differences in the north of the sub-domain, where the difference in Figure 2.3a,c is not as high as in Figure 2.3b. This is interesting because GLC2000 and ESACCI-LC share similar land cover type fractions, as seen in Figures 2.1 and 2.2b,e. These results demonstrate that apart from the LC fraction, it is also necessary to study the role of LC distribution in regional climate modeling.

Over the Alpine area, the simulated temperature shows differences ranging between −3 and +3 °C compared to the observed temperature (Figure 2.3). The orographic and soil moisture settings in the COSMO-CLM play an important role in affecting the temperature distribution. The long-term snow cover may also affect the temperature simulation in this case. Future studies should further investigate the relationship between the temperature and the elevation and soil moisture settings in COSMO-CLM.

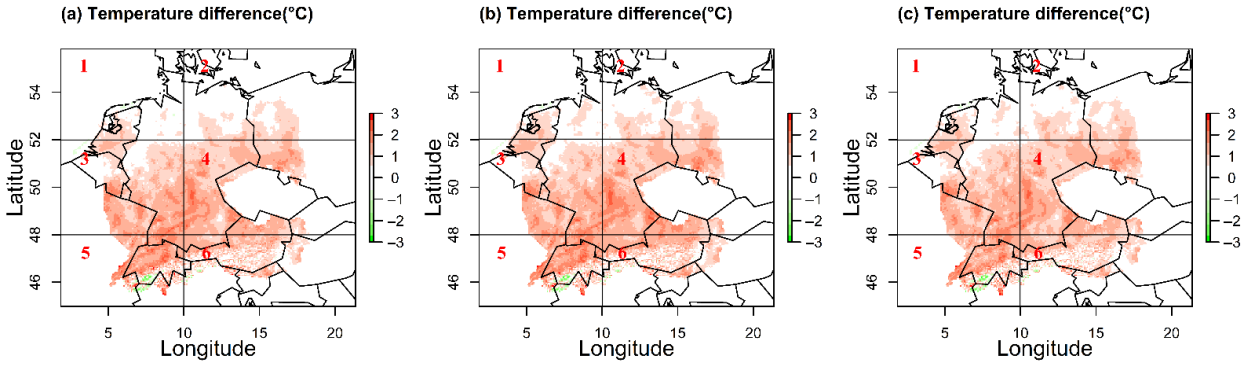

Figure 2.3. Summer 1999 mean temperature differences between simulations and HYRAS observations: (a) GlobCover2009, (b) GLC2000, and (c) ESACCI-LC. Numbers 1 to 6 refer to the six different sub-regions used to conduct the statistical significance test (Table 2.4).

The statistical significance test at the 95% confidence level for the simulated temperature difference to HYRAS and for each of the six sub-areas, as shown in Figures 2.3 and 2.4, are presented in Table 2.4. Non-significant differences denote a good agreement between the simulations and the observations. In total, ESACCI-LC shows a better agreement with HYRAS compared to GlobCover 2009 and GLC2000. Over southwestern Germany (area 3, 3), ESACCI-LC indicates non-significant differences, while the GlobCover 2009 and GLC2000 simulated results show a noticeable difference to observations according to the significance t-test.

Table 2.4. Statistical significance test results (t-value) of the summer temperature differences (°C) between the simulated temperature and the HYRAS observations: Critical t-value = 1.960; results lower than the t-value are marked with * and are in bold.

	GlobCover 2009	GLC2000	ESACCI-LC
Area 1	**36.6**	**35.5**	**36.5**
Area 2	**22.4**	**25**	**26.9**
Area 3	**38.4**	**36.4**	–18.4 *
Area 4	**66.9**	**75.2**	**39.1**
Area 5	**26.0**	**25.5**	–75.6 *
Area 6	**57.2**	**59.5**	**27.7**

In winter (Figure 2.4), the simulated seasonal mean temperature is in good agreement with the observational data over most of the area, except for the Alpine area. The COSMO-CLM output temperature based on the ESACCI-LC is similar to GlobCover 2009 compared to GLC2000. Although the GLC2000 and ESACCI LC maps have a similar land cover fraction, the simulation output does not support this similarity, denoting that, the land cover fraction may not be the decisive component of the LC maps for the simulated temperature.

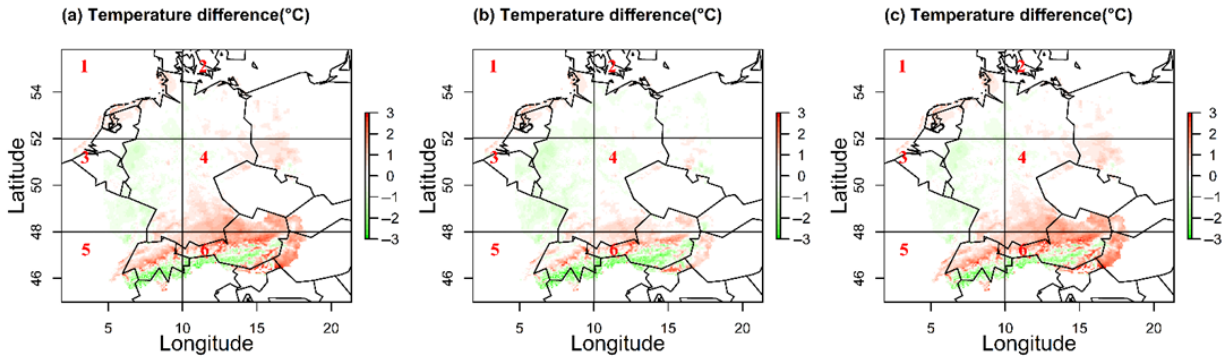

Figure 2.4. Winter 1999/2000 mean temperature differences between simulations and HYRAS observations: (a) GlobCover2009, (b) GLC2000, and (c) ESACCI-LC. Numbers 1 to 6 refer to six different sub-regions used to conduct the statistical significance test (Table 2.5).

Table 2.5. Statistical significance test results (t-value) of the winter temperature differences (°C) between the simulated temperature and the HYRAS observations: Critical t-value = 1.960; results lower than the t-value are marked with * and are in bold.

	GlobCover 2009	GLC2000	ESACCI-LC
Area 1	**–8.8 ***	**–7.6 ***	**–12.6 ***
Area 2	15.9	15.6	13.5
Area 3	9.7	12.3	**–4.42 ***
Area 4	11.6	9.8	**–0.6 ***
Area 5	30.0	31.4	**–0.4 ***
Area 6	23.6	23.8	**5.1**

A much better performance is evident for all simulations with the different LC maps and all sub-regions during the winter season (Figure 2.3 and Table 2.5). The simulated temperature with ESACCI-LC shows more realistic results compared to HYRAS, except in areas 5 and 6. According to Table 2.5, the GlobCover 2009 and GLC2000 results show a remarkable difference over the whole region, especially over the south of Germany and the Alpine area. As for the summer analysis, a relationship between the LC fraction and the regional climate simulation in terms of seasonal temperature does not hold (Figure 2.3 and Table 2.4), which also reinforces the need to further investigate the effects of LC distributions.

We also calculated the overall bias for the six areas, as well as the whole domain (see Table 2.6). Table 6 indicates that the simulated temperature shows a greater difference in summer compared to winter. In summer, the temperature was overestimated by COSMO-CLM with three different land cover maps. In contrast, the winter temperature was mostly underestimated over Germany, except over the areas 5 and 6.

Overall, COSMO-CLM performs better in winter compared to summer. We expect this is because of the vegetation scheme, the parameterization of elevation change and the snow cover in COSMO-CLM. It is necessary to conduct further studies in this area.

Table 2.6. The bias of the simulated temperature compared to HYRAS over the six areas, as well as the whole area, both in summer and in winter.

	Summer			Winter		
	ESACCI-LC	GlC2000	GlobCover 2009	ESACCI-LC	GlC2000	GlobCover 2009
Area 1	**1.25**	**1.18**	**1.24**	**–0.33**	**–0.14**	**–0.17**
Area 2	**0.59**	**0.54**	**0.49**	**–0.12**	**–0.07**	**–0.06**
Area 3	**1.26**	**1.15**	**1.23**	**–0.03**	**0.37**	**0.32**
Area 4	**0.65**	**0.65**	**0.57**	**–0.10**	**0.003**	**0.02**
Area 5	**0.97**	**0.85**	**0.88**	**0.18**	**1.10**	**1.05**
Area 6	**0.94**	**0.91**	**0.88**	**–0.06**	**0.24**	**0.23**
Whole region	**0.95**	**0.89**	**0.89**	**–0.09**	**0.17**	**0.16**

2.4.2. Impacts of Different Land Cover Types on the COSMO-CLM Output LAI

To answer the question on how the LAI (leaf area/ground area, m2/m2) react according to different land cover data sets, we compared the summer and winter LAI based on the three land cover data sets. The GlobCover 2009 data set has been used as the reference data.

The simulated summer and winter LAIs are shown in Figure 2.5. The simulations show an agreement over the European study area. Differences over specific areas, such as the Alps, northern Iberian Peninsula, smaller parts of Germany and France are more pronounced (±0.6 m2/m2) during the summer. During the winter, the LAI differences are significantly smaller (up to +/− 0.2 m2/m2) between the ESACCI-LC/GLC2000 and the GlobCover 2009.

The highest LAI differences are found in the summer over the Alpine area (Figure 5). These differences may be related to the orography, snow cover, and elevation parametrization in COSMO-CLM. The different classification systems that are used for the creation of the land cover maps may also impact the simulations as seen by the high differences over the northern Iberian Peninsula that is characterized by different land cover types due to the different classification

systems used by the LC maps. In winter, the LAI distribution is more homogenous (Figure 2.5) indicating the higher sensitivity of the COSMO-CLM model during summer.

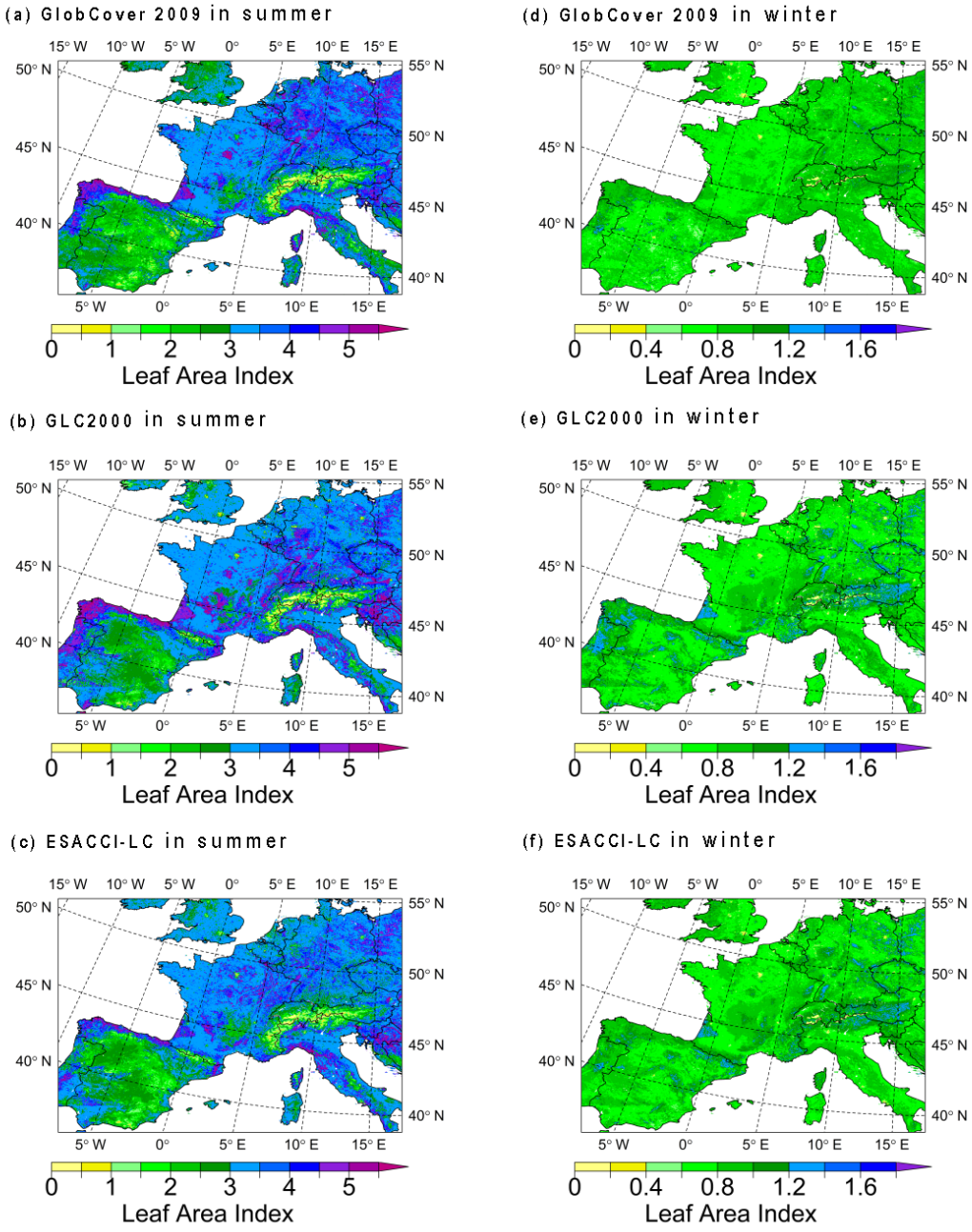

Figure 2.5. Simulated winter and summer LAI: (a) summer GlobCover2009, (b) summer ESACCI-LC, (c) summer GLC2000, (d) winter GlobCover2009, (e) winter ESACCI-LC, and (f) winter GLC2000.

As for the temperature assessment, the European study has been divided into six different regions (see Figure 2.11 in Appendix B) according to the LC fraction differences in order to evaluate the COSMO-CLM output (LAI and plant cover) via a differences statistical significance test. The six areas: southern England, Germany, France with Belgium and the Netherlands, the Iberian Peninsula, Switzerland/Austria, and Italy, are shown in Table 2.7 together with the t-test results for LAI. The areas of southern England, Germany, France with Belgium, and the Netherlands show good agreement between the two LC maps and the reference data set. Larger deviations are found over complex topography areas as the Iberian Peninsula, the Alpine area, and Italy. Over the complex orographically Alpine area, larger significant differences are found for both winter and summer.

Table 2.7. Statistical significance test results (t-value) of the LAI differences between two land cover data sets and GlobCover 2009. Results lower than the critical t-value (1.960) are marked with * and are in bold.

	Summer		**Winter**	
t-value	ESACCI-LC	GLC2000	ESACCI-LC	GLC2000
Southern England	26.	**–62.5 ***	**–38.0 ***	**–39.1 ***
Germany	3.1	**–17.5 ***	**–15.0 ***	8.6
France, Belgium, and the Netherlands	**–9.0 ***	1.5	**–51.5 ***	4.7
Iberian Peninsula	10.8	29.9	15.1	13.9
Switzerland/Austria	57.9	22.4	8.5	40.3
Italy	35.6	10.7	**–9.3 ***	56.6

In the summer, smaller differences characterize the ESACCI-LC simulations compared to GLC2000 over the areas with lower terrain complexity (Figure 2.6). The GLC2000 summer map shows a clear overestimation of the LAI over the Iberian Peninsula. The same map is characterized by a significant underestimation over the northern Alpine areas, in contrast to the overestimation of LAI over the southern rim. Most of the sub-regions show smaller LAI differences of around ±0.2 during winter with lower sensitivity to the two different land cover maps (Figure 2.6).

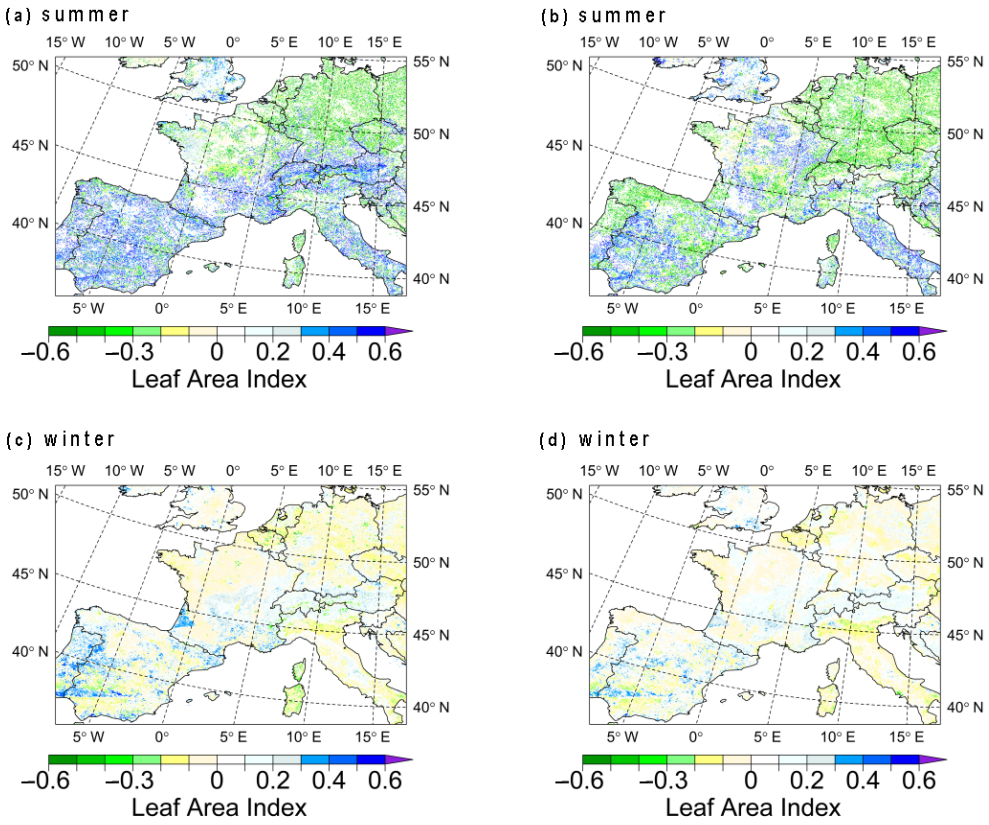

Figure 2.6. Winter and summer simulated LAI deviations with respect to GlobCover 2009: (a) ESACCI-LC summer, (b) GLC2000 summer, (c) ESACCI-LC winter and (d) GLC2000 winter.

2.4.3. Impacts of Different land Cover Types on the COSMO-CLM Output Plant Coverage

With the aim to investigate how the plant coverage is changing with the different land cover data sets, we compared the simulated summer and winter plant cover with three land cover data sets and looked at their differences with respect to the reference data set GlobCover 2009. Figure 2.7 presents the mean seasonal simulated plant coverage simulated with the three different land cover data sets (GlobCover 2009, GLC2000, and ESA-CCI-LC). It is obvious and expected that during winter, the plant coverage is lower than during the summertime, especially over central Europe (Germany, the Netherlands, and France). Seasonal vegetation, such as crops, which are under agricultural rest conditions during winter over these regions, is a major feature of this difference.

In the summer, the three simulations show similar plant coverage, while differences are concentrated over the Iberian Peninsula and the Alpine area (Figure 2.7). Lower plant coverage is

produced over both areas with GlobCover 2009. In winter, the simulated plant coverage shows smaller differences between the three land cover data sets. Larger differences can be seen over the Alpine area (Figure 2.7), where the simulations show strong variation, mainly due to the high elevation range and the forest vegetation type. The Alpine area has different LC fractions because the land cover classification system varies among the LC maps (see Figure 2.2e). Further work should investigate the relationship between these.

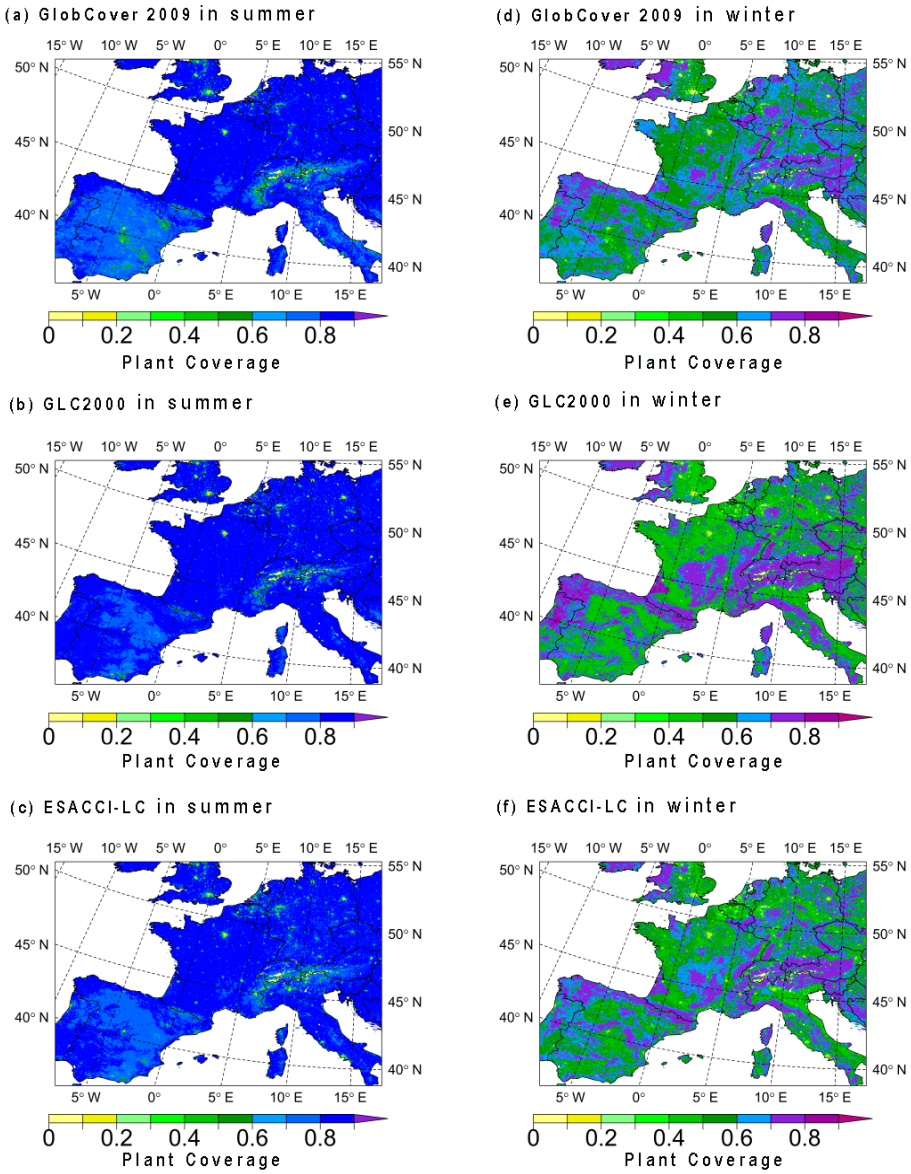

Figure 2.7. Seasonal simulated plant coverage: (a) GlobCover2009 in summer, (b) ESACCI-LC in summer, (c) GLC2000 in summer, (d) GlobCover2009 in winter, (e) ESACCI-LC in winter, and (f) GLC2000 in winter.

The simulated plant coverage with ESACCI-LC is lower overall than the GlobCover 2009 both in summer and winter (Figure 2.8, Table 2.8). Plant coverage differences between the two simulations are maximized over the high plant coverage areas, compared to the lower plant coverage areas. Differences between GlobCover 2009 and GLC2000 are less pronounced. Nevertheless, the difference between the simulated plant coverage based on ESACCI-LC and GlobCover 2009 is not as obvious as it is between GLC2000 and GlobCover 2009. During summer, ESACCI-LC simulations seem to agree well with the reference map over most of the area, when compared with GLC2000 (Figure 2.8). The ESACCI-LC map performs better for plant coverage, especially in summer.

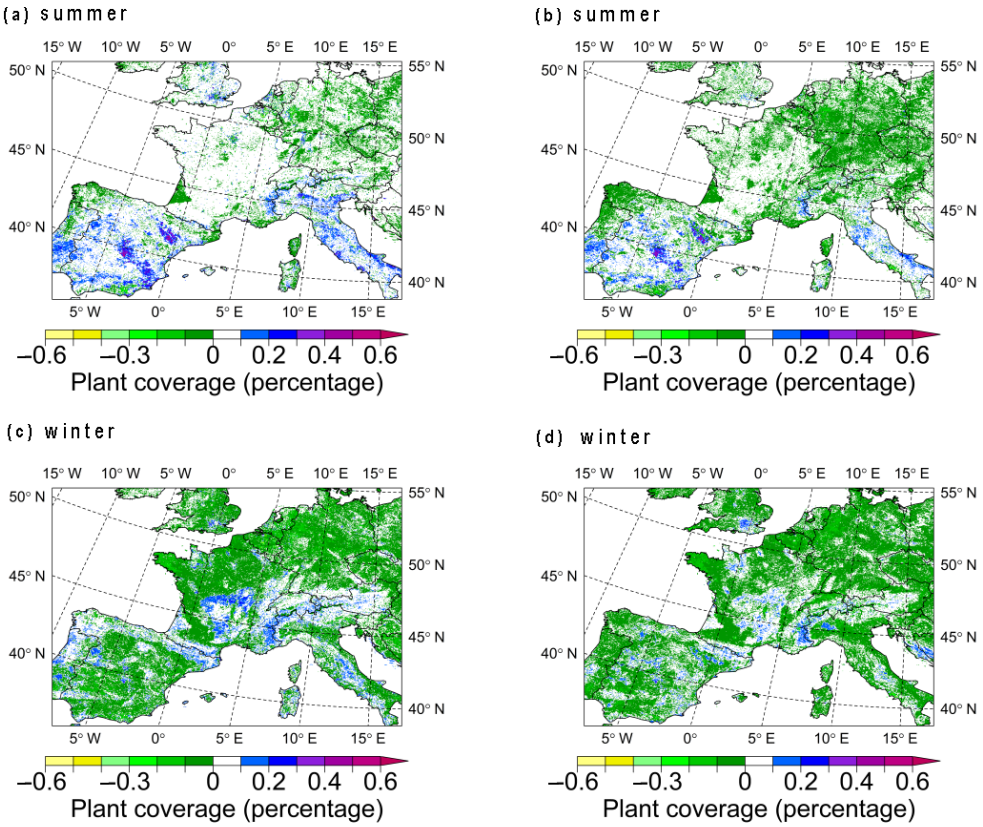

Figure 2.8. Winter and summer simulated plant coverage deviations with respect to GlobCover 2009: (a) ESACCI-LC summer, (b) GLC2000 summer, (c) ESACCI-LC winter, and (d) GLC2000 winter.

Table 2.8. Statistical significance test results (t-value) of the plant cover differences between two land cover data sets and GlobCover 2009. Results lower than the critical t-value (1.960) are marked with * and are in bold.

	Summer		Winter	
***t*-value**	**ESACCI-LC**	**GLC2000**	**ESACCI-LC**	**GLC2000**
Southern England	**–27.7 ***	**–23.2 ***	4.5	**–64.2 ***
Germany	**–3.9 ***	10.2	16.1	**–0.6 ***
France, Belgium, and the Netherlands	**–9.7 ***	22.6	**–9.9 ***	**–40.839 ***
Iberian Peninsula	**–1.5 ***	**–0.2 ***	10.7	**–14.9 ***
Switzerland/Austria	13.6	41.6	38.9	**–8.2 ***
Italy	17.4	38.8	25.6	2.3

2.4.4. Relationship between Differences in Land Cover Data Sets and Differences in the Simulated Temperature

In this section, we address the connections between different land cover maps/fraction effects and temperature, LAI, and plant coverage in the COSMO-CLM regional climate simulation. LAI and plant coverage influence the evapotranspiration levels, where a higher LAI or plant coverage lead to higher evapotranspiration and greater evaporation reduces the air temperature, evaporation cooling, due to energy absorption. To investigate how the differences between the land cover data sets (LAI and plant coverage) translate into the differences seen in the simulated temperature, we prepared a scatter plot between the differences in land cover data and the simulated results in summer (Figure 2.9 in Appendix B) and winter (Figure 2.9 in Appendix B) of ESACCI-LC vs. GlobCover 2009 and GLC2000 vs. GlobCover 2009. We can see that the temperature is affected more by the LAI in summer (Figure 2.9a,c) and winter (Figure 2.10a,c). In summer, the temperature shows a negative relationship between the differences in the LAI and differences in temperature. This means that an increase in LAI results in a temperature decrease in the COSMO-CLM output. In winter, this relationship is not as distinct as in summer but still follows the same pattern. The temperature does not react as much to plant coverage as to change in LAI during both seasons (Figures 2.9b,d and 2.10b,d). A slightly negative relationship between plant coverage and temperature is seen in the winter.

2.4.5. Impact of the Classification System and Land Cover Unifying Methodology

As mentioned earlier, the land cover maps are produced with different classification systems. These classification systems are categorized into supervised (human-guided) and unsupervised

(calculated by the software) (Jog and Dixit, 2016; Bernabé and Plaza, 2010). Different classification systems result in differences in land cover maps both in terms of fraction and distribution by using even the same source data. The sensitivity of COSMO-CLM to different land cover maps and fractions is related also to the classification systems used to produce them. Therefore, to study the impacts of different LC maps on regional climate simulation, we unified the legend of the three used LC maps. By unifying the legend, we can compare the differences without concerning the non-identical land cover type definition of three land cover maps.

Further, re-gridding the three land cover maps into the same target horizontal resolution by EXTPAR because the different spatial resolutions could also influence the simulation results.

2.5. Conclusions

In this study, we applied three different LC maps (GlobCover 2009, GLC2000, and ESACCI-LC) as the lower boundary input data to perform simulations with COSMO-CLM over a large part of Europe at a 3 km horizontal resolution. The analysis of air temperature, LAI and plant coverage showed that COSMO-CLM is sensitive to different LC maps and fractions. A comparison of the simulated temperature output shows that all simulations with the three different LC maps provided reliable results compared to the observational data. The analysis also showed that the LAI and plant coverage have different feedback based on different land cover types, especially over the areas with high diversity in LC fractions (over southern Germany, and the Alpine area) and density vegetation coverage (e.g., over the northern Iberian Peninsula). Nevertheless, the simulated results indicate different feedback to different LC maps and fractions in summer and winter. Generally, the model performed better for the winter compared to the summer. The different regional representations of COSMO-CLM also indicate that the soil moisture, atmospheric circulation, evaporative demand, elevation, and snow cover schemes are located in the frame of land cover impacts. A comprehensive study of all of these factors is important in terms of high accuracy in climate modeling.

This study indicated that different LC maps and different LC fractions, as lower boundaries of COSMO-CLM have significant impacts on the simulated air temperature, the LAI, and plant coverage. The questions raised in the introduction can be answered as follows:

- The seasonal temperature outputs of the COSMO-CLM based on these three data sets closely resemble the observations. Over most of the research domain, according to the temperature anomaly comparison with observational data, all three LC maps provided reliable COSMO-CLM simulation results. While over the Alpine area, the results showed higher deviation (differences of –3 to +3 K), further studies are needed to investigate the effects of soil moisture and orography on temperature.
- The simulated temperature is sensitive to different land cover maps and fractions. The temperature shows higher dependence on land cover fractions in summer compared to winter.
- Different LC maps affect the LAI, as well as the plant coverage. The regional and local simulation results responded differently towards the land cover maps and fractions. The area covered by forest with a heterogeneous land cover combination showed high sensitivities related to different land cover maps.
- The COSMO-CLM output did not show a corresponding difference in the LC fraction. In our experiments, GLC2000 and ESACCI-LC showed similar LC fractions compared to GlobCover 2009, but the COSMO-CLM output showed greater similarity between ESACCI-LC and GlobCover 2009. This suggests that we not only need to check the differences in LC fraction but also the differences in LC distribution, and this will be the next step of our research.

In future studies, we will analyze how heterogeneous land cover types and seasonal land cover types affect climate and will also assess the role of land cover in regional climate modeling. Furthermore, how to select the appropriate land cover maps is in the scope of the study. Investigating how regional climate sensitively responds to different land cover distributions is necessary.

Author Contributions

Conceptualization: M.Z., M.H.T., and J.L.; methodology: M.Z., M.H.T. and J.L.; software development: M.Z., M.H.T., and E.H.; validation: M.Z.; analysis and statistical evaluation: M.Z., M.H.T., E.X., and J.L.; writing process and interpretation of results: all authors. All authors have read and agreed to the published version of the manuscript.

Acknowledgments

Computational resources were made available by the German Climate Computing Center (DKRZ) through support from the Federal Ministry of Education and Research in Germany (BMBF). We acknowledge the support of the German Weather Service, the ESA Climate Change Initiative—Land Cover led by UCLouvain (2017), ESA 2010, and UCLouvain, website: {http://due.esrin.esa.int/page_globcover.php}{ESA DUE GlobCover}, accessed on 17 December 2019, Global Land Cover 2000 database. European Commission, Joint Research Centre 2003 for supplying the research data and software which we have used in this paper. The SPOT/PROBA-V LAI data product was generated by the land service of Copernicus, the Earth Observation programme of the European Commission. The research leading to the current version of the LAI product has received funding from various European Commission Research and Technical Development programmes. The product is based on SPOT/VGT 1 km data ((c) CNES/PROBA-V 1 km data ((c) ESA and distributed by VITO) last access date: 28/9/2018. This research was funded by the German Research Foundation (DFG), grant number 401857120. The authors acknowledge Jürgen Helmert (German Met Office) for his important input to the different sections.

Conflicts of Interest:

The authors declare no conflict of interest.

Appendix A. Abbreviations

LC: Land Cover

GLC2000: Global Land Cover Map for the year 2000

JRC: Joint Research Center

COSMO: Consortium for Small-scale Modeling

CCLM: COSMO model in Climate Mode

PFTs: Plant Function Types

ESA: European Space Agency

CCI: Climate Change Initiative

EO: Earth Observation

UNFCCC: United Nations Framework Convention on Climate Change

GCS: Geographic Coordinate System

NWP: Numerical Weather Prediction

EXTPAR: External Parameter for Numerical Weather Prediction and Climate Application

WCRP: World Climate Research Programme

CORDEX: Coordinated Regional Downscaling Experiment

CDD: Consecutive Dry-Day

DKRZ: German Climate Computing Center

MBE: Mean Bias Error

Appendix B. Figures

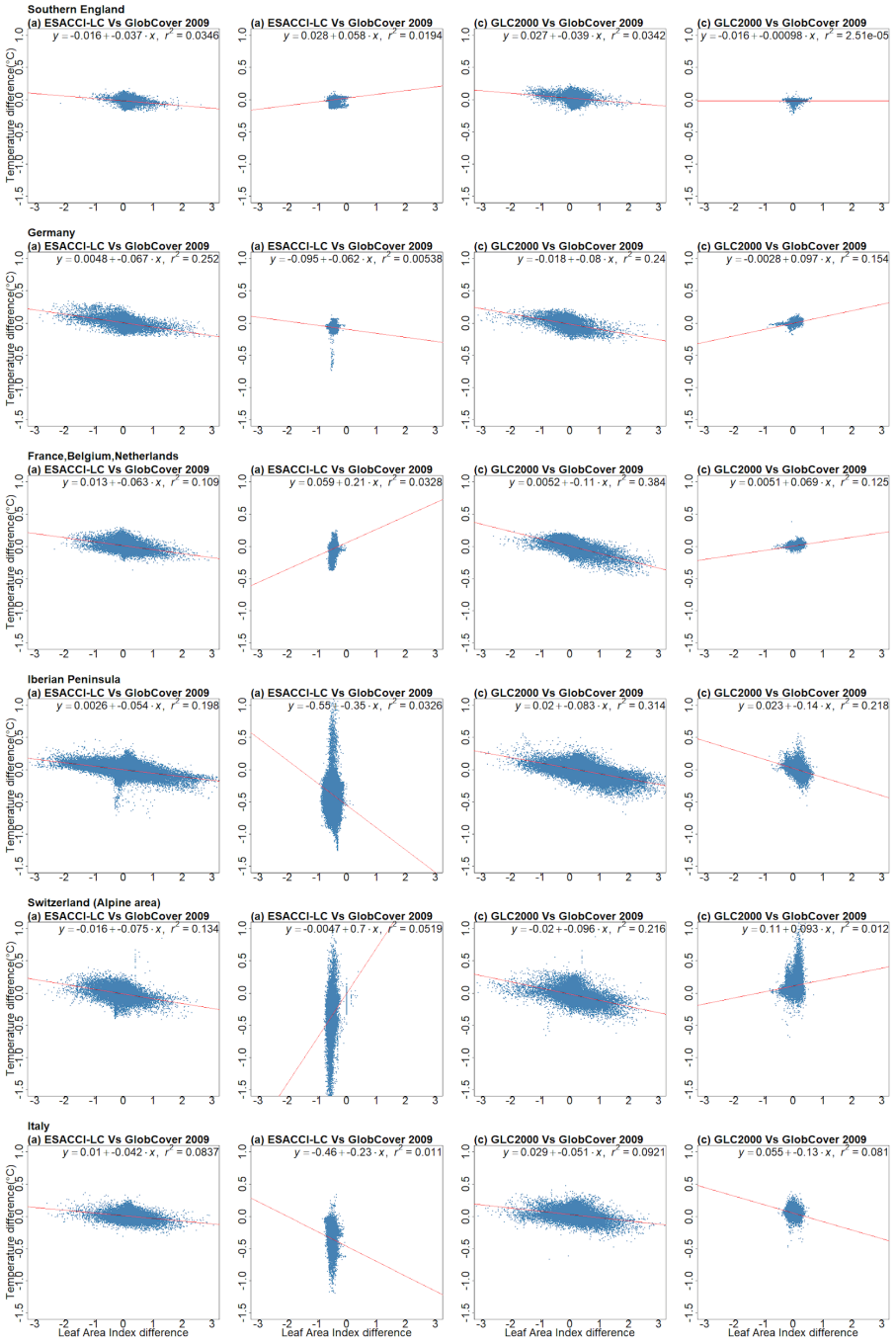

Figure 2.9. (a) LAI differences between land cover ESACCI-LC and GlobCover 2009 vs. temperature differences of ESACCI-LC and GlobCover 2009 in summer. (b) LAI differences between land cover ESACCI-LC and GlobCover 2009 vs. temperature differences of ESACCI-LC and GlobCover 2009 in winter. (c) LAI differences between land cover GLC2000 and GlobCover 2009 vs. temperature differences of GLC2000 and GlobCover 2009 in summer. (d) LAI differences between land cover GlC2000 and GlobCover 2009 vs. temperature differences of GLC2000 and GlobCover 2009 in winter.

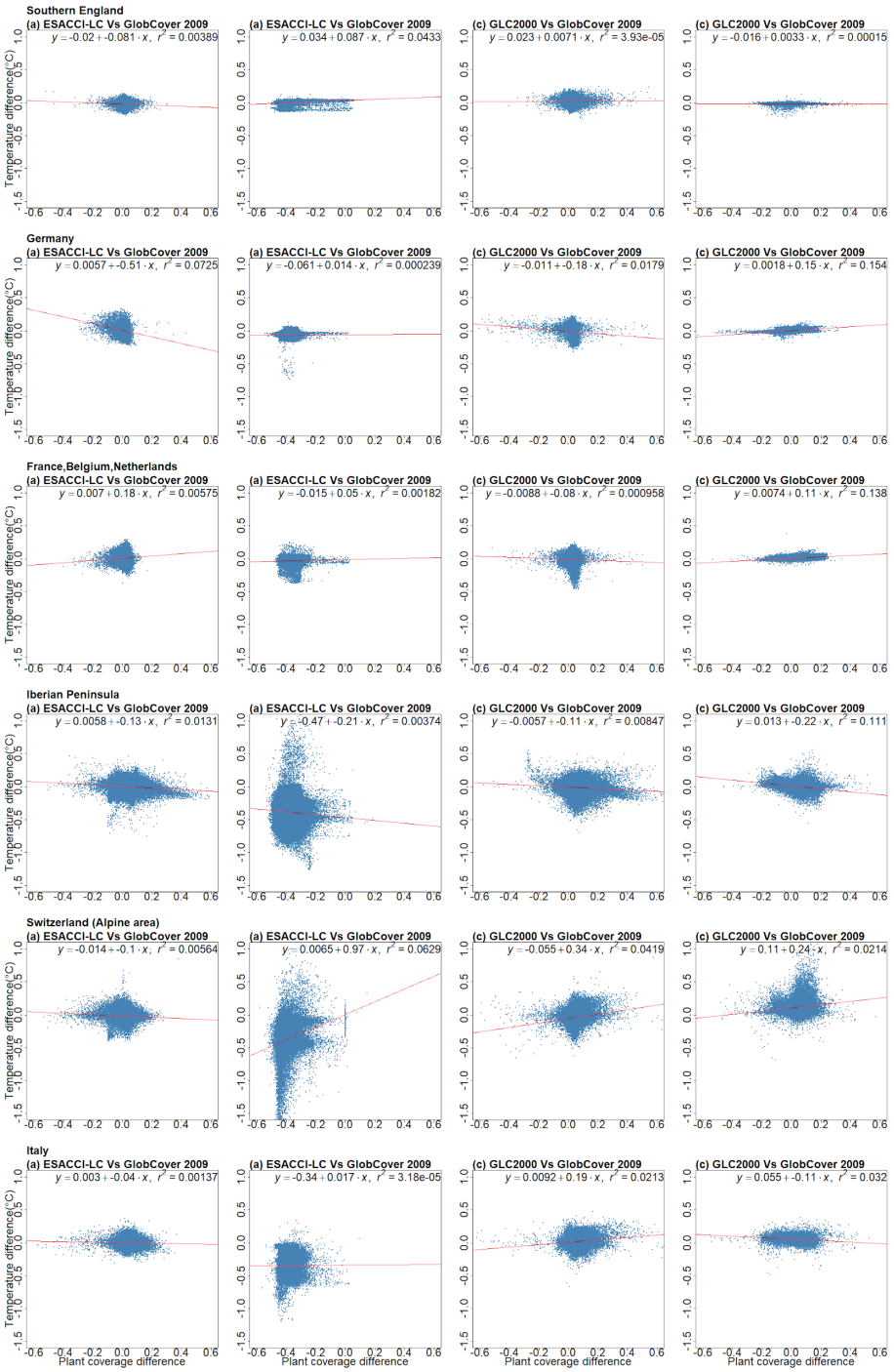

Figure 2.10. (a) Plant coverage differences between land cover ESACCI-LC and GlobCover 2009 vs. temperature differences of ESACCI-LC and GlobCover 2009 in summer. (b) Plant coverage differences between land cover ESACCI-LC and GlobCover 2009 vs. temperature difference of ESACCI-LC and GlobCover 2009 in winter. (c) Plant coverage differences between land cover GLC2000 and GlobCover 2009 vs. temperature difference of GLC2000 and GlobCover 2009 in summer. (d) Plant coverage differences between land cover GLC2000 and GlobCover 2009 vs. temperature differences of GLC2000 and GlobCover 2009 in winter.

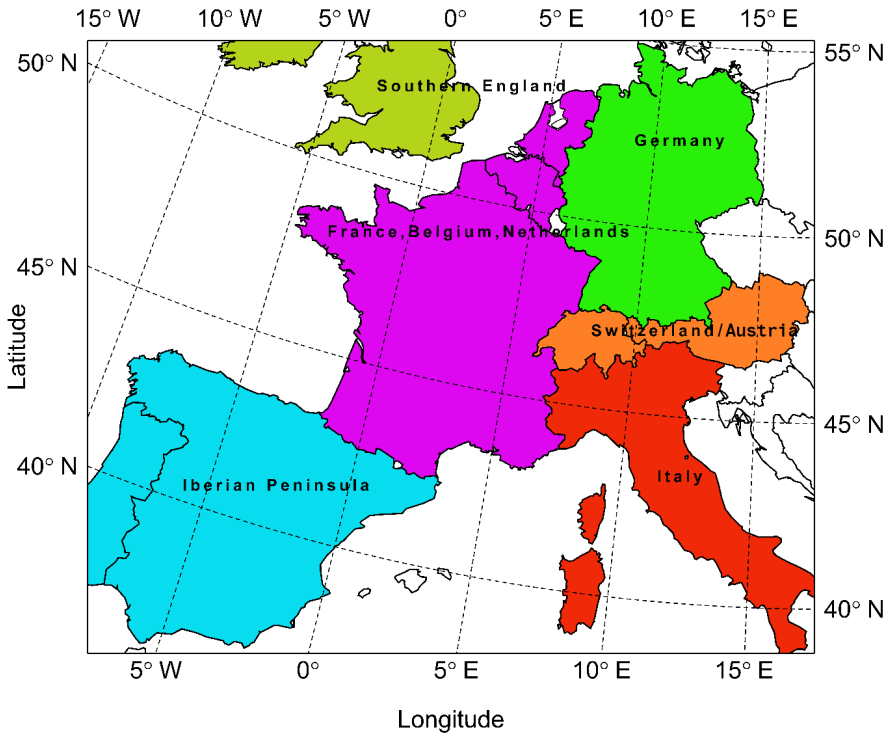

Figure 2.11. Six sub-domains used in the LAI and plant cover analysis.

Appendix C. Tables

Table 2.9: Landcover Transfer Table.

Value of LC (ESACCI-LC)	Land Cover Type of ESACCI-LC	Value of LC (GlobCover 2009) GlobCover LC Type/ESACCI LC Type	Land Cover Type of GlobCover 2009	Value of LC (GLC2000)	Land Cover Type of GLC2000
10	Cropland, rainfed	14/2	Rainfed croplands	16	cultivated and managed areas
11	Herbaceous cover				
12	Tree or shrub cover				
20	Cropland, irrigated or post-flooding	11/1	irrigated croplands	16	cultivated and managed areas
30	Mosaic cropland (>50%)/natural vegetation (tree, shrub, herbaceous cover) (<50%)	20/3	mosaic cropland (50–70%)—vegetation (20–50%)	17	mosaic crop/tree/natural vegetation
40	Mosaic natural vegetation (tree, shrub, herbaceous cover) (>50%)/cropland (<50%)	30/4	mosaic vegetation (50–70%)—cropland (20–50%)	18	mosaic crop/shrub or grass
50	Tree cover, broadleaved, evergreen, closed to open (>15%)	40/5	closed broadleaved evergreen forest	1	evergreen broadleaf tree
60	Tree cover, broadleaved, deciduous, closed to open (>15%)	50/6	closed broadleaved deciduous forest	2	deciduous broadleaf tree closed
61	Tree cover, broadleaved, deciduous, closed (>40%)				

62	Tree cover, broadleaved, deciduous, open (15–40%)	60/7	Open broadleaved deciduous forest	3	deciduous broadleaf tree open
70	Tree cover, needleleaved, evergreen, closed to open (>15%)	70/8	Closed (>40%) needleleaved evergreen forest (>5 m)	4	evergreen needleleaf tree
71	Tree cover, needleleaved, evergreen, closed (>40%)				
72	Tree cover, needleleaved, evergreen, open (15–40%)	90/9 Open (15–40%) needleleaved deciduous or evergreen forest (>5 m)		5 deciduous needleleaf tree	
80	Tree cover, needleleaved, deciduous, closed to open (>15%)				
81	Tree cover, needleleaved, deciduous, closed (>40%)				
82	Tree cover, needleleaved, deciduous, open (15–40%)				
90	Tree cover, mixed leaf type (broadleaved and needleleaved)	100/10	mixed broadleaved and needleleaved forest	6	mixed leaf tree
100	Mosaic tree and shrub (>50%) / herbaceous cover (<50%)	110/11	Mosaic Forest/Shrubland (50–70%)/Grassland (20–50%)	11	evergreen shrubs closed-open
110	Mosaic herbaceous cover (>50%) / tree and shrub (<50%)	120/12	Mosaic Grassland (50–70%) / Forest/Shrubland (20–50%)	9	mosaic tree / other natural vegetation
120	Shrubland	130/13	Closed to open (>15%) shrubland (<5 m)	12	deciduous shrubs closed-open
121	Evergreen shrubland				
122	Deciduous shrubland				
130	Grassland	140/14	Closed to open (>15%) grassland	13	herbaceous cover closed-open
140	Lichens and mosses	150/15	Sparse (>15%) vegetation (woody vegetation, shrubs, grassland)	14	sparse herbaceous or grass
150	Sparse vegetation (tree, shrub, herbaceous cover) (<15%)				
152	Sparse shrub (<15%)				
153	Sparse herbaceous cover (<15%)				
160	Tree cover, flooded, fresh or brakish water	160/16	closed to open forest regulary flooded	7	fresh water flooded tree
170	Tree cover, flooded, saline water	170/17	closed forest or shrubland permanently flooded	8	saline water flooded tree
180	Shrub or herbaceous cover, flooded, fresh/saline/brackish water	180/18	Closed to open grassland regularly flooded	15	flooded shrub or herbaceous
190	Urban areas	190/19	Artificial surfaces	22	artificial surfaces
200	Bare areas	150/15	Sparse (>15%) vegetation (woody vegetation, shrubs, grassland)	14	sparse herbaceous or grass
201	Consolidated bare areas				
202	Unconsolidated bare areas				
210	Water bodies	210/21	Water bodies	20	water bodies
220	Permanent snow and ice	220/22	Permanent snow and ice	21	snow and ice
230	undefined	230/23	undefined	23	undefined

References

Wang, S.; Kang, S.; Zhang, L.; Li, F. Modelling Hydrological Response to Different Land-Use and Climate Change Scenarios in the Zamu River Basin of Northwest China. Hydrol. Process. Int. J. 2008, 22, 2502–2510.

Betts, R.A.; Falloon, P.D.; Goldewijk, K.K.; Ramankutty, N. Biogeophysical Effects of Land Use on Climate: Model Simulations of Radiative Forcing and Large-Scale Temperature Change. Agric. For. Meteorol. 2007, 142, 216–233.

Wramneby, A.; Smith, B.; Samuelsson, P. Hot Spots of Vegetation-Climate Feedbacks under Future Greenhouse Forcing in Europe. J. Geophys. Res. Atmos. 2010, 115, D21119.

Arora, V.K.; Montenegro, A. Small Temperature Benefits Provided by Realistic Afforestation Efforts. Nat. Geosci. 2011, 4, 514–518.

Davin, E.L.; Rechid, D.; Breil, M.; Cardoso, R.M.; Coppola, E.; Hoffmann, P.; Jach, L.L.; Katragkou, E.; de Noblet-Ducoudré, N.; Radtke, K.; et al. Biogeophysical Impacts of Forestation in Europe: First Results from the LUCAS (Land Use and Climate across Scales) Regional Climate Model Intercomparison. Earth Syst. Dyn. 2020, 11, 183–200. https://doi.org/10.5194/esd-11-183-2020.

Steiner, A.L.; Pal, J.S.; Rauscher, S.A.; Bell, J.L.; Diffenbaugh, N.S.; Boone, A.; Sloan, L.C.; Giorgi, F. Land Surface Coupling in Regional Climate Simulations of the West African Monsoon. Clim. Dyn. 2009, 33, 869–892.

Lu, L.; Pielke, R.A., Sr.; Liston, G.E.; Parton, W.J.; Ojima, D.; Hartman, M. Implementation of a Two-Way Interactive Atmospheric and Ecological Model and Its Application to the Central United States. J. Clim. 2001, 14, 900–919.

Davin, E.L.; Stöckli, R.; Jaeger, E.B.; Levis, S.; Seneviratne, S.I. COSMO-CLM2: A New Version of the COSMO-CLM Model Coupled to the Community Land Model. Clim. Dyn. 2011, 37, 1889–1907. https://doi.org/10.1007/s00382-011-1019-z.

Pielke, R.A.; Avissar, R.; Raupach, M.; Dolman, A.J.; Zeng, X.; Denning, A.S. Interactions between the Atmosphere and Terrestrial Ecosystems: Influence on Weather and Climate. Glob. Chang. Biol. 1998, 4, 461–475.

Betts, R. Implications of Land Ecosystem-Atmosphere Interactions for Strategies for Climate Change Adaptation and Mitigation. Tellus B Chem. Phys. Meteorol. 2007, 59, 602–615.

Avissar, R.; Pielke, R.A. The Impact of Plant Stomatal Control on Mesoscale Atmospheric Circulations. Agric. For. Meteorol. 1991, 54, 353–372. https://doi.org/10.1016/0168-1923(91)90013-G.

Bonan, G.B.; Levis, S.; Kergoat, L.; Oleson, K.W. Landscapes as Patches of Plant Functional Types: An Integrating Concept for Climate and Ecosystem Models. Glob. Biogeochem. Cycles 2002, 16, 5-1–5-23.

Feddema, J.J.; Oleson, K.W.; Bonan, G.B.; Mearns, L.O.; Buja, L.E.; Meehl, G.A.; Washington, W.M. The Importance of Land-Cover Change in Simulating Future Climates. Science 2005, 310, 1674–1678.

Luca, A.D.; Argüeso, D.; Evans, J.P.; de Elía, R.; Laprise, R. Quantifying the Overall Added Value of Dynamical Downscaling and the Contribution from Different Spatial Scales. J. Geophys. Res. Atmos. 2016, 121, 1575–1590. https://doi.org/10.1002/2015JD024009.

Pitman, A.J. The Evolution of, and Revolution in, Land Surface Schemes Designed for Climate Models. Int. J. Climatol. J. R. Meteorol. Soc. 2003, 23, 479–510.

Brovkin, V.; Sitch, S.; Von Bloh, W.; Claussen, M.; Bauer, E.; Cramer, W. Role of Land Cover Changes for Atmospheric CO2 Increase and Climate Change during the Last 150 Years. Glob. Chang. Biol. 2004, 10, 1253–1266.

Seneviratne, S.I.; Corti, T.; Davin, E.L.; Hirschi, M.; Jaeger, E.B.; Lehner, I.; Orlowsky, B.; Teuling, A.J. Investigating Soil Moisture–Climate Interactions in a Changing Climate: A Review. Earth-Sci. Rev. 2010, 99, 125–161.

Stéfanon, M.; Schindler, S.; Drobinski, P.; de Noblet-Ducoudré, N.; Andrea, F.D. Simulating the Effect of Anthropogenic Vegetation Land Cover on Heatwave Temperatures over Central France. Clim. Res. 2014, 60, 133–146.

Giorgi, F.; Mearns, L.O. Approaches to the Simulation of Regional Climate Change: A Review. Rev. Geophys. 1991, 29, 191–216.

Tölle, M.H.; Gutjahr, O.; Busch, G.; Thiele, J.C. Increasing Bioenergy Production on Arable Land: Does the Regional and Local Climate Respond? Germany as a Case Study. J. Geophys. Res. Atmos. 2014, 119, 2711–2724. https://doi.org/10.1002/2013JD020877.

Torma, C.; Giorgi, F.; Coppola, E. Added Value of Regional Climate Modeling over Areas Characterized by Complex Terrain—Precipitation over the Alps. J. Geophys. Res. Atmos. 2015, 120, 3957–3972. https://doi.org/10.1002/2014JD022781.

Alestalo, M. The Energy Budget of the Earth–Atmosphere System in Europe. Tellus 1981, 33, 360–371.

Jacob, D.; Petersen, J.; Eggert, B.; Alias, A.; Christensen, O.; Bouwer, L.; Braun, A.; Colette, A.; Déqué, M.; Georgievski, G.; et al. EURO-CORDEX: New High-Resolution Climate Change Projections for European Impact Research. Reg. Environ. Chang. 2014, 14, 563–578. https://doi.org/10.1007/s10113-013-0499-2.

Kotlarski, S.; Keuler, K.; Christensen, O.B.; Colette, A.; Déqué, M.; Gobiet, A.; Goergen, K.; Jacob, D.; Lüthi, D.; van Meijgaard, E.; et al. Regional Climate Modeling on European Scales: A Joint Standard Evaluation of the EURO-CORDEX RCM Ensemble. Geosci. Model Dev. 2014, 7, 1297–1333. https://doi.org/10.5194/gmd-7-1297-2014.

Diffenbaugh, N.S. Atmosphere-Land Cover Feedbacks Alter the Response of Surface Temperature to CO2 Forcing in the Western United States. Clim. Dyn. 2005, 24, 237–251.

Foley, J.A.; Levis, S.; Prentice, I.C.; Pollard, D.; Thompson, S.L. Coupling Dynamic Models of Climate and Vegetation. Glob. Chang. Biol. 1998, 4, 561–579. https://doi.org/10.1046/j.1365-2486.1998.t01-1-00168.x.

Yokohata, T.; Kinoshita, T.; Sakurai, G.; Pokhrel, Y.; Ito, A.; Okada, M.; Masaki, T.I.; Nishimori, M.; Hanasaki, N.; Takahashi, K. MIROC-INTEG1: A Global Bio-Geochemical Land Surface Model with Human Water Management, Crop Growth, and Land-Use Change. Geosci. Model Dev. Discuss. 2019. https://doi.org/10.5194/gmd-2019-184.

Tölle, M.H.; Engler, S.; Panitz, H.-J. Impact of Abrupt Land Cover Changes by Tropical Deforestation on Southeast Asian Climate and Agriculture. J. Clim. 2016, 30, 2587–2600. https://doi.org/10.1175/JCLI-D-16-0131.1.

Wilhelm, M.; Davin, E.L.; Seneviratne, S.I. Climate Engineering of Vegetated Land for Hot Extremes Mitigation: An Earth System Model Sensitivity Study. J. Geophys. Res. Atmos. 2015, 120, 2612–2623. https://doi.org/10.1002/2014JD022293.

Fosser, G.; Khodayar, S.; Berg, P. Benefit of Convection Permitting Climate Model Simulations in the Representation of Convective Precipitation. Clim. Dyn. 2015, 44, 45–60. https://doi.org/10.1007/s00382-014-2242-1.

Pal, S.; Chang, H.-I.; Castro, C.L.; Dominguez, F. Credibility of Convection-Permitting Modeling to Improve Seasonal Precipitation Forecasting in the Southwestern United States. 2019, 7, 11. https://doi.org/10.3389/feart.2019.00011.

Meredith, E.P.; Ulbrich, U.; Rust, H.W.; Truhetz, H. Present and Future Diurnal Hourly Precipitation in 0.11° EURO-CORDEX Models and at Convection-Permitting Resolution. Environ. Res. Commun. 2021, 3, 055002. https://doi.org/10.1088/2515-7620/abf15e.

Breil, M.; Rechid, D.; Davin, E.L.; de Noblet-Ducoudré, N.; Katragkou, E.; Cardoso, R.M.; Hoffmann, P.; Jach, L.L.; Soares, P.M.M.; Sofiadis, G.; et al. The Opposing Effects of Reforestation and Afforestation on the Diurnal Temperature Cycle at the Surface and in the Lowest Atmospheric Model Level in the European Summer. J. Clim. 2020, 33, 9159–9179. https://doi.org/10.1175/JCLI-D-19-0624.1.

Heck, P.; Lüthi, D.; Wernli, H.; Schär, C. Climate Impacts of European-Scale Anthropogenic Vegetation Changes: A Sensitivity Study Using a Regional Climate Model. J. Geophys. Res. Atmos. 2001, 106, 7817–7835.

Garnaud, C.; Sushama, L.; Verseghy, D. Impact of Interactive Vegetation Phenology on the Canadian RCM Simulated Climate over North America. Clim. Dyn. 2015, 45, 1471–1492. https://doi.org/10.1007/s00382-014-2397-9.

Wouters, H.; Varentsov, M.; Blahak, U.; Schulz, J.-P.; Schattler, U.; Bucchignani, E.; Demuzere, M. User Guide for TERRA URB v2.2: The Urban-Canopy Land-Surface Scheme of the COSMO Model. 12p. Available online: http://cosmo-model.cscs.ch/content/tasks/workGroups/wg3b/docs/terra_urb_user.pdf (accessed on 24 November 2021).

GLOBCOVER Products Description and Validation Report. Available online: https://www.researchgate.net/profile/O_Arino/publication/260137807_GLOBCOVER_products_description_and_validation_report/links/576bf8a808aef0e50da8a271/GLOBCOVER-products-description-and-validation-report.pdf (accessed on 25 May 2020).

Arino, O.; Perez, J.R.; Kalogirou, V.; Defourny, P.; Achard, F. GlobCover 2009. Available online: https://epic.awi.de/id/eprint/31046/1/Arino_et_al_GlobCover2009-a.pdf (accessed on 25 May 2020).

Yin, K.; Xu, S.; Zhao, Q.; Huang, W.; Yang, K.; Guo, M. Effects of Land Cover Change on Atmospheric and Storm Surge Modeling during Typhoon Event. Ocean Eng. 2020, 199, 106971. https://doi.org/10.1016/j.oceaneng.2020.106971.

Zhong, Y.; Luo, C.; Hu, X.; Wei, L.; Wang, X.; Jin, S. Cropland Product Fusion Method Based on the Overall Consistency Difference: A Case Study of China. Remote Sens. 2019, 11, 1065. https://doi.org/10.3390/rs11091065.

Bartholomé, E.; Belward, A.S. GLC2000: A New Approach to Global Land Cover Mapping from Earth Observation Data. Int. J. Remote. Sens. 2005, 26, 1959–1977. Available online: https://www.tandfonline.com/doi/abs/10.1080/01431160412331291297 (accessed on 25 May 2020).

Lamarche, C.; Santoro, M.; Bontemps, S.; D'Andrimont, R.; Radoux, J.; Giustarini, L.; Brockmann, C.; Wevers, J.; Defourny, P.; Arino, O. Compilation and Validation of SAR and Optical Data Products for a Complete and Global Map of Inland/Ocean Water Tailored to the Climate Modeling Community. Remote Sens. 2017, 9, 36. https://doi.org/10.3390/rs9010036.

Bounoua, L.; DeFries, R.; Collatz, G.J.; Sellers, P.; Khan, H. Effects of Land Cover Conversion on Surface Climate. Clim. Chang. 2002, 52, 29–64.

Rauthe, M.; Steiner, H.; Riediger, U.; Mazurkiewicz, A.; Gratzki, A. A Central European Precipitation Climatology—Part I: Generation and validation of a high-resolution gridded daily data set (HYRAS). Meteorol. Z. 2013, 22, 235–256.

Tiedtke, M. Parameterization of Cumulus Convection in Large-Scale Models. In Physically-Based Modelling and Simulation of Climate and Climatic Change: Part 1; Schlesinger, M.E., Ed.; NATO ASI Series; Springer: Dordrecht, The Netherlands, 1988; pp. 375–431, ISBN 978-94-009-3041-4.

Rockel, B.; Will, A.; Hense, A. Regional Climate Modelling with COSMO-CLM (CCLM). Meteorol. Z. 2008, 17, 347–348.

Schulz, J.-P.; Vogel, G.; Becker, C.; Kothe, S.; Rummel, U.; Ahrens, B. Evaluation of the Ground Heat Flux Simulated by a Multi-Layer Land Surface Scheme Using High-Quality Observations at Grass Land and Bare Soil. Meteorol. Z. 2016, 25, 607–620. https://doi.org/10.1127/metz/2016/0537.

Ritter, B.; Geleyn, J.-F. A Comprehensive Radiation Scheme for Numerical Weather Prediction Models with Potential Applications in Climate Simulations. Mon. Weather Rev. 1992, 120, 303–325. https://doi.org/10.1175/1520-0493(1992)120<0303:ACRSFN>2.0.CO;2.

Young, K.C. A Numerical Simulation of Wintertime, Orographic Precipitation: Part I. Description of Model Microphysics and Numerical Techniques. J. Atmos. Sci. 1974, 31, 1735–1748. https://doi.org/10.1175/1520-0469(1974)031<1735:ANSOWO>2.0.CO;2.

Smiatek, G.; Rockel, B.; Schättler, U. Time Invariant Data Preprocessor for the Climate Version of the COSMO Model (COSMO-CLM). Meteorol. Z. 2008, 17, 395–405. https://doi.org/10.1127/0941-2948/2008/0302.

Smiatek, G.; Helmert, J.; Gerstner, E.-M. Impact of Land Use and Soil Data Specifications on COSMO-CLM Simulations in the CORDEX-MED Area. Meteorol. Z. 2016, 25, 215–230. https://doi.org/10.1127/metz/2015/0594.

Asensio, H.; Messmer, M. External Parameters for Numerical Weather Prediction and Climate Application EXTPAR v5_0: User and Implementation Guide. 45p. Available online: http://www.cosmo-model.org/content/support/software/ethz/EXTPAR_user_and_implementation_manual_202003.pdf (accessed on 24 November 2021).

Dee, D.P.; Uppala, S.M.; Simmons, A.J.; Berrisford, P.; Poli, P.; Kobayashi, S.; Andrae, U.; Balmaseda, M.A.; Balsamo, G.; Bauer, D.P. The ERA-Interim Reanalysis: Configuration and Performance of the Data Assimilation System. Q. J. R. Meteorol. Soc. 2011, 137, 553–597. https://doi.org/10.1002/qj.828.

Welch, B.L. The Generalization of 'Student's' Problem When Several Different Population Variances Are Involved. Biometrika 1947, 34, 28–35. https://doi.org/10.2307/2332510.

Hartmann, E.; Schulz, J.-P.; Seibert, R.; Schmidt, M.; Zhang, M.; Luterbacher, J.; Tölle, M.H. Impact of Environmental Conditions on Grass Phenology in the Regional Climate Model COSMO-CLM. Atmosphere 2020, 11, 1364. https://doi.org/10.3390/atmos11121364.

Jog, S.; Dixit, M. Supervised Classification of Satellite Images. In Proceedings of the 2016 Conference on Advances in Signal Processing (CASP), Pune, India, 9–11 June 2016; pp. 93–98.

Bernabé, S.; Plaza, A. A New System to Perform Unsupervised and Supervised Classification of Satellite Images from Google Maps. In Satellite Data Compression, Communications, and Processing VI; SPIE: Bellingham, WA, USA, 2010; Volume 7810, pp. 261–270.

3. Regional paleoclimate simulation over the Nile River basin: a model evaluation

An extend abstract for publication in the proceeding of Recent Advances in Environmental Science from the Euro-Mediterranean and Surrounding Regions (3rd Edition).

Mingyue Zhang[1], Eva Hartmann[1], Elena Xoplaki[1, 3], Sebastian Wagner[2]

[1] Department of Geography, Climatology, Climate Dynamics and Climate Change, Justus-Liebig University Giessen, Giessen, Germany

[2] HZG: Helmholtz-Zentrum Geesthacht

[3] Center for international Development and Environmental Research, Justus Liebig University Giessen, Giessen, Germany

mingyue.zhang@geogr.uni-giessen.de

Abstract

The Nile Basin has been the focus of research on the links between climate variability, extreme events and social events over the last 2000 years of history. Un-fortunately, we currently only have global climate and Earth system model data with low spatial resolution for this period. To understand how climate affects society, we must rely on proxy data, as global climate models lack the necessary regional process detail. Our goal is to enhance our understanding of the historical climate of the Nile Basin on a regional scale using the customized COSMO-CLM paleoclimate model. We intend to run simulations with COSMO-CLM (forced by MPI-ESM-LR) by using the "past2k" simulation set up with an optimized configuration for both the present (1979-2019 CE) and paleo periods (500-2000 BCE). at resolutions of around 50 km and 12 km. In this approach, we tried to systematically consider orbital, solar, and volcanic influences, as well as changes in vegetation, land use, and greenhouse gas concentrations in the simulation. We found that the temperature simulations are overall in agreement with the reanalysis data and the observational record. However, it is worth noting that our precipitation simulations performed relatively weakly, especially in the Nile basin.

Keywords: Paleoclimate, Nile basin, COSMO-CLM

3.1 Introduction

Over the past 2000 years, there has been a notable interests on the climate variations, extreme climate events, and their interactions with societal changes within the Nile River basin. The Nile River system and thus the water availability of the massive drainage basin that crosses different hydroclimate zones from the sources to the delta are affected by various atmospheric patterns. It is necessary to look at the regional Nile River basin atmospheric circulation in a higher horizontal resolution. Nevertheless, the impact of climate on societies is assessed mainly through the exist proxy records (such as lake sediments), lacking the detailed insights provided by regional climate model simulations with continuous temporal resolution and the specific atmospheric circulation patterns affecting this region. Recently, the examination of the current and future climate as well as the climate variability, within the Nile Basin is conducted within the MENA-CORDEX program, using various regional climate models (with a resolution ranging from 25 to 50 km). However, when it comes to studying the past climate, we are limited to global circulation model (GCM) or earth system model (ESM) simulations characterized by coarse horizontal resolutions, typically at a minimum of 100 kilometers spatial resolution. To study the past climate at the regional scale, regional climate models (RCM) are therefore needed, allowing a considerably increased horizontal resolution of up to 10 x 10 km. The MENA region has been identified as a hot spot for future climate change (Planton et al., 2012; Cramer et al., 2018; Zittis et al., 2021). To produce useful climate predictions and prepare adequate responses to the impact of climate change on these vulnerable and already impacted areas (Kelley et al., 2015), a better understanding of the past climate is of great importance. Our objective is to enhance our comprehension of the historical climate within the Nile River basin on a regional scale, achieved by employing a modified paleoclimate version of the COSMO-CLM.

To determine the optimal settings for the CCLM, test simulations were conducted for 2017-2018 in the study area. As indicated in Bucchignani et al. (2016), it has been found that the parameters regarding albedo and aerosols play a major role in reasonably simulate the climate over this area and may be the reason for significant biaes in comparison to observational data.

3.2 Data and Methods

3.2.1. ERA-Interim data sets

ERA-Interim, a globally atmospheric reanalysis data set, which is a reanalyzed and homogenized observation data and has been used in many different applications (such as model input, model evaluation). This dataset offers a remarkable horizontal resolution of 0.125°.

3.2.2 Model description

The COSMO-CLM (COnsortium for Small-scale MOdeling-CLimate Mode) is a limited area model that also has a climate version (Rockel et al., 2008). We planned several simulations, which are shown in Table 1. In Experiment Eval_44 (0.44°) and Eval_11_nest (0.11°), we used reanalysis data ERAInterim as the forcing data of COSMO-CLM, it is simulated from 1979 to 2019. While the Experiment Present_44 (0.44°) and Present_11_nest (0.11°) are forced by the "past2k" data generated by MPI-ESM. Further on, the fully forced MPI-ESM simulations at resolution 1.875 at the global scale is planned for BCE500 to CE2000. With this fully forced MPI-ESM data, a simulation at 0.44° horizontal resolution over the Nile River basin will be performed from BCE500 to CE2000. On the top of this, several simulations at 0.11° horizontal resolution will be performed over selected special period which has major volcanic eruptions, for example from 1220-1290, and 525 to 575. All the simulations are running under the German Climate Computing Center (Deutsches Klimarechenzentrum, DKRZ; https://www.dkrz.de/about-en/about-us?set_language=en&cl=en).

Table 3.1. Overview of the planned simulations

Experiments	Description	Resolution	Simulation years
Eval_44	Present climate–ERA Interim (finished)	0.44	1979-2019(40)
Eval_11_nest	Present climate–ERA Interim (finished)	0.11	1979-2019 (40)
Present_44	Present climate – MPI-ESM (finished)	0.44	1970-2000 (30)
Present_11_nest	Present climate – MPI-ESM (finished)	0.11	1970-2000 (30)
MPI-ESM_2021	MPI-ESM fully forced	1.875	1-2000(1999)

Transient_44	Transient – MPI-ESM	0.44	1-2000(1999)
Early_LIA_11_nest	Early_LIA– MPI-ESM	0.11	1220-1290(70)
LALIA_11_nest	LALIA– MPI-ESM	0.11	525-575(50)

3.3 Results and discussions

3.3.1 Annual cycle

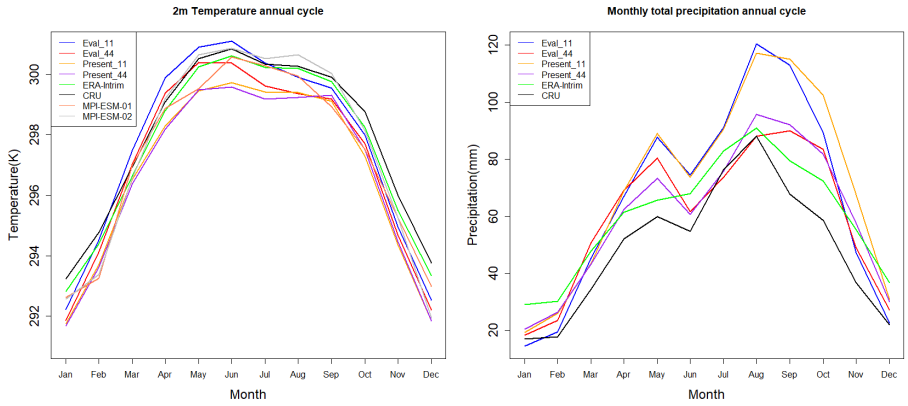

(a) (b)

Figure 3.1. Annual cycle of (a) 2m temperature and (b) precipitation.

From Fig. 3.1, we can see that the 2-meter temperature over the Nile basin are well simulated with COSMO-CLM both in 0.44 and 0.11° horizontal resolution, compare to the forcing data ERA-Interim and the observational data CRU (Climatic Research Unit). However, the 2-meter temperature shows better accordance in the 0.11° simulation, compared to the 0.44° simulation. Contrariwise, the precipitation shows better performance in the 0.44° simulation compared to the 0.11° simulation.

3.3.2 Temperature and Precipitation difference map

A difference map indicates "Model results" minus "Observation/reanalysis data". From the difference map (Fig. 3.2 and Fig. 3.3), we can see that both temperature and precipitation shows better result in summer (June, July and August) and winter (December, January and February), but higher bias in spring (March, April and May) and autumn (September, October and November)

compare to ERA-Interim. And the difference of the simulation compared to reanalysis data is up to +6k in the south of Nile River basin, and -6k in Ethiopia. This is accepted considering the complex atmospheric circulation over this region. The precipitation also shows higher bias in these region compared to other parts of the simulation area. We referenced to the MENA-CORDEX simulation, which is performed at 0.44° with COSMO-CLM also, it concludes that the simulated precipitation shows large range of variation in this region. In addition, when comparing the result of temperature and precipitation in both 0.11° and 0.44° separately, it suggests that there is a less significant added value of 0.11° simulation compared to 0.44°. Over the Ethiopia highland, the 0.11° simulation results show much higher variability compared to 0.44°. This might relate to the orography procedure in COSMO-CLM, for example, the Ethiopian Highlands and the East African Plateau have high elevations and have a large impact on the regional climate.

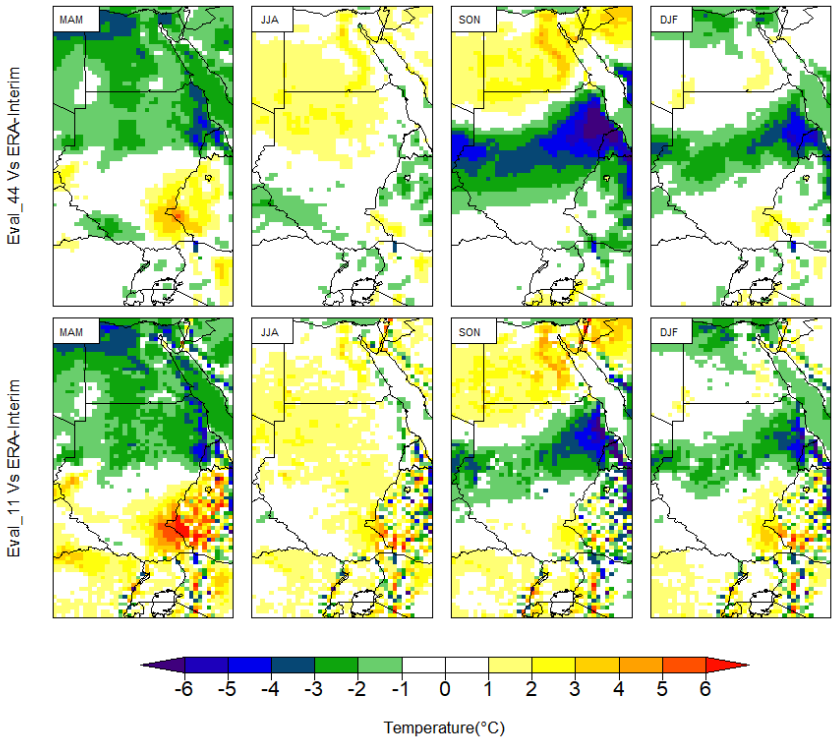

Figure 3.2. Seasonal 2m temperature difference map of Eval_44 (upper panel) and Eval_11 (lower panel) compared to ERA-Interim.

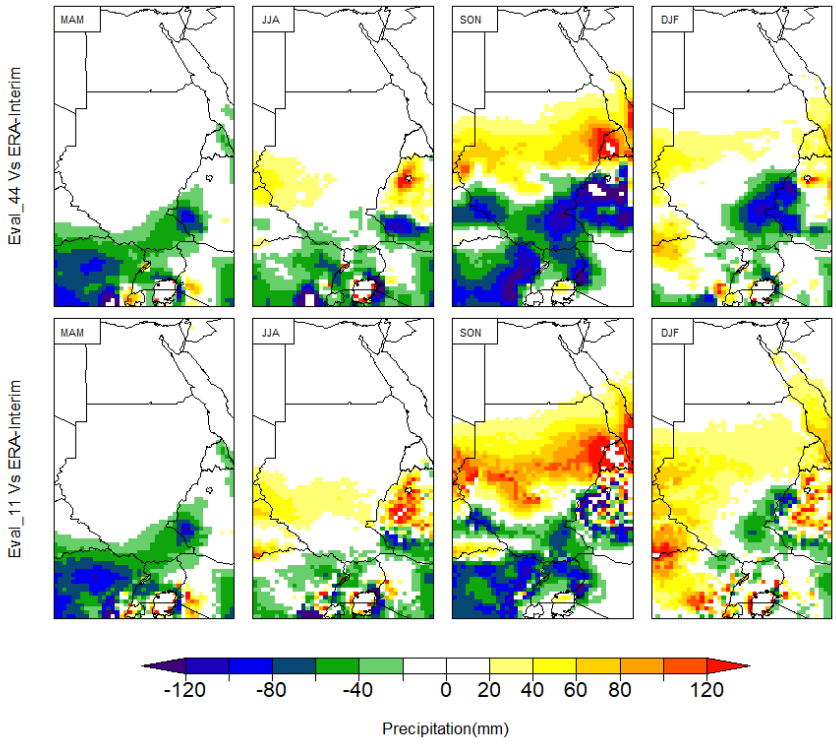

Figure 3.3. Seasonal precipitation difference map of Eval_44 (upper panel) and Eval_11 (lower panel) compare to ERA-Interim.

3.4 Conclusions

In this study, we performed several simulations over the Nile River basin with COSMO-CLM to identify the optimum settings for the Paleoclimate aspects. The present day simulations show that the temperature and precipitation are reasonably simulated compared to reanalysis and observational data in general, despite that in some region, there is high variability. This is understandable, considering the complex atmosphere circulation over this region.

Nevertheless, further evaluation is necessary, for instance, statistical index can be calculated to in order to deeply analysis the simulation results. Additionally, if the CCLM correctly captured convection and cloud cover in the greater southern areas of the domain which affected by the tropical convection is needed.

Moreover, the local climate appears to be markedly influenced by factors such as orography and land-sea interactions, potentially resulting in disagreements when compared to observational data. These could be closely studied under specific spatial resolution in future research.

References

Cramer, W., Guiot, J., Fader, M., Garrabou, J., Gattuso, J.-P., Iglesias, A., Lange, M. A., Lionello, P., Llasat, M. C., Paz, S., Peñuelas, J., Snoussi, M., Toreti, A., Tsimplis, M. N., and Xoplaki, E.: Climate change and interconnected risks to sustainable development in the Mediterranean, Nature Clim Change, 8, 972–980, https://doi.org/10.1038/s41558-018-0299-2, 2018.

Kelley, C. P., Mohtadi, S., Cane, M. A., Seager, R., and Kushnir, Y.: Climate change in the Fertile Crescent and implications of the recent Syrian drought, Proceedings of the National Academy of Sciences, 112, 3241–3246, https://doi.org/10.1073/pnas.1421533112, 2015.

Planton, S., Lionello, P., Artale, V., Aznar, R., Carrillo, A., Colin, J., Congedi, L., Dubois, C., Elizalde, A., Gualdi, S., Hertig, E., Jacobeit, J., Jordà, G., Li, L., Mariotti, A., Piani, C., Ruti, P., Sánchez Gómez, E., Sannino, G., and Tsimplis, M.: The Climate of the Mediterranean Region in Future Climate Projections, in: The Climate of the Mediterranean Region, 449–502, https://doi.org/10.1016/B978-0-12-416042-2.00008-2, 2012.

Rockel, B., Will, A., and Hense, A.: Regional climate modelling with COSMO-CLM (CCLM), Meteorol. Z. (Stuttg.), 17, 2008.

Zittis, G., Hadjinicolaou, P., Almazroui, M., Bucchignani, E., Driouech, F., El Rhaz, K., Kurnaz, L., Nikulin, G., Ntoumos, A., Ozturk, T., Proestos, Y., Stenchikov, G., Zaaboul, R., and Le-lieveld, J.: Business-as-usual will lead to super and ultra-extreme heatwaves in the Middle East and North Africa, npj Clim Atmos Sci, 4, 1–9, https://doi.org/10.1038/s41612-021-00178-7, 2021.

4. The climate of the Eastern Mediterranean and the Nile River basin 2000 years ago using the fully forced COSMO-CLM simulation

Submitted to: Climate of the Past on 09.27.2023.

Mingyue Zhang[1], Eva Hartmann[1], Sebastian Wagner[2], Muralidhar Adakudlu[3], Niklas Luther[3], Christos Zerefos[4], Elena Xoplaki[1, 3]

[1]Climatology, Climate Dynamics and Climate Change, Department of Geography, Justus Liebig University of Giessen, Giessen, 35390, Germany

[2]Helmholtz-Zentrum Hereon, Geesthacht, 21502, Germany

[3]Center for International Development and Environmental Research, Justus Liebig University of Giessen, Giessen, 35390, Germany

[4]Research Centre for Atmospheric Physics and Climatology, Academy of Athens, Athens, Greece

Correspondence to: Mingyue Zhang (Mingyue.zhang@geogr.uni-giessen.de)

Abstract

Understanding the past climate at regional scale, the impact of natural variability and sensitivity by studying the underlying dynamics and processes, can provide a point of reference for future climate conditions under anthropogenic forcing. The Eastern Mediterranean (EM) and Nile River basin (NR) regions are of particular interest for the study of past climate due to their location under the influence of major atmospheric teleconnections. We developed a high-resolution regional model for paleoclimate applications, COSMO-CLM, by integrating all external forcings and conducted a transient simulation from 500 BCE to 1850 CE. Principal Component Analysis (PCA) was applied for winter/summer precipitation and temperature to validate the model set up and showed very good agreement between simulated and observational/reanalysis data. Further, 400-362 BCE and 1800-1850 CE have been selected for the comparison of the mean climate conditions of the early Roman period (ERP) and pre-industrial times (PI). The comparison of temperature and precipitation suggests comparable mean climatic conditions with spatial differences in terms of variability within the study regions. Over the Eastern Mediterranean (EM), ERP is wetter and warmer in both winter and summer compared to PI, with higher variability in temperature and precipitation in summer than in winter. In the Nile River basin (NR), ERP summers were wetter and more variable compared to PI. The ERP over NR is warmer by approximately 0.5 °C in winter and cooler by 0.5 °C in summer, with low variability in winter and high variability in summer compared to PI. The relevant large-scale circulation of the two periods shows consistent spatial structures with the corresponding precipitation/temperature EOF patterns, albeit with varying amplitudes. The 2500 years transient simulation sheds light to the paleo climate conditions and relevant atmospheric circulation as well as processes of periods of interest in complex areas with detailed output and comprehensive forcing allowing for better representation of the regional climate variability and change. Comparison of simulated output with proxy records, reconstructions and detailed studies of specific events, e.g., volcanic eruptions, can help to capture the spatiotemporal extent of these events and their impact on climate variability and change, in addition to providing insights into their impact on societal change and human history.

4.1 Introduction

The global climate undergoes significant changes, characterized by rising temperatures, more intense, more frequent and more persistent extreme weather and climate events and shifting precipitation patterns (Hennessy et al., 2022). Anthropogenic climate change poses a great threat to ecosystems, economies, and human well-being worldwide (Pörtner et al., 2022). The historical context is critical when assessing present-day climate anomalies, attributing them to forcings and making statements regarding their frequency and severity in a long-term perspective (e.g. Luterbacher et al., 2016). Furthermore, the availability of paleoclimatic data spanning centuries to millennia is a vital resource for studying and characterizing climate changes, offering insights that enhance our comprehension of climate variability, trends, extremes, and contributing essential information for climate mitigation and adaptation strategies (Luterbacher et al., 2016; Luterbacher and Pfister, 2015; Haldon et al., 2014, 2018).

Studying climate at regional and local scales improves our understanding of the dynamical and physical processes involved. In order to prepare useful climate projections and adequate responses to the impacts of climate change on vulnerable areas (Kelley et al., 2015), a better understanding of the past climate at a high spatial resolution is of great importance. The Eastern Mediterranean (EM) and the Nile River Basin (NR) are located in an area of great climatic and societal interest with a very long history, with important civilizations inhabiting the area for several millennia. Today, the EM area faces substantial societal challenges, partially connected with climate change impacts, including migration and societal disruptions (Lange et al., 2020). The region also represents a prominent climate change hotspot with exceptionally intense warming that exceeds the continental and global averages, while the area experiences an increasing amount of extreme weather events such as heatwaves, droughts, dust storms, heavy precipitation and floods (Zittis et al., 2022).

EM is influenced by mid-latitude, subtropical and tropical weather systems (Alpert et al., 2005), which can lead to a range of extremes, including windstorms, hydrological and temperature extremes (Hochman et al., 2022). Situated in a transition zone between subtropical and mid-latitude climates and located at an atmospheric crossroad, the area is directly influenced by a variety of atmospheric circulation patterns and meteorological processes on different continents (Zittis et al.,

2022). For example, in the summer the South Asian Monsoon has a major impact on the Eastern Mediterranean, while in winter, the area may be affected by the variability of continental circulation anomalies linked to the Siberian High-Pressure System (Cramer et al., 2018; Paz et al., 2003). The extreme weather over EM, such as heavy precipitation, is mainly governed by the large-scale atmospheric circulation and its interaction with regional synoptic systems (i.e., Cyprus Lows, Red Sea Troughs, Persian Troughs, "Sharav" Lows) and high-pressure systems. Complex orographic features further play an important role in the generation of extreme weather (Hochman et al., 2022). Multiple atmospheric circulation patterns affect the NR region and the water availability of the huge drainage basin that crosses different hydroclimatic zones. The precipitation regime along the Nile catchment is mainly related to the West African monsoon, which itself is modulated by the Indian monsoon dynamics (Ménot et al., 2020). Over the central Ethiopian Highlands, the source region of the Blue Nile, 70% of the annual precipitation falls during summer (June-September) when the region is affected by the rain belt of the Intertropical Convergence Zone (ITCZ) and tropical convection clusters over the continental areas (Conway, 2000). The climate of the region is also influenced by monsoon systems that prevail around Lake Victoria and sections of the Ethiopian highlands (Camberlin, 2009). The moisture sources that actually affect the NR Basin originate from the Gulf of Guinea, the Indian Ocean and the northern inflow from the Mediterranean Sea and the Red Sea (Viste and Sorteberg, 2013). Most of the wet months in Ethiopia occur in connection with enhanced moisture transport from the north (Viste and Sorteberg, 2013).

As in the past, the Nile River is also today the main agricultural and economic water resource for multiple African countries (Singh et al., 2023). Among those, Egypt has always been heavily dependent on the Nile River flow, as one of the Ancient World "hydraulic civilizations" (Singh et al., 2023) and thus provides a unique laboratory to study societal vulnerability and response to climate variability (Manning et al., 2017). For example, the Nile floods had significant impacts on the Egyptians' prosperity, thus various strategies have been made to mitigate, adapt to and take advantage of the impacts of flooding, including technological advancements in water-lifting machines and innovative agricultural practices.

The study and better understanding of the climate of the past, its variability, the occurrence of extremes and their interaction with societies are of great significance and scientific interest. It is crucial for gaining insight into current and potential future environmental challenges, and understanding societal and cultural changes (Xoplaki et al., 2016, 2018). The Eastern Mediterranean and northeastern African areas offer a relatively dense network of natural archives and documentary evidence covering the past 2,000 years and indicate the heterogeneous and variable in time and across space climate of the past two millennia (Xoplaki et al., 2016, 2018, 2021; Zittis et al., 2022).

The Paleoclimate Modelling Intercomparison Project (PMIP) aims at understanding how the climate system responds to various climate forcings for the documented climate conditions that might differ between historical and current times (Kageyama et al., 2018). At its fourth phase, PMIP4 focuses as well on the comparison between climate reconstructions (based on physical, chemical or biological records) and climate modelling results addressing the ability of state-of-the-art numerical models to realistically simulate climate variability and change of the past, and whether their response to different external forcings is compatible with paleoclimatic evidence (Kageyama et al., 2018). Paleoclimate studies in the Eastern Mediterranean and the Nile Basin mostly rely on proxy records (García-Herrera et al., 2007), climate reconstructions (Luterbacher et al., 2016), and global paleoclimate models with a coarse spatial resolution (Giorgi and Lionello, 2008). The purpose of regional climate models (RCMs) is to refine climate data from coarse-resolution global climate models (GCMs). By doing so, RCMs offer more detailed information at smaller, sub-GCM-grid scales. This increased resolution is particularly valuable for studying regional phenomena and for conducting vulnerability, impacts, and adaptation assessments (Giorgi, 2019). Various studies in the field of present-day regional climate modelling (Worku et al., 2018; Alemseged and Tom, 2015; Bucchignani et al., 2016) demonstrated that the RCMs outperform their global counterparts in various aspects, mostly related to small-scale meteorological phenomena and the hydrological cycle. Armstrong et al. (2019) found that a regionally limited version of a high spatial resolution atmospheric GCM can more accurately simulate pre-industrial climate and enhance the representation of anomalies in certain past atmospheric processes compared to lower resolution GCMs. By comparing GCM and RCM simulations for different periods in the past, Gomez-Navarro et al. (2012) concluded that their regional model improves the

skill to reproduce high-frequency climate patterns over parts of the Mediterranean for the last millennium by better mimicking regional circulation patterns and local climate and hence reducing the biases of the driving GCM. Studies have also highlighted the more realistic representation of topography and the regional climate information that is valuable for paleoclimate studies (Renssen et al., 2001). Considering that the existing proxy and observational data over the study region are geographically restricted over specific parts of the area and the existing GCMs are too coarse, RCMs can help to close this gap by improving the spatial resolution (Bray and Von Storch, 2016). These facts support the need for a regional paleoclimate simulation in areas highly vulnerable to climate variability, such as EM and NR.

Climate variations are also related to changes in external forcing parameters (e.g., orbital, solar, volcanic, land use and greenhouse gases (GHG) (Gómez-Navarro and Zorita, 2013). The climate system is primarily driven by solar radiation, and the variations of solar irradiance can lead to changes at decadal to centennial time scales (Gray et al., 2010). Changes in orbital parameters such as eccentricity, obliquity, and precession also have important effects on the latitudinal and seasonal distribution of solar radiation at different temporal scales (Ludwig et al., 2016; Cubasch et al., 2006). As far as the volcanic forcing is concerned, of the impact of volcanic sulfate aerosols that are injected into the atmosphere by large tropical volcanic eruptions, leads to pronounced stratospheric warming and surface cooling (Robock, 2000; Crowley et al., 2008). Historical studies have matched the Nile flooding with the impact of volcanic eruptions (Manning et al., 2017). Greenhouse gases (GHGs) trap in turn the longwave radiation that is emitted by the Earth surface and lead to a continuous increase of energy in the climate system and effects on the global climate (Ramanathan and Feng, 2009). Furthermore, land use and land cover changes can affect climate by directly altering the surface solar and longwave radiation and indirectly impacting atmospheric turbulence (Pielke Sr et al., 2011; Zhang et al., 2021). When studying palaeoclimate in EM and NR, the climate models used are mainly GCMs, and these forcings are introduced in the GCM simulations. For example, the MPI-ESM-LR which we are using as the input data for the RCM, is fully forced with solar, orbital, volcanic, GHG and land use change (Jungclaus et al., 2017), but those forcings are not yet fully implemented in the RCM, especially for the paleoclimate simulation. Studies have shown that implementing some of the forcings into RCM can have a more accurate representation of regional climate variability (Ludwig et al., 2016, 2017b). Hence, the

respective changes in external forcings such as solar, orbital, volcanic, GHG and land use change must be implemented into the COSMO-CLM to make the RCM more realistic and consistent with its driving GCM.

Thus, we have, to our knowledge, developed the first highly resolved, fully forced, transient paleo regional climate simulation with COSMO-CLM for the period from 500 BCE to 1850 CE. The implementation of the forcings and sensitivity experiments are described in Hartmann et al. (submitted). A temporally and spatially highly resolved, regional simulation across the complete study area (Eastern Mediterranean and Nile River Basin, EMNR) allows the study of regional-to-local paleoclimate processes with higher accuracy. Further, it enables the exploration of the association between the regional climate patterns and the large-scale atmospheric circulation patterns from the GCM world. An asset of the simulation is its contribution to the study of the impact of the occurrence of extreme climate conditions on societies through interdisciplinary, collaborative research.

We present and exploit the advantages and breakthroughs of the fully forced, transient simulation by assessing the ability of the simulation to represent the climatic conditions of the area in space and time and the links with the large-scale circulation. The assessment is divided into two approaches, an evaluation during the present time and a comparison of two periods, one in the first millennium BCE and one in the pre-industrial times.

The paper is structured as follows: The section "Data and Methods" describes the RCM COSMO-CLM, the reanalysis and observation time series and provides information on the implemented methods. In the section "Results and Discussion", the findings of the analysis are presented and interpreted in detail. Finally, the "Conclusions" section summarizes the main findings and their significance and briefly discusses possible directions for future research.

4.2 Data and methods

4.2.1 Regional Climate Model Simulations

The COSMO-CLM (COnsortium for Small-scale MOdelling in CLimate Mode - CCLM) (Rockel et al., 2008) is a widely used RCM that has been used to investigate climate change under different

forcings, such as land use, orbital and GHG. The CCLM is originally designed to perform simulations from 1850 CE onward and its performance largely depends on the driving GCM (Armstrong et al., 2019). Multiple CCLM simulations have been recently performed at different resolutions up to very high convection-permitting resolution (Raffa et al., 2023) in the frame of the CORDEX (Coordinated Regional Climate Downscaling EXperiment, https://cordex.org/) initiative.

In this work, we revolutionize by implementing the CCLM in model version 5.0 with CLM version 16 to an adjusted paleoclimate version, fully forced with orbital, solar, GHG, volcanic and land-use changes (Hartmann et al., submitted). We performed a transient simulation from 500 BCE to 1850 CE at the Deutsches Klimarechenzentrum (DKRZ), which is forced with the new MPI-ESM-P simulation "Mythos" that is performed under the CMIP6 protocol after 1 AD (MPI-ESM-LR 'past2k') (Jungclaus et al., 2017) at ~1.875° resolution. The period 500 BCE until 1 BC is according to the external forcings used by Bader et al., (2020) in a simulation for the entire Holocene.

The implemented forcings in COSMO-CCLM are identical to those of MPI-ESM-P "Mythos" simulation, namely, the orbital forcing is represented by the eccentricity, the obliquity and the longitude of perihelion (Berger, 1978) and the solar forcing by the total solar irradiance (Jungclaus et al., 2017). The changes in GHG concentrations consist of CO2, CH4 and N2O (Meinshausen et al., 2017), while the volcanic forcing is based on the stratospheric aerosol optical depth (AOD) at 550 nm wavelength by Toohey and Sigl, (2017).

The interpolation of the driving data to the model is done with INT2LM in version 2.05 with CLM version 1 (INT2LM−v2.05clm1) (Schättler and Blahak, 2017). The time integration is the two-step Runge-Kutta scheme (Jameson et al., 1981) with a 300 seconds time step. The convection parameterization based on the Tiedtke scheme (Tiedtke, 1988) is used. The representation of albedo and aerosols are found to be the most important parameters in the studied region (see also Hartmann et al., submitted) and are set the same as in Bucchignani et al., (2016). The land surface model is TERRA-ML (Doms et al., 2011; Schulz et al., 2016). The simulations are carried out in a domain including the Eastern Mediterranean, the Middle East and the Nile River Basin from Lake Victoria to the Nile Delta (Fig. 4.1, 4° − 60° E, 5° S − 49° N). For the analysis of the precipitation, we consider the areas of the Eastern Mediterranean (EM, Fig 4.1b) and the Nile River Basin (NR, Fig.

4.1c) separately as the precipitation regimes are significantly different between the two regions. While for the analysis of temperature, we have selected a region, include the Eastern Mediterranean and Nile River basin (EMNR, Fig. 4.1a).

The following periods have been used for the assessment of the fully forced, transient CCLM simulation: i) present period (1980-2018) to validate the adjusted COSMO-CLM, ii) the pre-industrial period (PI; 1800-1850 CE), and iii) the Early Roman Period (ERP; 400-362 BCE) for the comparison of the mean climate conditions of the two periods and changes in the climate characteristics of the study region.

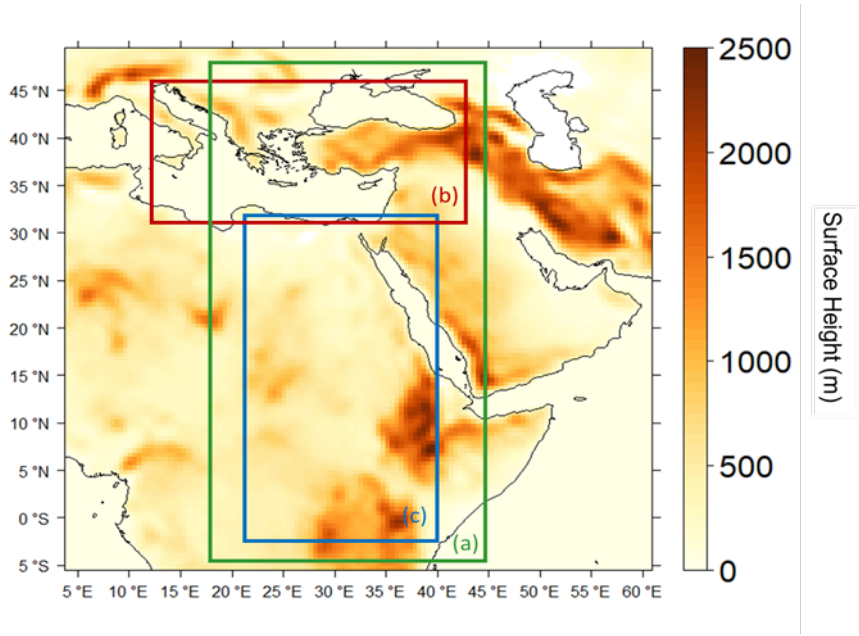

Figure 4.1. Topography of the study regions (a) EMNR: indicated with green rectangle, (b) EM: indicated with red rectangle, (c) NR: indicated with blue rectangle. Area (a) is used for the analysis of temperature and the other two areas (b, c) are used for the analysis of precipitation.

4.2.2 Observational Time Series and Reanalysis Data

We validate the CCLM output, with different observational and reanalysis data sets at 0.5° resolution for the present period, 1980-2018: the monthly mean temperature and total precipitation from CRU TS v.4.05 (Harris et al., 2020), the precipitation climatology from the Global Precipitation Climatology Centre V.2020 (GPCC) (Schneider et al., 2022); and finally the ERA-Interim temperature (Dee et al., 2011) as an additional comparison data set. We restrain from using

the ERA-Interim precipitation due to its dependence on GPCC observations. The CRU TS is the reference data set of the validation of the present CCLM simulation output.

4.2.3 Methods

4.2.3.1 Principal Component Analysis

Principal Component Analysis (PCA), also referred to as empirical orthogonal functions (EOFs), is a frequently applied technique in climate sciences and multivariate datasets to reduce the dimensions of the dataset and find a smaller number of independent variables conveying as much of the original information (w.r.t. to the variance) as possible (Wilks, 2011). The technique enables the investigation of spatial variability modes by detecting structures in the data (Gallacher et al., 2017; Bader et al., 2020).

Eq. (4.1) shows the covariance matrix C_{XX} (where XX represents the detrended seasonal anomalies of temperature and precipitation) is decomposed according to

$$C_{XX} \cdot e = \lambda \cdot e \tag{4.1}$$

This decomposition includes a restructuring of the covariance matrix C_{XX} with the most important patterns (eigenvectors, e) and their principal components (PCs) showing the highest amount of spatial variance (represented by the eigenvalue λ) within the full fields. The classic patterns, EOFs, are orthogonal, hence, the eigenvectors are uncorrelated. For some applications, this is a useful characteristic (i.e., setting up multiple regression models with predictors that are not collinear). In meteorological applications, however, the orthogonality constraint may be disadvantageous, because most processes in the real world are not orthogonal (Storch and Zwiers, 1984). We thus applied the VARIMAX rotation to obtain rotated EOFs (re_j, REOFs) that are physically more consistent than the non-rotated patterns. REOFs are thus used for the validation of the model set-up in the present period (1980 - 2018 CE), while non-rotated EOFs are implemented for the comparison of the mean climate conditions in PI and ERP times.

The PCs provide the temporal evolution of the (rotated) eigenvectors re_j and are calculated by projecting the original seasonal anomaly precipitation and temperature time series X onto the (rotated) eigenvectors re_j (REOFs), see Eq. (4.2):

$$PC_j = < X \mid re_j > \tag{4.2}$$

where $< \mid >$ denotes the dot product and j the index of the according principal component and rotated eigenvector, respectively.

4.2.3.2 Validation of the Model Set-up (1980-2018)

For the comparison between observed/reanalysis and simulated temperature and precipitation in the present time (1980-2018), we want to compare spatially homogeneous climatic regions in the study area of the simulated and observed datasets. For this purpose, spatial correlations between the first six REOFs of the reference dataset CRU and all REOFs of CCLM and GPCC are calculated to identify the best matching patterns among them. A two-sided t-test was conducted to address the correlations' significance. The retained first six CRU REOFs account for around 75% of the total explained variance in each season and eventually in each data set. For the regions definition, the 80th (75th) percentile of the precipitation (temperature) REOF loadings is calculated. For the "paired" REOFs, six regions are defined by those grid points that exceed the 80th (75th) percentiles of precipitation (temperature). Precipitation and temperature differences are then calculated with respect to the reference CRU data set for the period 1980-2018 and each region. Taylor diagrams (the Pearson correlation coefficient, the root-mean-square error (RMSE) error, and the standard deviation against the reference data CRU is shown) for each region are then prepared for the validation and skill assessment of the COSMO-CLM simulations.

4.2.3.3 Mean Climate Conditions: Pre-industrial and first millennium BCE

The mean climate conditions between the first millennium BCE and the pre-industrial times are investigated by addressing differences in mean values and standard deviations together with their statistical significance with a student's t-test at each grid point at the 95% confidence level. By examining temperature variations during these periods, we gain valuable insight into climatic trends and changes at the beginning and end of the simulation period. In order to investigate the

relevant atmospheric circulation in the two periods, the non-rotated temperature and precipitation PCs were linearly regressed onto the global sea level pressure (SLP) anomalies from the MPI-ESM-P simulation "Mythos" to estimate the local regression coefficients for the SLP field, see Eq. (4.3):

$$PC(j) = \beta_0(j,k) + \beta_1(j,k) * SLP(k) + \varepsilon(j,k) \quad (4.3)$$

The index k represents the grid-point index covering the geographical domain. $PC(j)$ is the jth non-rotated principal component and $\beta_1(j,k)$ presents the regression coefficients for the jth component on grid point k, and $SLP(k)$ is the SLP time series of grid point k. $\beta_0(j,k)$ is the intercept of the regression and $\varepsilon(j,k)$ as the noise component of grid point k for the jth non-rotated principal component. In our case $j = 1,2,3$, i.e., the leading three non-rotated PCs. Please note that in this study, only the regression coefficients $\beta_1(j,k)$ are used to plot the regression map.

4.3 Results and Discussion

4.3.1 Evaluation of the CCLM output

4.3.1.1 Precipitation – EM

The spatial correlations between the seasonal CRU, CCLM and GPCC REOFs for the period 1980-2018 are presented in Table 4.1. The two-sided t-test at the 95% confidence level showed that all correlations are significant. CRU and CCLM REOFs seem to agree well with the highest significant correlation of 0.94 for winter (DJF) and summer (JJA). Lower correlations, however, characterize mainly REOFs of lower explained variance.

Table 4.1. Spatial correlation of the CCLM with CRU and GPCC precipitation REOFs for winter (DJF) and summer (JJA) over the EM. All values are significant at the 95% significance level. Numbers in parentheses give the corresponding REOFs of each data set.

Winter (December to February)						
$r_{CRU\text{-}CCLM}$	0.70 (1 & 4)	0.85 (2 & 1)	0.91 (3 & 2)	0.74 (4 & 8)	0.74 (5 & 7)	0.88 (6 & 5)
$r_{GPCC\text{-}CCLM}$	0.62 (1 & 4)	0.83 (2 & 1)	0.92 (3 & 2)	0.66 (4 & 6)	0.85 (5 & 5)	0.65 (6 & 4)
Summer (June to August)						
$r_{CRU\text{-}CCLM}$	0.94 (1 & 1)	0.86 (2 & 3)	0.67 (3 & 2)	0.67 (4 & 5)	0.40 (5 & 5)	0.74 (6 & 11)
$r_{GPCC\text{-}CCLM}$	0.92 (1 & 1)	0.79 (2 & 3)	0.69 (3 & 11)	0.71 (4 & 4)	0.60 (5 & 2)	0.33 (6 & 2)

The derived winter and summer precipitation regions are shown in Figure 4.2. Each map is based on the paired REOFs of each data set with CRU, as shown in Table 4.1, and the regions are numbered according to the CRU REOFs ranking. For example, GPCC winter region 5 corresponds to GPCC REOF11 as the counterpart to CRU REOF5. The explained variance of each REOF is presented along the regions. The three precipitation data sets show a stronger agreement during winter over the EM. Some regions show a very good agreement between the data sets, such as the winter precipitation region 2 of CCLM (REOF1) and CRU (REOF2) over the Balkans. Other areas, such as the CCLM region 4 in winter do not agree well with CRU and GPCC, and the CCLM regions agree less well in the summer with both CRU and GPCC, especially along the Aegean Sea and the Black Sea coasts. In general, summer precipitation over the EM is mostly convective and thus very local, leading to a lack of agreement between the observational data sets and the simulation. The strong bias shown in Figure 4.3 might be due to an underestimation of its strength and cloud cover (Bucchignani et al., 2016).

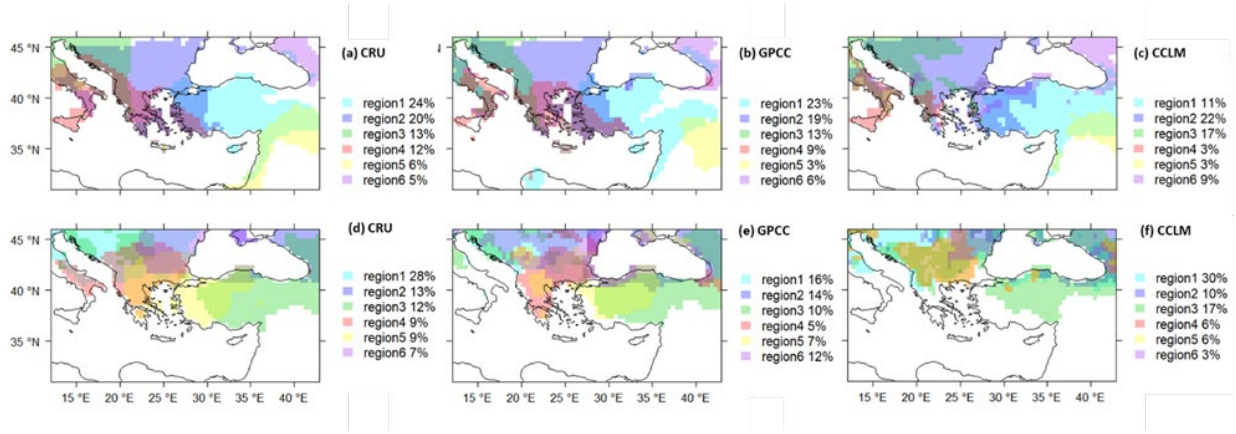

Figure 4.2. Regionalization of precipitation over the EM in winter (DJF, upper panel) and summer (JJA, lower panel) for CRU (a, d), GPCC (b, e) and CCLM (c, f). The total explained variance of the corresponding REOF is shown in the legend.

The mean regional total precipitation differences of the six regions for GPCC and CCLM with respect to the 1980-2018 mean total CRU winter and summer precipitation are shown in Figure 4.3. The simulated seasonal variability of precipitation agrees well with the two observational data sets, although the systematic underestimation of CCLM in summer is noticeable. Very good agreement is visible for winter precipitation in regions 2 and 3 around the west and south coast of the Black Sea area. The simulated mean total precipitation differences with respect to CRU for the

six regions show a correlation higher than 0.7 and comparable standard deviation for both seasons and data sets, implying that the CCLM is performing well in representing the precipitation variability in the EM region (see Figure 4.13).

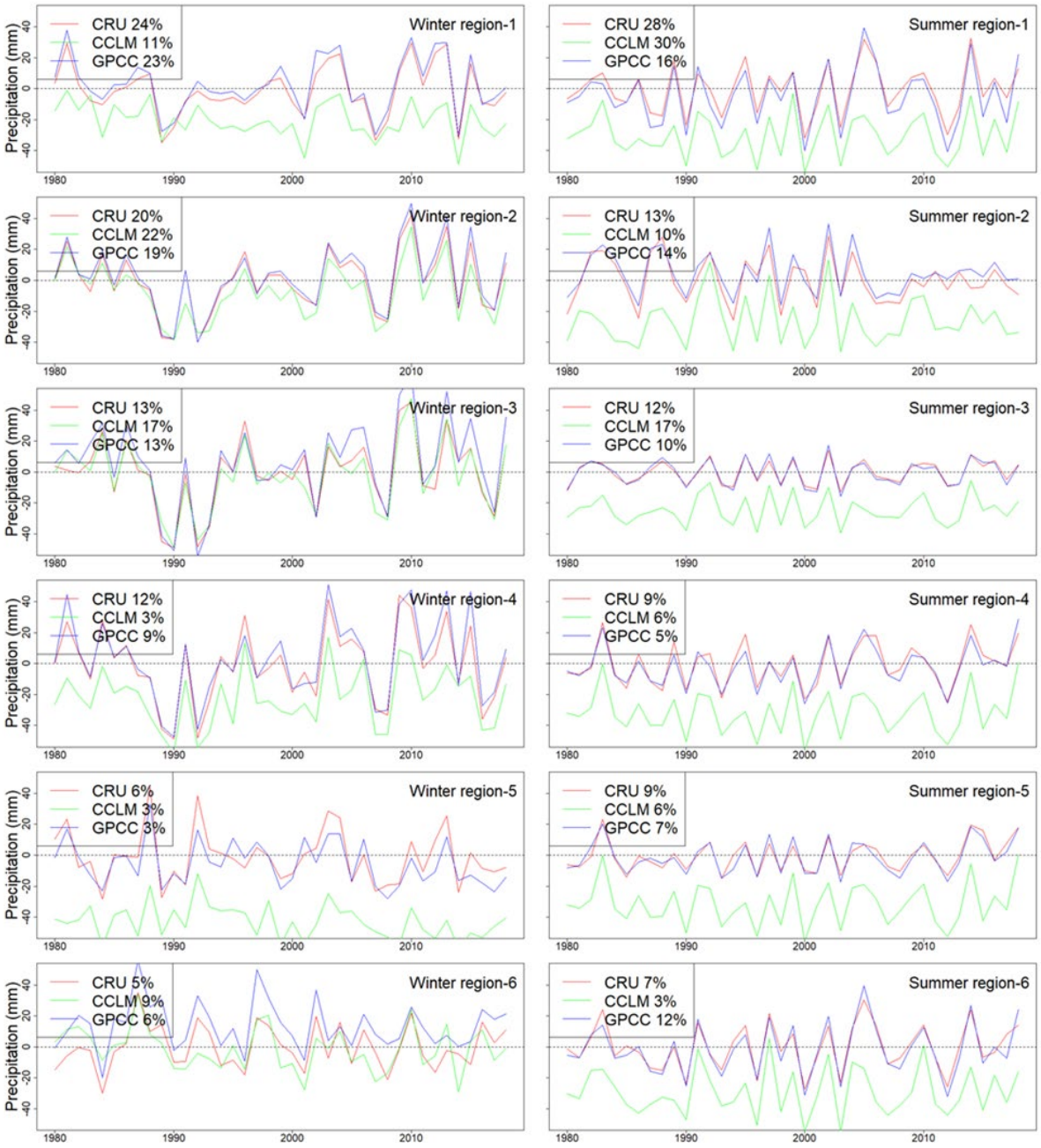

Figure 4.3. Seasonal mean total precipitation differences of EM regions with respect to the 1980-2018 mean total CRU winter (DJF) and summer (JJA) precipitation.

4.3.1.2 Precipitation – NR

The EM and NR are characterized by significantly different precipitation regimes, and we have thus separated the two areas for the analysis. The spatial correlation among the REOFs of the three data sets is calculated to determine the associated regions with respect to CRU, as presented in Table 4.2. The correlation of REOFs for precipitation in NR is for some pairs significantly lower compared to the correlations of EM. The CCLM does not perform as well in simulating precipitation over NR, which may be related to the effect of the Hadley circulation, strong convection in the ITCZ combined with subtropical advection of hot, dry air linked with the near-surface trade winds (Adam et al., 2016). The poorer performance of CCLM over the African region may further be connected to an inaccurate representation of cloud coverage, particularly along the ITCZ (Sørland et al., 2021). Finally, the NR station time series that enter the gridded CRU and GPCC data sets are sparse, which may also reduce their quality (Harris et al., 2020; Schneider et al., 2022).

Table 4.2. Spatial correlation of the CCLM with CRU and GPCC precipitation REOFs for winter (DJF) and summer (JJA) over the NR. All values are statistically significant at the 95% significance level. Numbers in parentheses give the corresponding REOFs of each data set.

Winter (December, January, February)						
$r_{CRU\text{-}CCLM}$	0.79 (1 & 2)	0.71 (2 & 1)	0.29 (3 & 9)	0.50 (4 & 5)	0.74 (5 & 1)	0.50 (6 & 4)
$r_{GPCC\text{-}CCLM}$	0.77 (1 & 2)	0.77 (2 & 1)	0.60 (3 & 3)	0.62 (4 & 5)	0.52 (5 & 6)	0.21 (6 & 4)
Summer (June, July, August)						
$r_{CRU\text{-}CCLM}$	0.64 (1 & 4)	0.56 (2 & 1)	0.37 (3 & 8)	0.63 (4 & 4)	0.40 (5 & 13)	0.26 (6 & 7)
$r_{GPCC\text{-}CCLM}$	0.55 (1 & 4)	0.60 (2 & 4)	0.48 (3 & 5)	0.32 (4 & 13)	0.18 (5 & 8)	0.41 (6 & 3)

Figure 4.4 shows the corresponding regions based on the REOFs for each of the three data sets (CRU, GPCC, and CCLM), the explained variance of each REOFs is shown for each region. Precipitation in NR is mainly concentrated in the southern part of the area, and south of the Sahara desert. In addition, the regions of CCLM over NR exhibit a less homogeneous pattern compared to the other two data sets. This may be also related to the parameterization of CCLM which is better optimized for Europe than other areas, especially compared to complex and completely different geographical regions such as NR (Sørland et al., 2021). In the summer, the regions shift farther north compared to winter, which is related to rainfall variability due to the seasonal shift of the ITCZ (Nicholson, 2018) and the monsoon rain band (Dieng et al., 2016). The explained variance

varies more between winter and summer compared to EM. For instance, the selected six leading REOFS of CCLM explain 70 % of the variance in winter but only 50 % in summer.

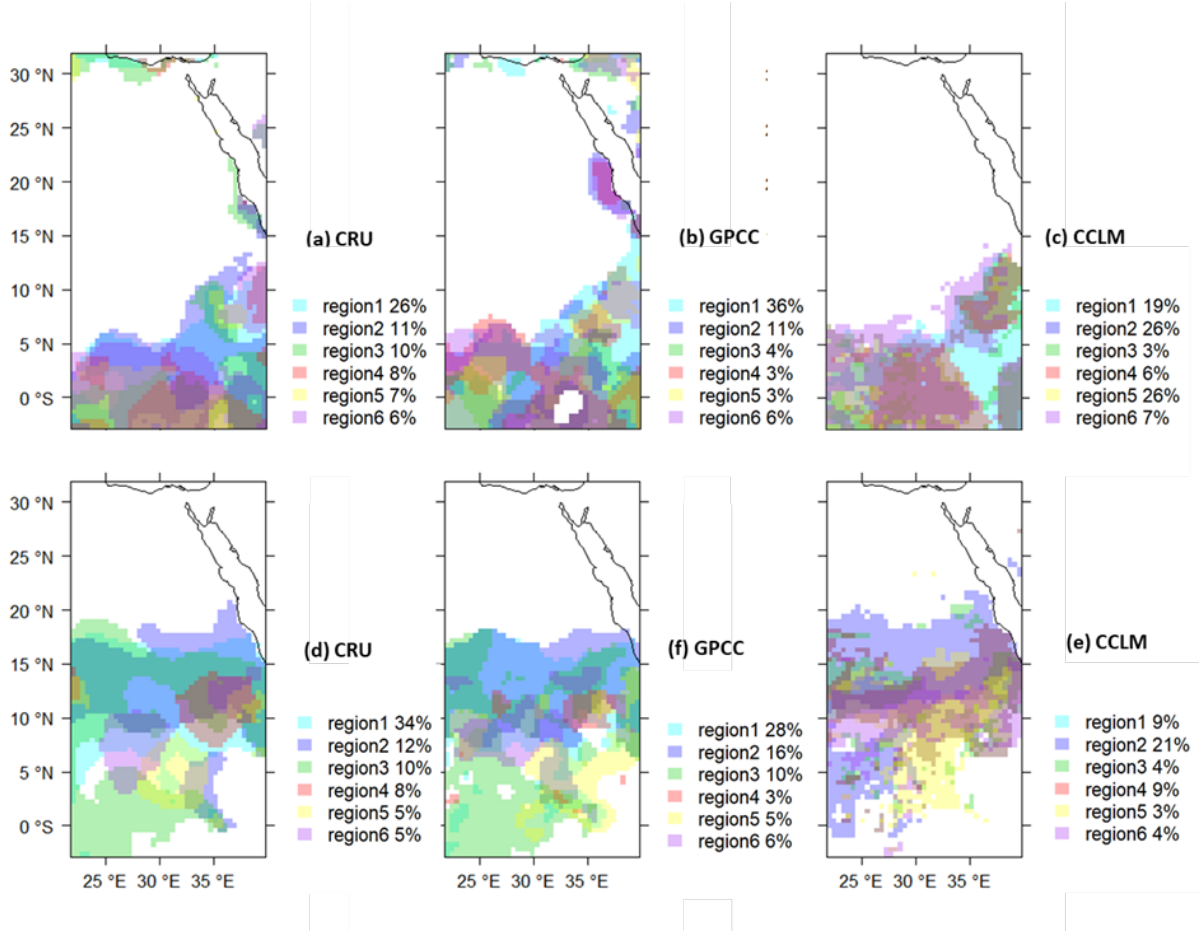

Figure 4.4. Regionalization of precipitation over the NR in winter (DJF, upper panel) and summer (JJA, lower panel) for CRU (a, d), GPCC (b, e) and CCLM (c, f). The total explained variance of the corresponding REOF is shown in the legend.

The seasonal precipitation differences, with respect to CRU (1980-2018), are presented for the six identified regions of NR (Fig. 4.5). Differences between the simulated and observed winter precipitation are smaller than those for EM, and all wet and dry extremes are overestimated by CCLM. In summer, there is a lack of agreement between the simulated and observed precipitation, in most cases, while the two observational data sets fail to agree as well. This is visible in the low correlations between the simulated and observational REOFs. As for the EM region, the Taylor Diagram illustrates the correlation and standard deviation of the seasonal mean total precipitation differences across the six regions in NR (Fig. 4.14). Compared to the EM region, the simulated

precipitation in NR exhibits larger biases in terms of standard deviation compared to CRU (Fig. 4.14).

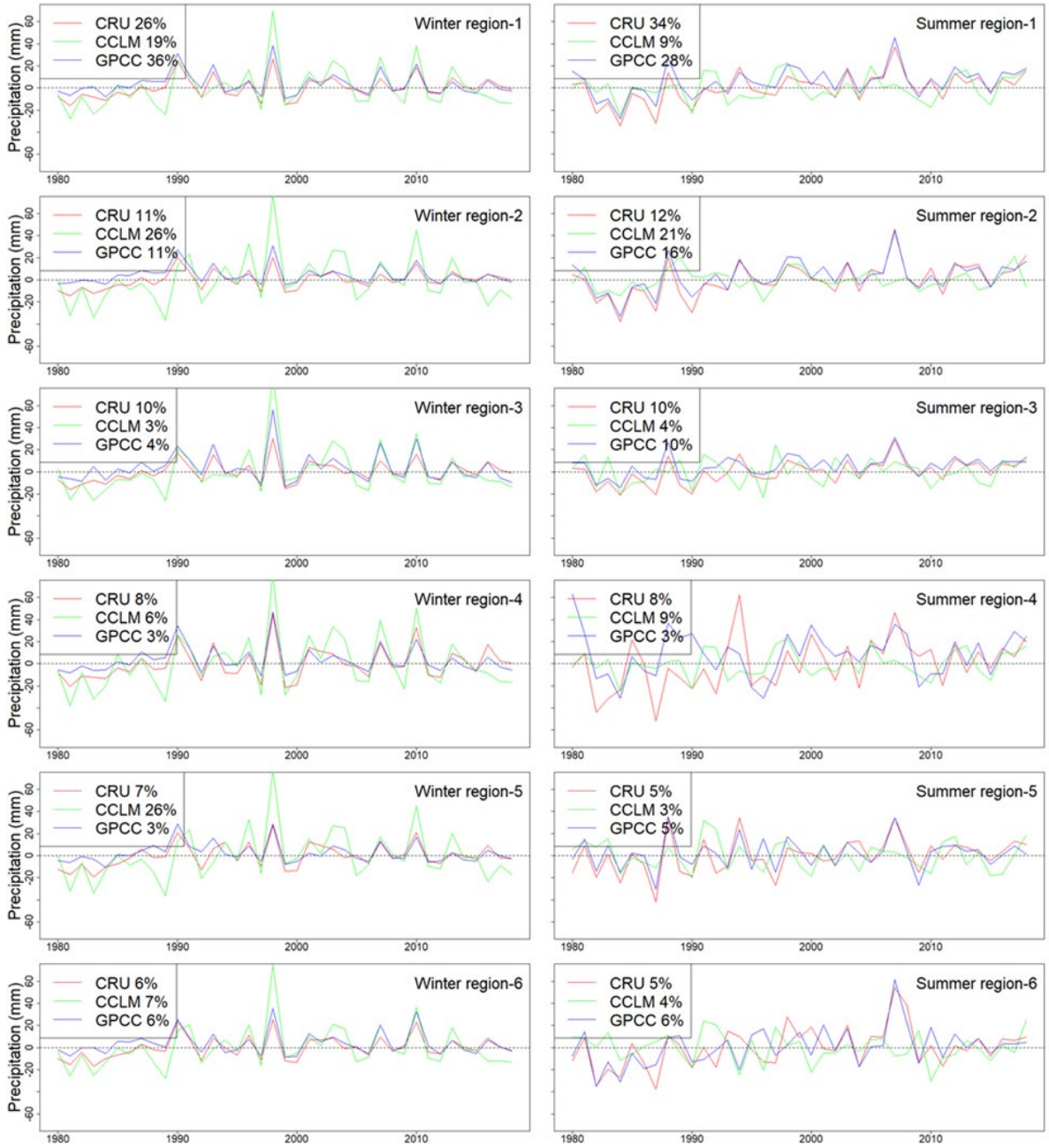

Figure 4.5. Seasonal mean total precipitation differences of NR regions with respect to the 1980-2018 mean total CRU winter (DJF) and summer (JJA) precipitation.

4.3.1.3 Temperature - EMNR

The temperature analysis encompasses the Eastern Mediterranean and Nile River Basin (EMNR). In Table 4.3 are presented the correlation coefficients between the three datasets REOFs (CRU-CCLM, CRU-ERA). The simulated temperature is highly correlated with both CRU and ERA-Interim data in winter and in summer, supporting the good performance of the RCM for this variable.

Figure 4.6 shows the regions based on the temperature REOFs of the three data sets and the explained variance of the REOFs for each region. The regions have a good agreement in space, which indicates as well the good agreement of the temperature variance of each region. Overall, the regions in all three data sets are spatially coherent regardless of the season. The mean regional temperature differences of the six regions for GPCC and CCLM with respect to the 1980-2018 mean total CRU winter (DJF) and mean summer (JJA) temperature are shown in Figure 4.15. A clear agreement between the interannual variability of the CCLM simulations and the observations/reanalysis is observed, however, differences are found mainly in the maximum and minimum temperatures for specific regions and seasons. In region 1, CCLM underestimates temperature both in winter and summer. Similarly, the simulated temperature is clearly lower in region 5 during winter and higher in region 6 during summer compared to the observational data sets. Such deviations from observations in the simulated temperature may be connected with differences in simulated cloud cover and other variables in the equatorial area affected by the ITCZ (Sørland et al., 2021).

An overall strong correlation between the CCLM seasonal mean temperature and the observational/reanalysis data sets is further illustrated in the Taylor diagrams (Fig 4.16). The over/underestimation of temperature in specific regions is observed in Figure B3, and those regions also show lower correlation to CRU data (Figure 4.16). During winter, a better agreement is observed between simulated and observational temperatures compared to summer.

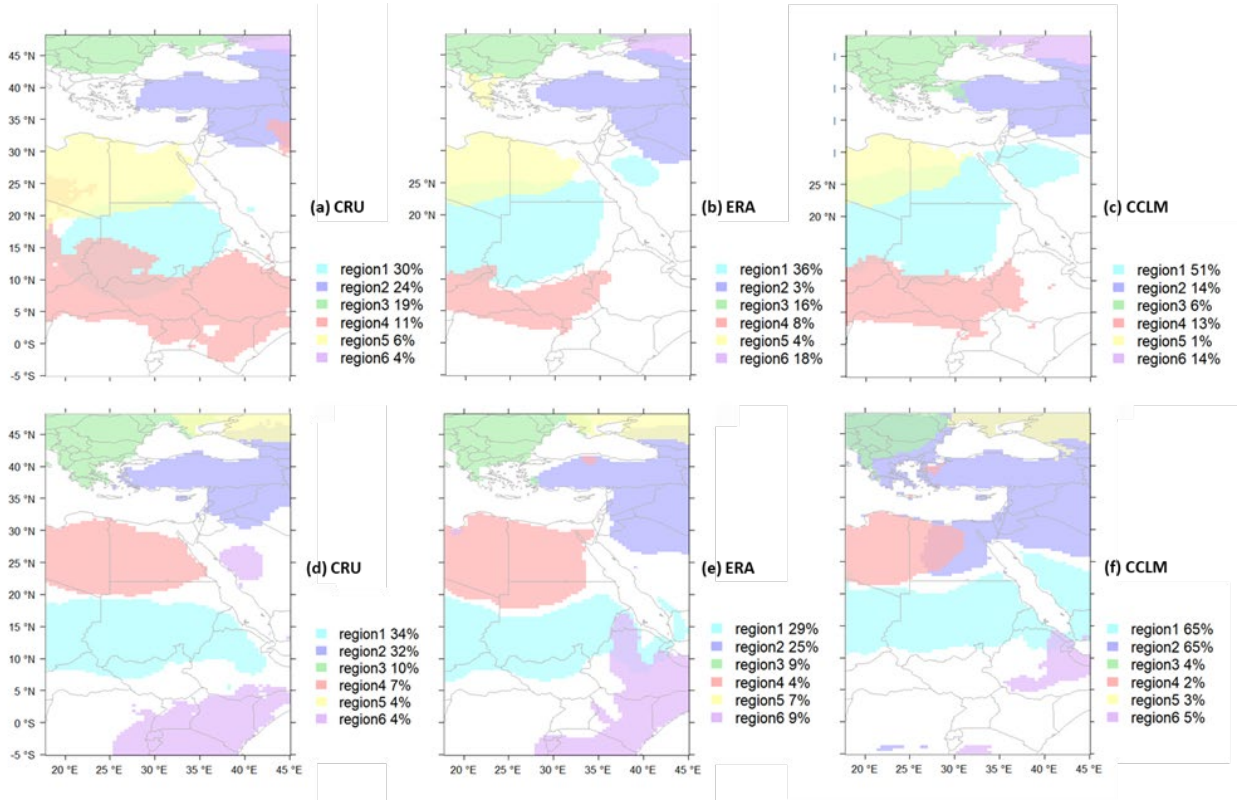

Figure 4.6. Regionalization of temperature over the EMNR in winter (DJF, upper panel) and summer (JJA, lower panel) for CRU (a, d), GPCC (b, e) and CCLM (c, f). The total explained variance of the corresponding REOF is shown in the legend.

4.3.2 Early Roman Period and Pre-Industrial climates: similarities and differences

In this section, we analyze the CCLM simulation for two periods in the past, namely the PI (1800-1850 CE) and ERP (400-362 BCE) periods. The selection of the two periods is based on two reasons: Firstly, both periods experienced a series of volcanic eruptions as reflected in the reconstructions by Toohey and Sigl, (2017), and secondly, the two periods represent the earliest and latest periods of our transient simulation (from 500 BCE to 1850 CE).

Figure 4.7 presents the precipitation and temperature annual cycle of the three regions (EM, NR and EMNR) and the selected two periods. The absolute monthly mean total precipitation and monthly mean temperature are displayed on the left y-axis, while the right y-axis represents the differences between the ERP and PI of each month for precipitation and temperature, respectively. Similar mean climate conditions characterize the two periods over the study area. The precipitation and temperature annual cycles of the two periods are similar, with slight differences for

precipitation in the NR, also reflected in EMNR. In the EM region, the largest differences in monthly precipitation of approximately 5 mm occur in April and in May, whereas in the NR region, the most notable differences of 15 mm occur in September. The ERP temperatures are approximately 1 °C warmer in September compared to the PI period in the EM and up to 1 °C cooler in May over the three study areas. Similar findings were obtained when comparing CCLM simulations with and without orbital forcing. The orbital forcing leads to increased autumn temperatures while causing a decrease in winter and spring temperatures (Hartmann et al., submitted). Nevertheless, it is important to note that Figure 4.7 represents the spatial mean of each region, and therefore, spatial variations may be averaged out.

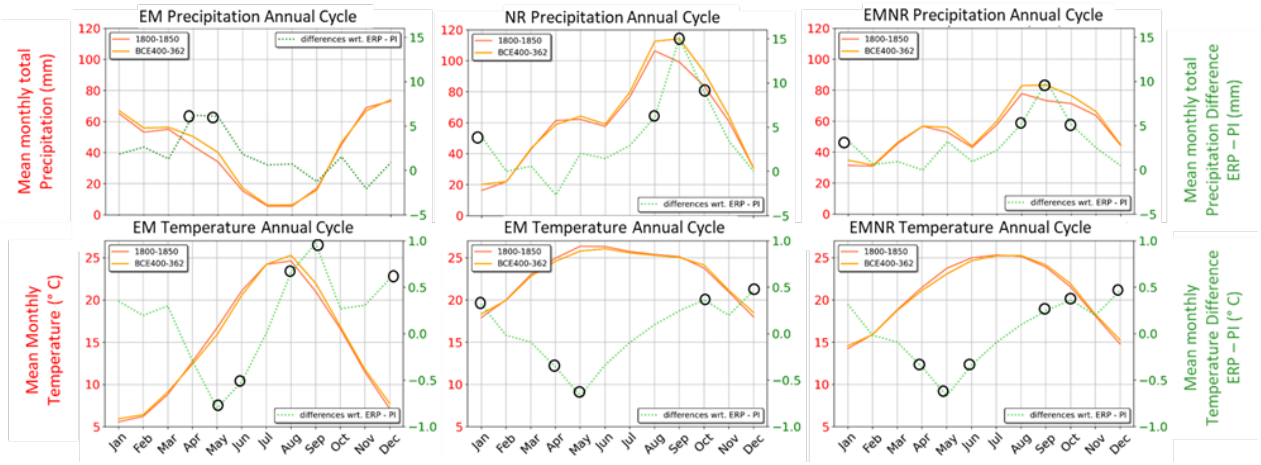

Figure 4.7. Precipitation and temperature annual cycle of the PI and ERP periods for EM, NR and EMNR. Monthly mean total precipitation and monthly mean temperature are presented on the left y-axis. Differences between ERP and PI (ERP minus PI) are shown on the right y-axis. Significant differences at a 95% confidence level according to a two-sided student t-test are marked with a black circle.

To explore the spatial differences between the two selected periods (ERP and PI) and the three regions (EM, NR, EMNR), we calculated the mean and standard deviation differences (ERP minus PI) for precipitation and temperature, shown in Figure 4.8. The dotted areas indicate statistically significant differences assessed with a t-test at the 95% confidence level.

There are notable differences in precipitation over the EM region (Fig. 4.8, upper panel, red rectangle), in both winter and summer. Compared to the PI period, the ERP winters experienced lower precipitation along the northern and eastern coasts of the Eastern Mediterranean Sea, and increased rainfall over the Balkans and the southern coast of the Black Sea. In addition, the ERP

winter season shows less variability over the entire Greek peninsula and more variability over the northern Balkans and southern Black Sea. Summers during the ERP period are relatively wetter across the entire EM region compared to the PI period, with statistically significant differences in some parts of the Balkans. The variability is higher in most parts of the EM region during the ERP summer period, except the eastern coast of the Black Sea. However, in both winter and summer, the mean differences are not statistically significant at the 95% level over most of the EM area.

The blue rectangles in the upper panel of Figure 4.8 show the precipitation differences between the two study periods for the NR region. During the winter, most of the NR region experienced drier conditions during the ERP compared to the PI. However, significantly wetter winters (about 20 mm) are found for the southwestern part of the NR region. In summer, the difference in rainfall between the two periods is more pronounced in the NR compared to the EM, with more areas experiencing statistically significant wetter conditions during the ERP than in the PI, and drier conditions over Southern Sudan and the Ethiopian Highlands. It is noteworthy that the standard deviation in the summer shows considerable differences across the NR region reflecting the underlying hydrological conditions and local-scale tropical convective activity.

The lower panel of Figure 4.8 shows the temperature differences for the three regions (EM, NR, EMNR). Accordingly, the ERP winters are warmer compared to the PI period, particularly over the EM and the northern parts of NR. Among the three studied regions, the difference in summer temperatures between the two periods is relatively small, within 0.5 °C. On the other hand, the standard deviation of temperature during the two periods shows distinct differences between summer and winter. The ERP winter temperature is overall less variable compared to the PI period, whereas the ERP summers show higher temperature variance (around 0.7 °C), especially over the EM region and the northern NR region compared to PI.

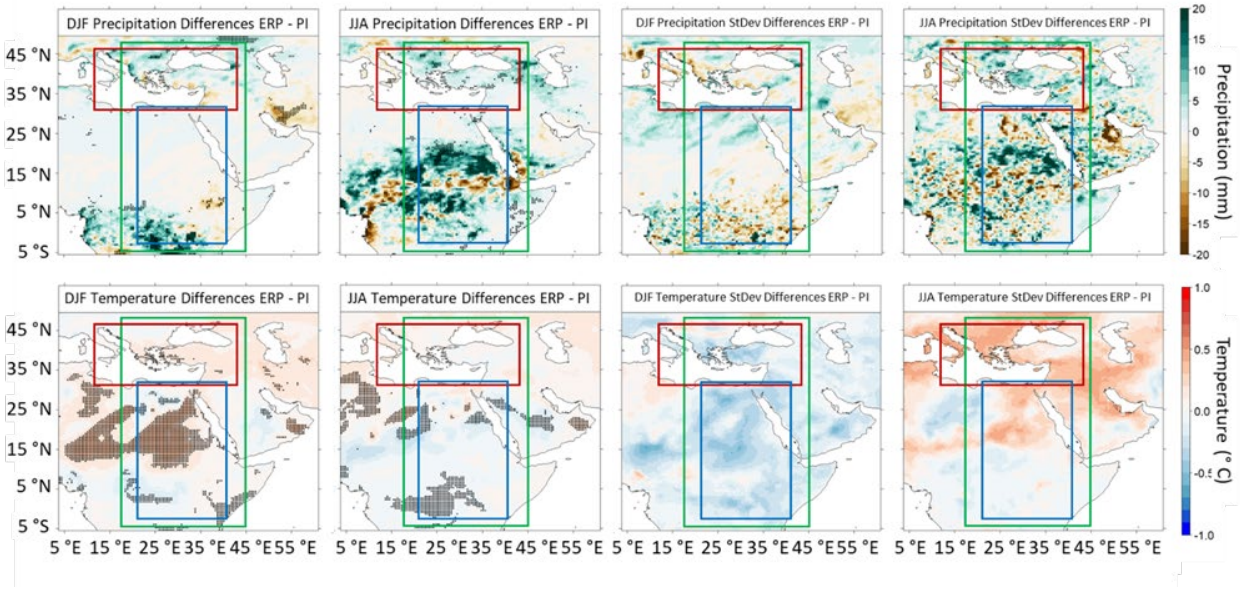

Figure 4.8. Seasonal differences (ERP minus PI) for winter (DJF) and summer (JJA) mean and standard deviation (StDev) of total precipitation over EM (red rectangle), NR (blue rectangle) and 2m air temperature over EMNR (green rectangle). Dotted areas indicate statistical significance at the 95% confidence level according to the local student's t-test.

4.3.3 Connection to atmospheric circulation

To establish the link between the large-scale atmospheric circulation and local climate in the ERP and PI periods, we explore in this section the connections between SLP and seasonal precipitation and temperature. We present results for winter precipitation over EM and summer temperature over EMNR and we restrict from using the precipitation data over the NR region part due to the limitations of CCLM to accurately simulate precipitation over the area. By examining the leading non-rotated EOFs, we gain insight into the dominant patterns of variability in winter precipitation and summer temperature within these two regions.

Figure 4.9 displays the three leading EOF patterns for the PI (a, b, c) and ERP (d, e, f) periods with the corresponding explained variance. For both periods, they show similar patterns with 75% cumulative total explained variance. EOF1 resembles the mean winter precipitation spatial distribution with highest precipitation anomalies along the western coasts of the peninsulas, indicating the influence of the westerly circulation and the land-sea interaction. The second EOF displays a dipole pattern with negative precipitation anomalies over the western and positive precipitation anomalies over the eastern part of EM, likely connected with the direct impact of the

large-scale circulation. The higher index EOF3 is characterized by a weaker dipole with distinct lower precipitation along the eastern coasts of the Black Sea and higher precipitation in the southern Mediterranean coastal areas. Smaller differences are observed in the total explained variance of each EOF of the two periods. This change in the relative amount of variance represented by the individual EOFs may indicate changes in the spatial structure of precipitation variability between the ERP and PI periods.

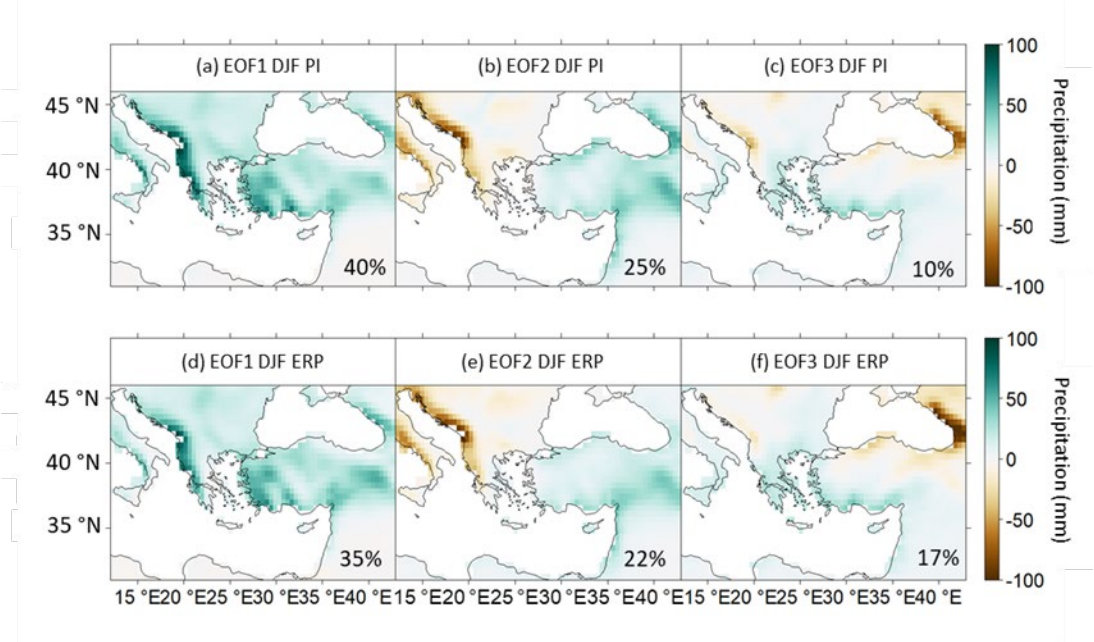

Figure 4.9. Patterns of the first three non-rotated EOFs of winter (DJF) precipitation for PI (1800-1850 CE; a, b, c) and ERP (400-362 BCE; d, e, f) and total explained variance for each EOF.

In Figure 4.10, the regression maps (i.e., the regression coefficients β_1 (j,k) according to Eq. (3)) are shown, between the three precipitation principal components (PC(j)) and the SLP fields from the driving MPI-ESM-P "Mythos" for the same periods. All regression maps show very similar spatial patterns, albeit with varying amplitudes between the two periods. This change in the amplitude of the regression coefficients may indicate variations in the robustness and strength of the underlying relationships between the precipitation PCs and the large-scale SLP fields.

The EOF1 positive winter precipitation anomalies along the western coasts of the peninsulas of EM (Fig. 4.9a, d) are connected with lower pressure over the Mediterranean (Fig. 4.10a, d) which is related to the higher frequency of cyclones from the Gulf of Genoa or of Atlantic origin moving

eastward, which, together with the orographical lifting, lead to high amounts of precipitation over these areas. The dipole structure of winter precipitation EOF2 (Fig. 4.9b, e) with drier conditions over western EM and wetter winters over its eastern part is linked to a statistically significant SLP dipole (or tripole for ERP, Fig. 4.10b, e) with stable anomalous anticyclonic conditions (SLP positive anomalies) over the Eastern Atlantic and western Europe and an anomalous trough with negative SLP anomalies over the east. The dry conditions over the eastern coasts of the Black Sea in EOF3 (Fig. 4.9c, f) are connected with the prevailing anomalous high pressure centered north of the Caspian Sea and extended over Eurasia (Fig. 4.10c, f). The ERP and PI periods represent a similar set of regression patterns with different intensity for winter with respect to the influence of large-scale circulation.

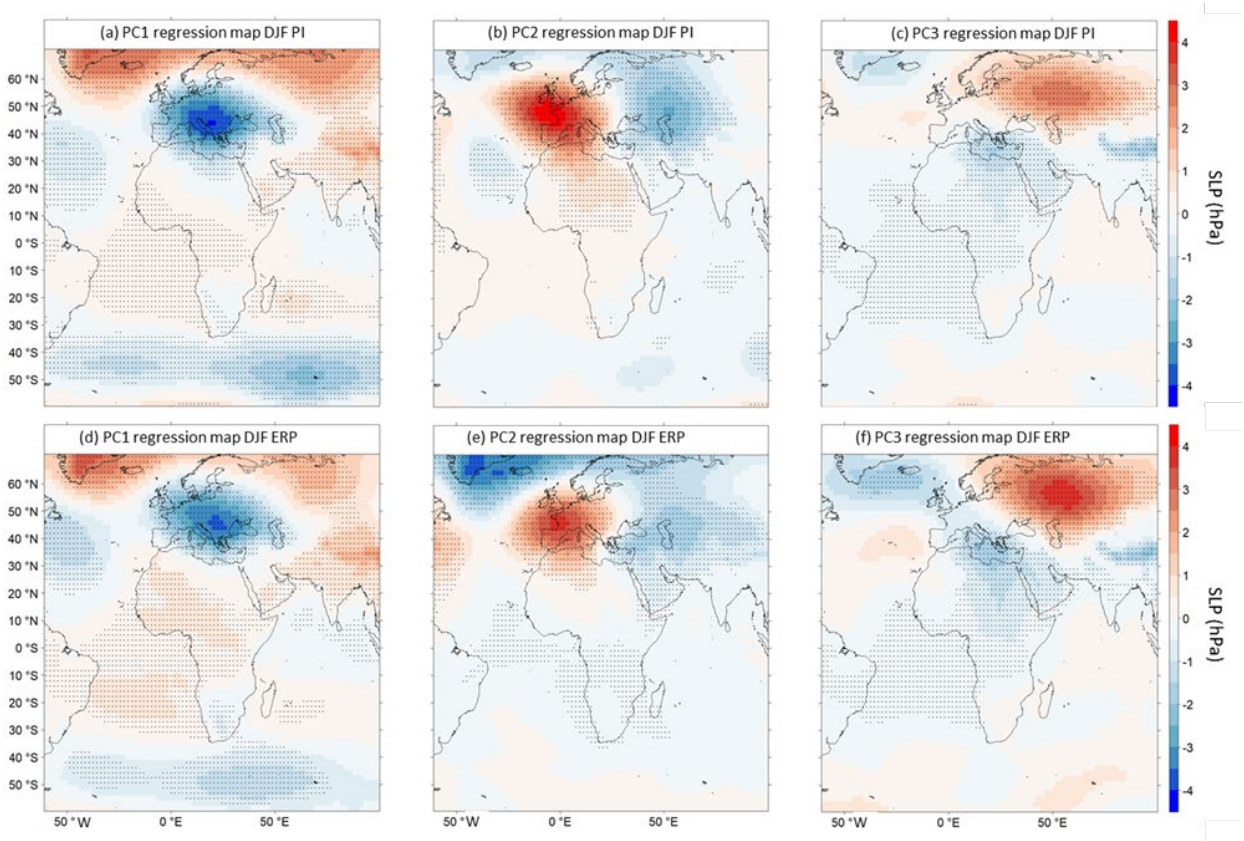

Figure 4.10. Regression maps between the PCs of the first three non-rotated winter (DJF) precipitation and SLP from the Mythos simulation for the PI (a, b, c) and ERP (d, e, f) periods. Statistical significance at the 95 % confidence level is denoted with dotted areas.

Figure 4.11 shows the leading three EOF patterns for summer 2m air temperatures over the EMNR region during the PI (a, b, c) and ERP (d, e, f) periods that together represent nearly 85% of the

total variance. Notably, the first EOF of the PI period explains nearly half of the variance, while the ERP period exhibits a lower but still high contribution of 40%. The EOF patterns show a high degree of similarity between the PI and ERP periods. The EOF1, as depicted in Figure 4.11 (a and d), shows a clear temperature dipole pattern, characterized by distinctive negative temperature anomalies over the African Sahel region (likely associated with ITCZ-related variability) and pronounced positive temperature anomalies over EM, extending to the Middle East and Egypt. This dipole structure indicates the presence of an apparent teleconnection between the Mediterranean Sea /Northern Africa and the Sahel region, resembling a temperature sea-saw pattern. The second EOF air temperature patterns (Fig. 4.11b, e) for the PI and ERP periods show positive anomalies throughout the entire EMNR area, while an intensified positive temperature anomalies signal is shown between 10 to 20 degrees north (Sahel). This pattern indicates similar variations of the two periods over the entire region that are uncorrelated to the temperature sea-saw depicted in EOF1. The EOF3 (Fig. 4.11c, f) shows weak negative temperature anomalies over the African Sahel region shifted slightly to the north, compared to EOF1, with negative anomalies extending over the Middle East and weak positive anomalies over the Balkans. This pattern shows lower values in the amount of explained variance.

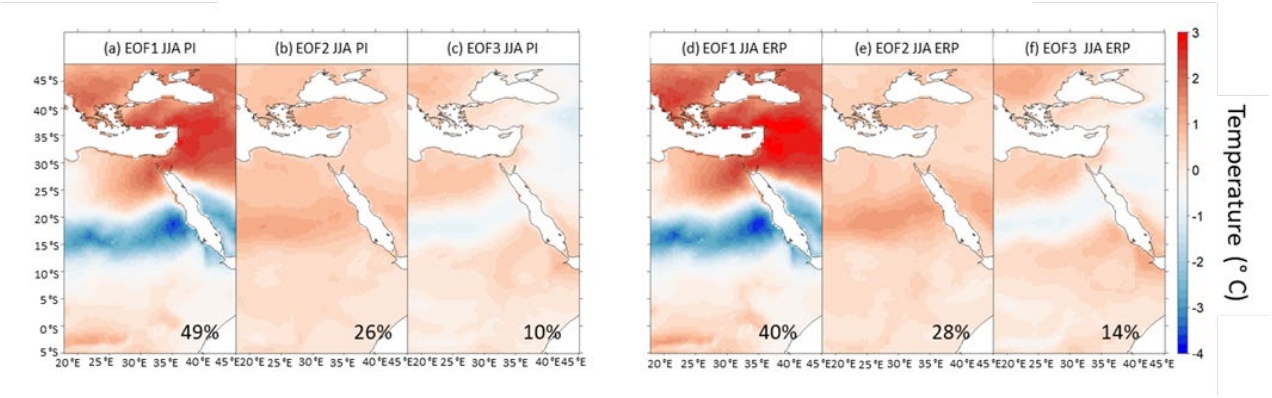

Figure 4.11. Patterns of the first three non-rotated EOFs of summer (JJA) temperature for PI (1800-1850 CE; a, b, c) and ERP (400-362 BCE; d, e, f) and total explained variance for each EOF.

The strong positive temperature anomalies over the northern and eastern part of the area and the belt of negative anomalies over the subtropical region in EOF1 is reflected in the SLP regression map (Fig. 4.12a, d). The EOF1 temperature pattern is related to negative SLP anomalies over the northern North Atlantic and positive anomalies over the central North Atlantic, potentially

connected with an intensified subtropical anticyclone, as well as negative anomalies over the extended study area, which may indicate the influence of the Persian trough extend from the Asian Monsoon trough (Lelieveld et al., 2012). Positive SLP anomalies are located over the belt of negative anomalies over the subtropical region. The EOF2 positive temperature anomalies over the entire EMNR area are connected to negative SLP anomalies over the region (Fig 4.12b, e). The higher temperatures over the area may be connected with an intensified Sahara heat low, which is an area of low surface pressure as a response high low-level temperatures (Lavaysse et al., 2009; Messager et al., 2010). The third EOF of the two periods (Fig. 4.11c, f) explains a smaller amount of variance and thus the interpretation of the patterns and the corresponding regression maps (Fig. 4.12c, f) is challenging and here not attempted.

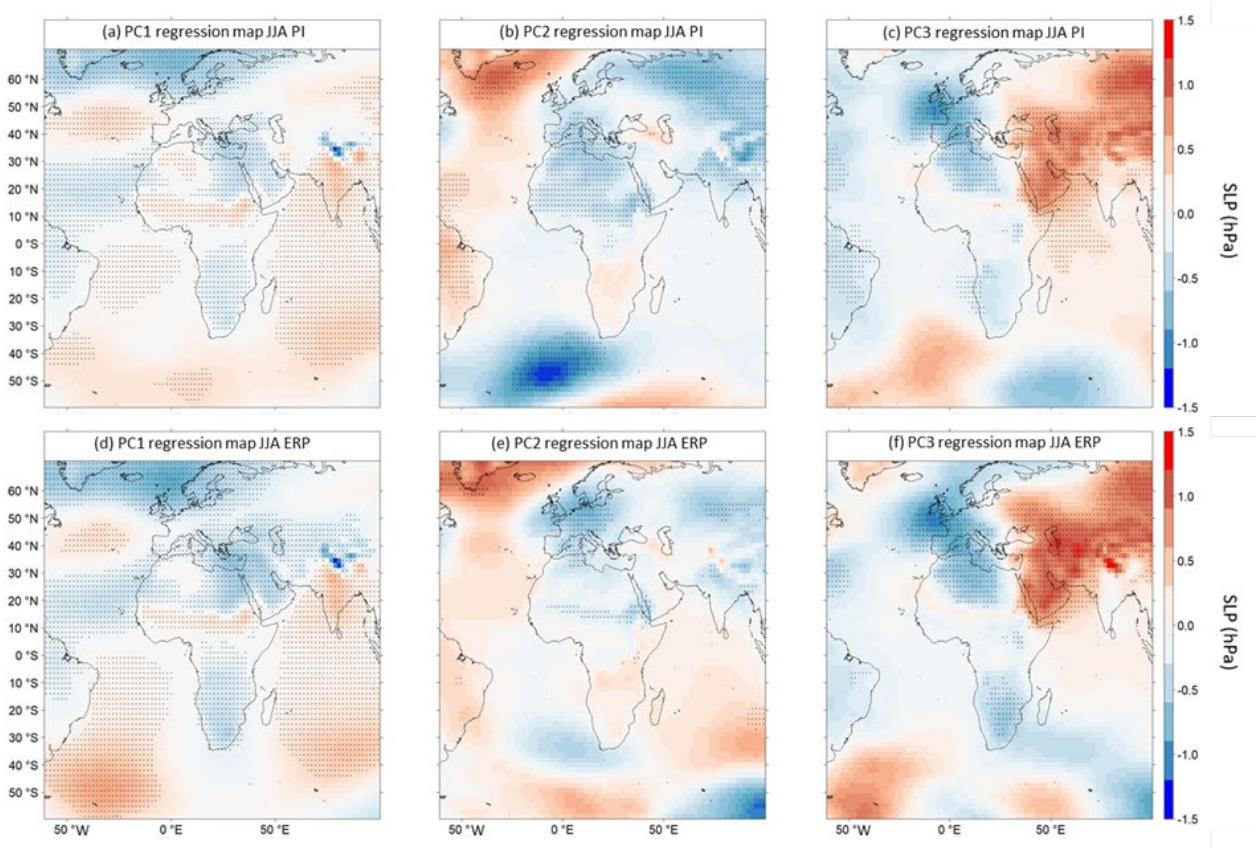

Figure 4.12. Regression maps between the PCs of the first three non-rotated summer (JJA) temperature and SLP from the Mythos simulation for the PI (a, b, c) and ERP (d, e, f) periods. Statistical significance at the 95 % confidence level is denoted with dotted areas.

4.4 Conclusions

In this study, we presented the first fully forced CCLM adapted for paleoclimatic applications including volcanic, solar, land-use, greenhouse gases, and orbital forcings with a spatial resolution of 0.44° over the extended area of the Eastern Mediterranean and the Nile River Basin. We evaluated the performance of the model in the present time (1980-2018) and compared the simulated climate for Early Roman Period, ERP (400-362 BCE) and the pre-industrial, PI (1800-1850 CE) period.

Our study demonstrates that the fully forced paleo CCLM can simulate reasonably the climate within the selected region. In general, the model exhibits better performance in simulating the seasonal air temperature compared to precipitation. Especially within the Nile River domain, the simulated precipitation is less accurate, possibly due to the model's limitations in representing convective processes linked to the ITCZ. Another important factor relates to the sparse network of observational data over those areas, further complicating a proper comparison between simulated and observed precipitation. In contrast, the model performs better in capturing precipitation patterns over the eastern Mediterranean, which is also located in a region associated with multiple circulations. The drying bias that occurs in the EM (especially in summer) may be related to the model's underestimation of total cloud cover. Moreover, the model tends to underestimate temperatures in northern Africa (around 10° - 32° N) during winter and the Sahel (10° - 20° N) during summer. During summer, temperatures in North Africa and the EM are showing a warm bias.

In terms of the annual cycle of precipitation and temperature, the average climatic conditions were comparable between the two periods, but the climatic variability varied across the study area. The ERP over the EM was generally wetter than the PI in both summer and winter, with greater variability in summer. In the NR region, there were no statistically significant differences during the ERP winter compared to the PI, while summers during the ERP were predominantly wetter and reflected a larger variability compared to the PI period. However, we have found that the CCLM has limitations in capturing a realistic rainfall pattern over the NR region.

The links between the regional precipitation and temperature patterns and large-scale features were investigated using a linear regression approach between the principal components of summer temperature and winter precipitation onto the sea level pressure. The according results indicate consistent associations between precipitation/temperature EOF patterns and corresponding SLP anomalies during both periods. The major winter precipitation patterns over EM shown in the principle component analysis are found to be related to the cyclones/anticyclones of the surrounding area (such as the Eastern Atlantic, the Western Europe) together with the orographical lifting. While, the NR region is located under the ITCZ and is subject to various circulation mechanisms, which poses a challenge for the model to accurately simulate local climate and its variability.

Future studies may involve adjusting physical parameters such as albedo, soil layers and aerosols to improve the performance of COSMO-CLM in capturing precipitation patterns in the NR region. Detailed investigations of the linkages between temperature and specific large-scale circulations in the EMNR region are also needed to provide a comprehensive understanding of the teleconnections in the study area. For paleoclimate research, comparing modeled data with proxy records is essential for a comprehensive understanding of climate variability and change over the past 2500 years. Additionally, establishing connections between abrupt climate events and profound historically documented societal developments can provide insights into the role of climate change in the context of historical socio-economic changes.

Appendix A

Table 4.3. Spatial correlation of the CCLM and ERA with the first six CRU temperature REOFs for winter (DJF) and summer (JJA) over the EMNR. All values are significant at the 95% significance level. Numbers in parentheses give the corresponding REOFs of each data set.

Winter (December, January, February)						
$r_{CRU\text{-}CCLM}$	0.79 (1 &1)	0.78 (2 & 2)	0.88 (3 & 5)	0.93 (4 & 3)	0.73 (5 & 10)	0.57 (6 & 2)
$r_{CRU\text{-}ERA}$	0.93 (1 & 1)	0.93 (2 & 2)	0.93 (3 & 5)	0.94 (4 & 3)	0.84 (5 & 4)	0.85 (6 & 10)
Summer (June, July, August)						
$r_{CRU\text{-}CCLM}$	-0.76 (1 & 1)	0.69 (2 & 1)	0.73 (3 & 3)	0.51 (4 & 9)	0.86 (5 & 6)	0.75 (6 & 2)
$r_{CRU\text{-}ERA}$	-0.77 (1 & 1)	0.64 (2 & 2)	0.78 (3 & 3)	0.83 (4 & 2)	0.90 (5 & 6)	0.67 (6 & 4)

Appendix B

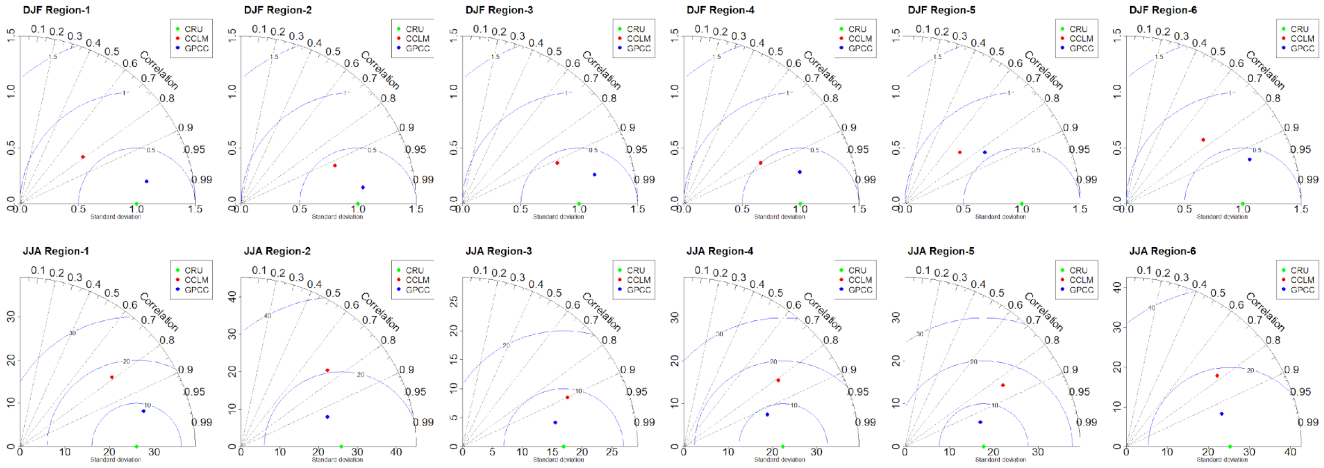

Figure 4.13. Taylor diagrams of winter (DJF) and summer (JJA) precipitation differences with respect to the CRU data set for the period 1980 – 2018 for the Eastern Mediterranean regions. The green dot indicated CRU data set, therefore the correlations showing in the plot is 1, and the blue (red) dot indicate the correlations between CCLM (GPCC) with CRU data sets.

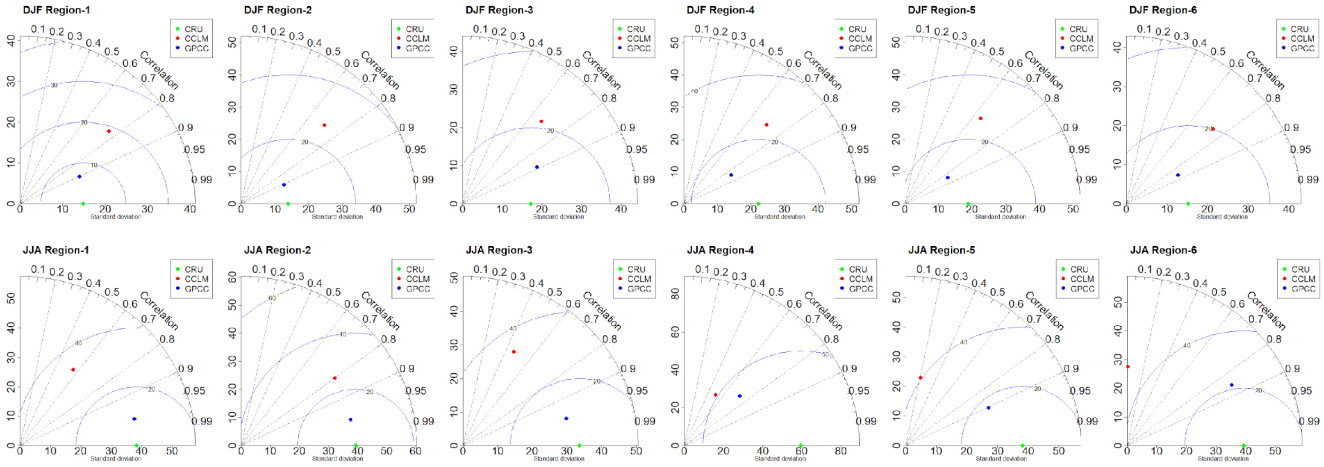

Figure 4.14. Taylor diagrams of winter (DJF) and summer (JJA) precipitation differences with respect to the CRU data set for the period 1980 – 2018 for the Nile River Basin regions. The green dot indicated CRU data set, therefore the correlations showing in the plot is 1, and the blue (red) dot indicate the correlations between CCLM (GPCC) with CRU data sets.

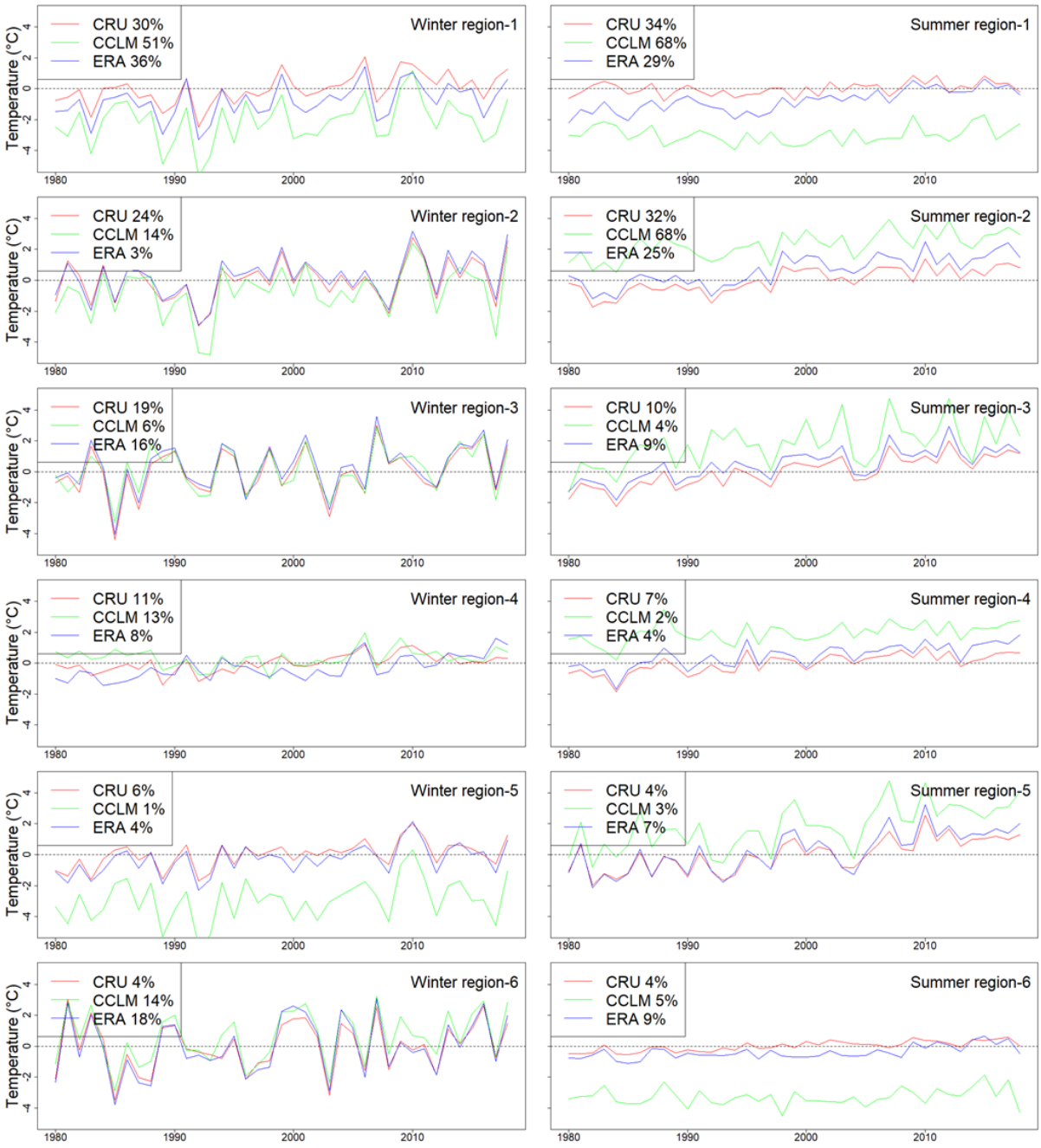

Figure 4.15. Seasonal mean total temperature differences of EMNR regions with respect to the 1980-2018 mean total CRU winter (DJF) and summer (JJA) temperature.

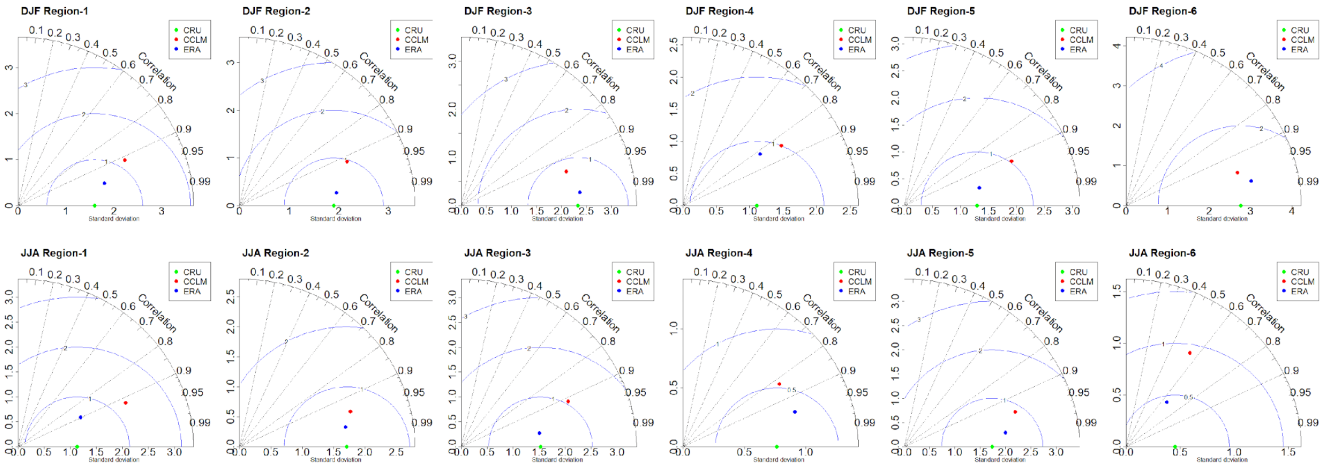

Figure 4.16. Taylor diagrams of winter (DJF) and summer (JJA) precipitation differences with respect to the CRU data set for the period 1980 – 2018 for the Eastern Mediterranean/Nile River Basin regions. The green dot indicated CRU data set, therefore the correlations showing in the plot is 1, and the blue (red) dot indicate the correlations between CCLM (ERA-Interim) with CRU data sets.

Code availability

The COSMO-CLM model is available and free of charge for all members of the CLM-Community via their website https://www.clmcommunity.eu/. The user must either be a member of the CLM-Community or the respective institute must possess an institutional license. The changes in the original source code for implementing the external forcings are described in detail in Hartmann et al., (submitted).

Data availability

The simulated data by COSMO-CLM in this paper is stored at the Deutsches Klimarechenzentrum (DKRZ).

Competing interests

The authors declare that they have no conflict of interest.

Author contribution

MZ and EH developed the model code and performed the simulations. EX, SW, MA and MZ contributed to the conceptualization of the manuscript. MZ conducted the formal analysis with the

support of SW and NL. MZ prepared the manuscript. All authors followed the analysis from the beginning, provided text and edited/commented the final version of the manuscript.

Acknowledgement

This work used resources of the Deutsches Klimarechenzentrum (DKRZ) granted by its Scientific Steering Committee (WLA) under project number bb1201. EX acknowledges support by the Greek "National Research Network on Climate Change and its Impact" (project code 200/937). EX, NL acknowledge support by the EU Horizon 2020 Project CLINT under Grant Agreement number 101003876. EX, MA acknowledge support by the German Federal Ministry of Education and Research (BMBF) project NUKLEUS (grant number 01LR2002F).

References

Adam, O., Schneider, T., Brient, F., and Bischoff, T.: Relation of the double-ITCZ bias to the atmospheric energy budget in climate models, Geophysical Research Letters, 43, 7670–7677, https://doi.org/10.1002/2016GL069465, 2016.

Alemseged, T. H. and Tom, R.: Evaluation of regional climate model simulations of rainfall over the Upper Blue Nile basin, Atmospheric Research, 161–162, 57–64, https://doi.org/10.1016/j.atmosres.2015.03.013, 2015.

Alpert, P., Price, C., Krichak, S. O., Ziv, B., Saaroni, H., Osetinsky, I., Barkan, J., and Kishcha, P.: Tropical tele-connections to the Mediterranean climate and weather, Advances in Geosciences, 2, 157–160, https://doi.org/10.5194/adgeo-2-157-2005, 2005.

Armstrong, E., Hopcroft, P. O., and Valdes, P. J.: Reassessing the Value of Regional Climate Modeling Using Paleoclimate Simulations, Geophysical Research Letters, 46, 12464–12475, https://doi.org/10.1029/2019GL085127, 2019.

Bader, J., Jungclaus, J., Krivova, N., Lorenz, S., Maycock, A., Raddatz, T., Schmidt, H., Toohey, M., Wu, C.-J., and Claussen, M.: Global temperature modes shed light on the Holocene temperature conundrum, Nature Communications, 11, https://doi.org/10.1038/s41467-020-18478-6, 2020.

Berger, A.: Long-Term Variations of Daily Insolation and Quaternary Climatic Changes, American Meteorological Society, 1978.

Bray, D. and Von Storch, H.: The Bray and von Storch 5th International Survey of Climate Scientists 2015/2016, https://doi.org/10.13140/RG.2.2.11802.85443, 2016.

Bucchignani, E., Cattaneo, L., Panitz, H.-J., and Mercogliano, P.: Sensitivity analysis with the regional climate model COSMO-CLM over the CORDEX-MENA domain, Meteorology and Atmospheric Physics, 128, 73–95, https://doi.org/10.1007/s00703-015-0403-3, 2016.

Camberlin, P.: Nile basin climates, in: The Nile, Springer, 307–333, 2009.

Conway, D.: The climate and hydrology of the Upper Blue Nile River, Geographical Journal, 166, 49–62, 2000.

Cramer, W., Guiot, J., Fader, M., Garrabou, J., Gattuso, J.-P., Iglesias, A., Lange, M. A., Lionello, P., Llasat, M. C., Paz, S., Peñuelas, J., Snoussi, M., Toreti, A., Tsimplis, M. N., and Xoplaki, E.: Climate change and interconnected risks to sustainable development in the Mediterranean, Nature Clim Change, 8, 972–980, https://doi.org/10.1038/s41558-018-0299-2, 2018.

Crowley, T., GA, Z., Vinther, B., Udisti, R., Kreutzs, K., Cole-Dai, J., and Castellano, E.: Volcanism and the Little Ice Age, PAGES Newslett., 16, 22–23, https://doi.org/10.1029/2002GL0166335, 2008.

Cubasch, U., Zorita, E., Kaspar, F., Gonzalez-Rouco, J. F., Storch, H. von, and Prömmel, K.: Simulation of the role of solar and orbital forcing on climate, Advances in Space Research, 37, 1629–1634, https://doi.org/10.1016/j.asr.2005.04.076, 2006.

Dee, D. P., Uppala, S. M., Simmons, A. J., Berrisford, P., Poli, P., Kobayashi, S., Andrae, U., Balmaseda, M. A., Balsamo, G., Bauer, P., Bechtold, P., Beljaars, A. C. M., van de Berg, L., Bidlot, J., Bormann, N., Delsol, C., Dragani, R., Fuentes, M., Geer, A. J., Haimberger, L., Healy, S. B., Hersbach, H., Hólm, E. V., Isaksen, L., Kållberg, P., Köhler, M., Matricardi, M., McNally, A. P., Monge-Sanz, B. M., Morcrette, J.-J., Park, B.-K., Peubey, C., de Rosnay, P., Tavolato, C., Thépaut, J.-N., and Vitart, F.: The ERA-Interim reanalysis: configuration and performance of the data

assimilation system, Quarterly Journal of the Royal Meteorological Society, 137, 553–597, https://doi.org/10.1002/qj.828, 2011.

Dieng, D., Smiatek, G., Heinzeller, D., and Kunstmann, H.: Simulation of the Rain Belt of the West African Monsoon (WAM) in High Resolution CCLM Simulation, in: High Performance Computing in Science and Engineering ´16, Cham, 547–558, https://doi.org/10.1007/978-3-319-47066-5_37, 2016.

Doms, G., Forstner, J., Heise, E., Reinhardt, T., Ritter, B., and Schrodin, R.: A Description of the Nonhydrostatic Regional COSMO Model, 161, 2011.

Gallacher, K., Miller, C., Scott, E. M., Willows, R., Pope, L., and Douglass, J.: Flow-directed PCA for monitoring networks, Environmetrics, 28, e2434, https://doi.org/10.1002/env.2434, 2017.

García-Herrera, R., Luterbacher, J., Lionello, P., González-Rouco, F., Ribera, P., Rodó, X., Kull, C., and Zerefos, C.: Reconstruction of past Mediterranean climate, Eos, Transactions American Geophysical Union, 88, 111–111, https://doi.org/10.1029/2007EO090010, 2007.

Giorgi, F.: Thirty Years of Regional Climate Modeling: Where Are We and Where Are We Going next?, Journal of Geophysical Research: Atmospheres, 124, 5696–5723, https://doi.org/10.1029/2018JD030094, 2019.

Giorgi, F. and Lionello, P.: Climate change projections for the Mediterranean region, Global and Planetary Change, 63, 90–104, https://doi.org/10.1016/j.gloplacha.2007.09.005, 2008.

Gómez-Navarro, J. J. and Zorita, E.: Atmospheric annular modes in simulations over the past millennium: No long-term response to external forcing, Geophysical Research Letters, 40, 3232–3236, https://doi.org/10.1002/grl.50628, 2013.

Gomez-Navarro, J. J., Wagner, S., Zorita, E., and Montavez, J. P.: Changes in distribution of daily temperature and precipitation between the Late Maunder Minimum and the 2nd half of the 20th century: A regional model study, 2012, PP21B-1990, 2012.

Gray, L. J., Beer, J., Geller, M., Haigh, J. D., Lockwood, M., Matthes, K., Cubasch, U., Fleitmann, D., Harrison, G., Hood, L., Luterbacher, J., Meehl, G. A., Shindell, D., van Geel, B., and White, W.: Solar Influences on Climate, Reviews of Geophysics, 48, https://doi.org/10.1029/2009RG000282, 2010.

Haldon, J., Roberts, N., Izdebski, A., Fleitmann, D., McCormick, M., Cassis, M., Doonan, O., Eastwood, W., Elton, H., Ladstätter, S., Manning, S., Newhard, J., Nicoll, K., Telelis, I., and Xoplaki, E.: The Climate and Environment of Byzantine Anatolia: Integrating Science, History, and Archaeology, The Journal of Interdisciplinary History, 45, 113–161, https://doi.org/10.1162/JINH_a_00682, 2014.

Haldon, J., Mordechai, L., Newfield, T. P., Chase, A. F., Izdebski, A., Guzowski, P., Labuhn, I., and Roberts, N.: History meets palaeoscience: Consilience and collaboration in studying past societal responses to environmental change, Proceedings of the National Academy of Sciences, 115, 3210–3218, https://doi.org/10.1073/pnas.1716912115, 2018.

Harris, I., Osborn, T. J., Jones, P., and Lister, D.: Version 4 of the CRU TS monthly high-resolution gridded multivariate climate dataset, Sci Data, 7, 109, https://doi.org/10.1038/s41597-020-0453-3, 2020.

Hartmann, E., Zhang, M., Xoplaki, E., Wagner, S., and Adakudlu, M.: Implementing External Climate Forcings into the COSMO-CLM - A Sensitivity Study around the Decade of the Samalas Volcanic Eruption in the EMME region, Geoscientific Model Development, submitted.

Hennessy, K., Lawrence, J., and Mackey, B.: IPCC Sixth Assessment Report (AR6): Climate Change 2022 - Impacts, Adaptation and Vulnerability: Regional Factsheet Australasia, 2022.

Hochman, A., Marra, F., Messori, G., Pinto, J. G., Raveh-Rubin, S., Yosef, Y., and Zittis, G.: Extreme weather and societal impacts in the eastern Mediterranean, Earth System Dynamics, 13, 749–777, https://doi.org/10.5194/esd-13-749-2022, 2022.

Jameson, A., Schmidt, W., and Turkel, E.: Numerical solution of the Euler equations by finite volume methods using Runge Kutta time stepping schemes, in: 14th Fluid and Plasma Dynamics

Conference, American Institute of Aeronautics and Astronautics, https://doi.org/10.2514/6.1981-1259, 1981.

Jungclaus, J. H., Bard, E., Baroni, M., Braconnot, P., Cao, J., Chini, L. P., Egorova, T., Evans, M., González-Rouco, J. F., Goosse, H., Hurtt, G. C., Joos, F., Kaplan, J. O., Khodri, M., Klein Goldewijk, K., Krivova, N., LeGrande, A. N., Lorenz, S. J., Luterbacher, J., Man, W., Maycock, A. C., Meinshausen, M., Moberg, A., Muscheler, R., Nehrbass-Ahles, C., Otto-Bliesner, B. I., Phipps, S. J., Pongratz, J., Rozanov, E., Schmidt, G. A., Schmidt, H., Schmutz, W., Schurer, A., Shapiro, A. I., Sigl, M., Smerdon, J. E., Solanki, S. K., Timmreck, C., Toohey, M., Usoskin, I. G., Wagner, S., Wu, C.-J., Yeo, K. L., Zanchettin, D., Zhang, Q., and Zorita, E.: The PMIP4 contribution to CMIP6 – Part 3: The last millennium, scientific objective, and experimental design for the PMIP4 past1000 simulations, Geoscientific Model Development, 10, 4005–4033, https://doi.org/10.5194/gmd-10-4005-2017, 2017.

Kageyama, M., Braconnot, P., Harrison, S. P., Haywood, A. M., Jungclaus, J. H., Otto-Bliesner, B. L., Peterschmitt, J.-Y., Abe-Ouchi, A., Albani, S., Bartlein, P. J., Brierley, C., Crucifix, M., Dolan, A., Fernandez-Donado, L., Fischer, H., Hopcroft, P. O., Ivanovic, R. F., Lambert, F., Lunt, D. J., Mahowald, N. M., Peltier, W. R., Phipps, S. J., Roche, D. M., Schmidt, G. A., Tarasov, L., Valdes, P. J., Zhang, Q., and Zhou, T.: The PMIP4 contribution to CMIP6 – Part 1: Overview and over-arching analysis plan, Geoscientific Model Development, 11, 1033–1057, https://doi.org/10.5194/gmd-11-1033-2018, 2018.

Kelley, C. P., Mohtadi, S., Cane, M. A., Seager, R., and Kushnir, Y.: Climate change in the Fertile Crescent and implications of the recent Syrian drought, Proceedings of the National Academy of Sciences, 112, 3241–3246, https://doi.org/10.1073/pnas.1421533112, 2015.

Lange, M. A., Llasat, M. C., Snoussi, M., Graves, A., Tellier, J. L., Queralt, A., and Vagliasindi, G. M.: First Mediterranean Assessment Report – Chapter 1: Introduction, Zenodo, https://doi.org/10.5281/zenodo.7100592, 2020.

Lavaysse, C., Flamant, C., Janicot, S., Parker, D. J., Lafore, J.-P., Sultan, B., and Pelon, J.: Seasonal evolution of the West African heat low: a climatological perspective, Clim Dyn, 33, 313–330, https://doi.org/10.1007/s00382-009-0553-4, 2009.

Lelieveld, J., Hadjinicolaou, P., Kostopoulou, E., Chenoweth, J., El Maayar, M., Giannakopoulos, C., Hannides, C., Lange, M. A., Tanarhte, M., Tyrlis, E., and Xoplaki, E.: Climate change and impacts in the Eastern Mediterranean and the Middle East, Climatic Change, 114, 667–687, https://doi.org/10.1007/s10584-012-0418-4, 2012.

Ludwig, P., Schaffernicht, E., Shao, Y., and Pinto, J.: Regional atmospheric circulation over Europe during the Last Glacial Maximum and its links to precipitation, Journal of Geophysical Research Atmospheres, 121, 2130–2145, https://doi.org/10.1002/2015JD024444, 2016.

Ludwig, P., Pinto, J., Raible, C., and Shao, Y.: Impacts of Surface Boundary Conditions on Regional Climate Model Simulations of European Climate during the Last Glacial Maximum, Geophysical Research Letters, 44, 5086–5095, https://doi.org/10.1002/2017GL073622, 2017.

Luterbacher, J. and Pfister, C.: The year without a summer, Nature Geosci, 8, 246–248, https://doi.org/10.1038/ngeo2404, 2015.

Luterbacher, J., Werner, J. P., Smerdon, J. E., Fernández-Donado, L., González-Rouco, F. J., Barriopedro, D., Ljungqvist, F. C., Büntgen, U., Zorita, E., Wagner, S., Esper, J., McCarroll, D., Toreti, A., Frank, D., Jungclaus, J. H., Barriendos, M., Bertolin, C., Bothe, O., Brázdil, R., Camuffo, D., Dobrovolný, P., Gagen, M., García-Bustamante, E., Ge, Q., Gómez-Navarro, J. J., Guiot, J., Hao, Z., Hegerl, G. C., Holmgren, K., Klimenko, V. V., Martín-Chivelet, J., Pfister, C., Roberts, N., Schindler, A., Schurer, A., Solomina, O., Gunten, L. von, Wahl, E., Wanner, H., Wetter, O., Xoplaki, E., Yuan, N., Zanchettin, D., Zhang, H., and Zerefos, C.: European summer temperatures since Roman times, Environ. Res. Lett., 11, 024001, https://doi.org/10.1088/1748-9326/11/2/024001, 2016.

Manning, J. G., Ludlow, F., Stine, A. R., Boos, W. R., Sigl, M., and Marlon, J. R.: Volcanic suppression of Nile summer flooding triggers revolt and constrains interstate conflict in ancient Egypt, Nat Commun, 8, 900, https://doi.org/10.1038/s41467-017-00957-y, 2017.

Meinshausen, M., Vogel, E., Nauels, A., Lorbacher, K., Meinshausen, N., Etheridge, D. M., Fraser, P. J., Montzka, S. A., Rayner, P. J., Trudinger, C. M., Krummel, P. B., Beyerle, U., Canadell, J. G., Daniel, J. S., Enting, I. G., Law, R. M., Lunder, C. R., O'Doherty, S., Prinn, R. G., Reimann,

S., Rubino, M., Velders, G. J. M., Vollmer, M. K., Wang, R. H. J., and Weiss, R.: Historical greenhouse gas concentrations for climate modelling (CMIP6), Geoscientific Model Development, 10, 2057–2116, https://doi.org/10.5194/gmd-10-2057-2017, 2017.

Ménot, G., Pivot, S., Bouloubassi, I., Davtian, N., Hennekam, R., Bosch, D., Ducassou, E., Bard, E., Migeon, S., and Revel, M.: Timing and stepwise transitions of the African Humid Period from geochemical proxies in the Nile deep-sea fan sediments, Quaternary Science Reviews, 228, 106071, https://doi.org/10.1016/j.quascirev.2019.106071, 2020.

Messager, C., Parker, D. J., Reitebuch, O., Agusti-Panareda, A., Taylor, C. M., and Cuesta, J.: Structure and dynamics of the Saharan atmospheric boundary layer during the West African monsoon onset: observations and analyses from the research flights of 14 and 17 July 2006, Quarterly Journal of the Royal Meteorological Society, 136, 107–124, https://doi.org/10.1002/qj.469, 2010.

Nicholson, S. E.: The ITCZ and the Seasonal Cycle over Equatorial Africa, Bulletin of the American Meteorological Society, 99, 337–348, https://doi.org/10.1175/BAMS-D-16-0287.1, 2018.

Paz, S., Tourre, Y. M., and Planton, S.: North Africa-West Asia (NAWA) sea-level pressure patterns and their linkages with the Eastern Mediterranean (EM) climate, Geophysical Research Letters, 30, https://doi.org/10.1029/2003GL017862, 2003.

Pielke Sr, R., Pitman, A., Niyogi, D., Mahmood, R., Mcalpine, C., Hossain, F., Klein Goldewijk, K., Nair, U., Betts, R., Fall, S., Reichstein, M., Kabat, P., and de NOBLET, N.: Land Use/Land Cover Changes and Climate: Modeling Analysis and Observational Evidence, Wiley Interdisciplinary Reviews: Climate Change, 2, 828–850, https://doi.org/10.1002/wcc.144, 2011.

Pörtner, H.-O., Roberts, D. C., Tignor, M. M. B., Poloczanska, E. S., Mintenbeck, K., Alegría, A., Craig, M., Langsdorf, S., Löschke, S., Möller, V., Okem, A., and Rama, B. (Eds.): Climate Change 2022: Impacts, Adaptation and Vulnerability. Contribution of Working Group II to the Sixth Assessment Report of the Intergovernmental Panel on Climate Change., 2022.

Raffa, M., Adinolfi, M., Reder, A., Marras, G. F., Mancini, M., Scipione, G., Santini, M., and Mercogliano, P.: Very High Resolution Projections over Italy under different CMIP5 IPCC scenarios, Sci Data, 10, 238, https://doi.org/10.1038/s41597-023-02144-9, 2023.

Ramanathan, V. and Feng, Y.: Air pollution, greenhouse gases and climate change: Global and regional perspectives, Atmospheric Environment, 43, 37–50, https://doi.org/10.1016/j.atmosenv.2008.09.063, 2009.

Renssen, H., Isarin, R. F. B., Jacob, D., Podzun, R., and Vandenberghe, J.: Simulation of the Younger Dryas climate in Europe using a regional climate model nested in an AGCM: preliminary results, Global and Planetary Change, 30, 41–57, https://doi.org/10.1016/S0921-8181(01)00076-5, 2001.

Richman, M. B. and Lamb, P. J.: Pattern analysis of growing season precipitation in Southern Canada, Atmosphere-Ocean, 25, 137–158, https://doi.org/10.1080/07055900.1987.9649268, 1987.

Robock, A.: Volcanic eruptions and climate, Reviews of Geophysics, 38, 191–219, https://doi.org/10.1029/1998RG000054, 2000.

Rockel, B., Will, A., and Hense, A.: Regional climate modelling with COSMO-CLM (CCLM), Meteorol. Z. (Stuttg.), 17, 2008.

Schättler, U. and Blahak, U.: in: A Description of the Nonhydrostatic Regional COSMO-Model, 2017.

Schneider, U., Finger P, Rustemeier E, Ziese M, and Hänsel S: Global Precipitation Analysis Products of the GPCC, 2022.

Schulz, J.-P., Vogel, G., Becker, C., Kothe, S., Rummel, U., and Ahrens, B.: Evaluation of the ground heat flux simulated by a multi-layer land surface scheme using high-quality observations at grass land and bare soil, Meteorologische Zeitschrift, 25, 607–620, https://doi.org/10.1127/metz/2016/0537, 2016.

Singh, R., Tsigaridis, K., LeGrande, A. N., Ludlow, F., and Manning, J. G.: Investigating hydroclimatic impacts of the 168–158 BCE volcanic quartet and their relevance to the Nile River basin and Egyptian history, Climate of the Past, 19, 249–275, https://doi.org/10.5194/cp-19-249-2023, 2023.

Sørland, S. L., Brogli, R., Pothapakula, P. K., Russo, E., Van de Walle, J., Ahrens, B., Anders, I., Bucchignani, E., Davin, E. L., Demory, M.-E., Dosio, A., Feldmann, H., Früh, B., Geyer, B., Keuler, K., Lee, D., Li, D., van Lipzig, N. P. M., Min, S.-K., Panitz, H.-J., Rockel, B., Schär, C., Steger, C., and Thiery, W.: COSMO-CLM regional climate simulations in the Coordinated Regional Climate Downscaling Experiment (CORDEX) framework: a review, Geoscientific Model Development, 14, 5125–5154, https://doi.org/10.5194/gmd-14-5125-2021, 2021.

Storch, H. V. and Zwiers, F. W.: Statistical Analysis in Climate Research, 1st ed., Cambridge University Press, https://doi.org/10.1017/CBO9780511612336, 1984.

Tiedtke, M.: Parameterization of Cumulus Convection in Large-Scale Models, in: Physically-Based Modelling and Simulation of Climate and Climatic Change, edited by: Schlesinger, M. E., Springer Netherlands, Dordrecht, 375–431, https://doi.org/10.1007/978-94-009-3041-4_9, 1988.

Toohey, M. and Sigl, M.: Volcanic stratospheric sulfur injections and aerosol optical depth from 500 BCE to 1900 CE, Earth System Science Data, 9, 809–831, https://doi.org/10.5194/essd-9-809-2017, 2017.

Viste, E. and Sorteberg, A.: Moisture transport into the Ethiopian highlands, International Journal of Climatology, 333, 249–263, https://doi.org/10.1002/joc.3409, 2013.

Wilks, D. S.: Statistical Methods in the Atmospheric Sciences, Academic Press, 698 pp., 2011.

Worku, G., Teferi, E., Bantider, A., Dile, Y. T., and Taye, M. T.: Evaluation of regional climate models performance in simulating rainfall climatology of Jemma sub-basin, Upper Blue Nile Basin, Ethiopia, Dynamics of Atmospheres and Oceans, 83, 53–63, https://doi.org/10.1016/j.dynatmoce.2018.06.002, 2018.

Xoplaki, E., Fleitmann, D., Luterbacher, J., Wagner, S., Haldon, J. F., Zorita, E., Telelis, I., Toreti, A., and Izdebski, A.: The Medieval Climate Anomaly and Byzantium: A review of the evidence on climatic fluctuations, economic performance and societal change, Quaternary Science Reviews, 136, 229–252, https://doi.org/10.1016/j.quascirev.2015.10.004, 2016.

Xoplaki, E., Luterbacher, J., Wagner, S., Zorita, E., Fleitmann, D., Preiser-Kapeller, J., Sargent, A. M., White, S., Toreti, A., Haldon, J. F., Mordechai, L., Bozkurt, D., Akçer-Ön, S., and Izdebski, A.: Modelling Climate and Societal Resilience in the Eastern Mediterranean in the Last Millennium, Hum Ecol, 46, 363–379, https://doi.org/10.1007/s10745-018-9995-9, 2018.

Xoplaki, E., Luterbacher, J., Luther, N., Behr, L., Wagner, S., Jungclaus, J., Zorita, E., Toreti, A., Fleitmann, D., Izdebski, A., and Bloomfield, K.: Hydrological Changes in Late Antiquity: Spatio-Temporal Characteristics and Socio-Economic Impacts in the Eastern Mediterranean, in: Climate Change and Ancient Societies in Europe and the Near East: Diversity in Collapse and Resilience, edited by: Erdkamp, P., Manning, J. G., and Verboven, K., Springer International Publishing, Cham, 533–560, https://doi.org/10.1007/978-3-030-81103-7_18, 2021.

Zhang, M., Tölle, M. H., Hartmann, E., Xoplaki, E., and Luterbacher, J.: A Sensitivity Assessment of COSMO-CLM to Different Land Cover Schemes in Convection-Permitting Climate Simulations over Europe, Atmosphere, 12, 1595, https://doi.org/10.3390/atmos12121595, 2021.

Zittis, G., Almazroui, M., Alpert, P., Ciais, P., Cramer, W., Dahdal, Y., Fnais, M., Francis, D., Hadjinicolaou, P., Howari, F., Jrrar, A., Kaskaoutis, D. G., Kulmala, M., Lazoglou, G., Mihalopoulos, N., Lin, X., Rudich, Y., Sciare, J., Stenchikov, G., Xoplaki, E., and Lelieveld, J.: Climate Change and Weather Extremes in the Eastern Mediterranean and Middle East, Reviews of Geophysics, 60, e2021RG000762, https://doi.org/10.1029/2021RG000762, 2022.

5. Conclusions

5.1 Acknowledgements

For finishing my doctorate study, I would like to express my deepest gratitude to my supervisor, Professor. Dr. Jürg Luterbacher and Dr. Elena Xoplaki for their unwavering guidance, valuable insights, and constant encouragement throughout my Ph.D. journey. Their dedication to fostering my academic growth and providing critical feedback has been instrumental in shaping the course of my research.

I am profoundly grateful to my mentors, Dr. Sebastian Wagner, whose expertise and guidance have been invaluable. His continuous support, thoughtful discussions, and willingness to share his knowledge have enriched my understanding of my research field and encouraged me toward achieving my goals. I also want to express my gratitude to Prof. Andreas Dittmann, who have provided valuable insights during my PhD study.

I extend my heartfelt appreciation to my colleagues through the whole journey of my PhD study: Eva Harmann, Dr. Muralidhar Adakudlu, Niklas Luther, Lorine Behr, Dr. Qing Lin, Dr. Yanet Díaz Esteban, Dr. Edgar Espitia, Dr. Fatemeh Heidari, Dr. Odysseas Vlachopoulos, Viviana Quezada, Dr. Stefanie Talento, Tim R. Sperzel, Dr. Angelika Palarz, Dr. Tine Nilsen, Dr. Florian Ellsäßer, Dr. Stella Dafka. Our discussions, spirited debates, and shared challenges have not only expanded my research horizons but have also created an environment conducive to learning and growth. Together, we have formed a community that thrives on mutual support and the pursuit of knowledge.

The support of Mrs. Andrea Goetzl, Justus Liebig University Giessen and the Geography faculty and staff has been invaluable, providing me with a nurturing academic environment and access to resources that have been instrumental in my research journey.

Lastly, I want to express my deepest gratitude and love to my family and friends for their constant support, patience, and encouragement throughout this journey. Their belief in my abilities has been a precious source of motivation.

This work would not have been possible without the collective support and mentorship of these individuals. I am truly fortunate to have had such a dedicated and inspiring group of individuals by my side.

山高路远，来日方长。但愿人长久，千里共婵娟。

With heartfelt gratitude,

Mingyue Zhang, 30.08.2023, Giessen